

A Theoretical Analysis of Single Coal Particle Behavior during Spontaneous Devolatilization and Combustion

Dissertation

zur Erlangung des akademischen Grades

Doktoringenieur (Dr.-Ing.)

von: M.Tech Shabi Ulzama

geb. am: 01.07.1978

in: Moradabad, India

genehmigt durch die Fakultät für Verfahrens- und Systemtechnik
der Otto-von-Guericke-Universität Magdeburg

Gutachter: Prof. Dr.-Ing. E.Tsotsas
Prof. Dr.-Ing. Eckehard Specht
Prof. Dr.-Ing. J.Schmidt

eingereicht am: 02.04.2007

Promotionskolloquium am: 26.04.2007

Preface

This dissertation presents the major results of my research performed between 2003 and 2007 at the Institute of fluid dynamics and thermodynamics (ISUT), Otto-von-Guericke-Universität Magdeburg, Germany. I would like to grab this opportunity to express my gratitude to all those who helped me and gave me the possibility to complete this thesis.

First and foremost, I would like to thank Prof. Dr.-Ing. E. Specht for enabling me to write this thesis at university of Magdeburg. I am also especially grateful to him for showing me his systematic approach of analyzing and modeling chemical processes. My second thanks goes to Prof. Dr.-Ing. habil. Evangelos Tsotsas for the co-operation and disposition as a referee of my thesis work.

I would like to thank Hermann Woche who during my thesis unremittingly helped me in assembling and conducting experiments. I also like to thank to the people of the mechanical workshop for their commitment and help, even when they were 'fully booked' with other tasks.

I would also like to take this opportunity in thanking all my friends who have been patient enough despite eagerly waiting for the completion of my thesis to see me as a successful person in my professional as well as real life.

My last thanks goes to the persons most dearest to me: my life companion and my family.

Shabi Ulzama

Magdeburg, 26.04.2007

Contents

	Page
Kurzzusammenfassung	iv
Abstract	vi
1. Introduction	
1.1 Coal: Utilization	1
1.2 Coal: Past, Present and Future	2
1.3 Motivation and Scope of this Work	8
2. An Analytical Study of Droplet Combustion under Microgravity	
2.1 Introduction	10
2.2 Model Formulation	12
2.2.1 Droplet Combustion Time	14
2.2.2 Flame Dynamics	15
2.3 Simulation Results	16
2.3.1 Droplet and Flame Structure Characteristics	17
2.3.2 Estimation of Gasification Rate	19
2.3.3 Influence of Vaporization Enthalpy on Burning Behavior	20
2.3.4 Flame Stand-off Ratio	21
2.3.5 Influence of Ambient Oxygen Concentration on Flame Structure	22
2.4 Concluding Remark	22
3. Modeling Coal Particle Behavior under Devolatilization	
3.1 Introduction	24
3.2 Single Coal Particle Devolatilization Modeling	26
3.3 Simulation Results	29
3.3.1 Particle's Surface Temperature	30
3.3.2 Flame Dynamics	31
3.4 Concluding Remark	32
4. Coke Gasification in an Environment of CO₂	
4.1 Introduction	34
4.2 Langmuir-Hinshelwood Semi Global Kinetics	37
4.3 Experiments	43
4.3.1 Experimental Setup and Materials used	43
4.3.2 Mass Transfer Calculations	47
4.4 Experimental Results	48
4.4.1 Measurement of Mass Transfer Coefficient	48
4.4.2 Intrinsic Kinetic Parameters for Coke Gasification in CO ₂ Environment	50
4.4.3 Determination of Sorption Coefficient of CO ₂	53
4.4.4 Determination of Sorption Coefficient of CO	55
4.4.5 Apparent Kinetic Parameters for Coke Gasification in CO ₂ Environment	58
4.5 Concluding Remark	65
5. Modeling Coal Combustion	

5.1	Introduction	66
5.2	Reaction Mechanism	71
5.3	Gas Phase Modeling	72
5.4	Simulation Results	74
5.4.1	Species Concentration and Gas Phase Temperature Profile	74
5.5	Solid Phase Modeling	75
5.5.1	Model Formulation	75
5.6	Simulation Results	79
5.6.1	Total Conversion Time	79
5.7	Mathematical Modeling for a Special Case of Combustion with Air Excess Number ≤ 1	80
5.7.1	Model Formulation	80
5.8	Simulation Results	82
5.8.1	Time History of Fractional Conversion and Particle Shrinkage	83
5.8.2	Total Combustion Time	83
5.8.3	Particle Temperature Variation	85
5.8.4	Oxygen Concentration Profile inside the Particle	85
5.9	Concluding Remark	86
6.	Conclusions and Outlook	87
7.	Nomenclature	91
8.	Bibliography	93
9.	Figure Index	102
10.	Table Index	105
11.	Appendix A: The BVP Solver	106

Kurzzusammenfassung

Ziel dieser Arbeit ist daher die methodische Analyse der folgenden Prozesse zu untersuchen: Analyse der Verdampfung der flüssigen Kohlenanteile, Effekt von Strahlung und Konvektion während der Verbrennung, Wärmeübergang im inneren der Partikel, Reaktionsgrad während des Kontaktes von reaktionsfähigen Gasen mit Kohlenpartikeln.

Das Modellbaukonzept des Kohlenverdampfungsprozesses ist dem der Verdampfung eines Flüssigkeitstropfens ähnlich. Unterschiedlich ist aber, dass während der Verdampfung der flüchtige Teil einen konstanten Durchmesser aufweist, während dessen der Tropfendurchmesser bei der Verbrennung abnimmt. Ein analytisches Modell, das auf der Annahme der kombinierten stationären und instationären Prozesse basiert, wird erläutert, um die zeitabhängige, sphärische Verbrennung eines einzigen Tropfens unter dem Effekt der Schwerkraft auf Mikrolevel darzustellen. Das Modell konzentriert sich auf Voraussagen bezüglich der folgenden Parameter: Variation des Tropfen- und Flammendurchmessers während der Verbrennung, Einfluss der Verdampfungsenthalpie auf das Verbrennungsverhalten, die durchschnittliche Verbrennungsgleichung und der Effekt des Konzentrationswechsels des umgebenden Sauerstoffs auf die Flammenstruktur.

Das Modell der Tropfenverbrennung wurde erfolgreich angewendet für die Beschreibung der Verdampfung der Kohlenpartikel, wo die weiteren prozessbeschränkenden Annahmen gemacht worden sind. Das Modell beschreibt den Mechanismus der Wärme- und Stoffübertragung in der Partikel-, Flammen- und Umgebung. Der diffuse Transport des Dampfes wurde mit zeitunabhängigem Zustandsverhalten erklärt dem zeitabhängigen diffusen Transport des Oxydationsmittels gegenüber. Weiterhin hat die Dateninkompatibilität, die durch die Bestimmung des kinetischen Koeffizienten beim Vergasen der Kohle mit CO_2 entstand, Experimentaluntersuchungen benötigt. Diese Arbeit beinhaltet Versuchsziele für die Neubestimmung des kinetischen Gleichungskoeffizienten der Boudouard Reaktion, der vom Kohlentyp abhängt. Weiterhin sind theoretische Analyse durchgeführt worden, um die Bedeutung der Boudouard Reaktion während der unterstöchiometrischen Verbrennungsprozesse darzustellen. Die Versuchs- und die Modellierungsergebnisse in dieser Arbeit beweisen, dass die Boudouard-Reaktion einen großen Einfluss auf den Prozess ($\lambda \leq 1$) hat und von der im Prozess verwendeten Kohlentyp abhängt. Die Simulationen über die Verbrennung der einzelnen Partikel wurden mit Hilfe eines instationären Modells durchgeführt, das eine

ausführliche Beschreibung des Transportphänomens und der chemischen Reaktion enthält. Das Ergebnis der Simulation ist mit den in der Literatur vorhandenen Versuchsergebnissen verglichen worden.

Abstract

The objective of this work has been to systematically analyze coal devolatilization, the radiation and convection effect over combustion, internal conduction within coal particle, and the reaction rates in circumstances where highly reactive gases come in contact with coal particle.

The modeling concept of coal devolatilization is similar to that of the liquid droplet combustion except that volatiles emitted from the coal particle which has a constant diameter during devolatilization unlike droplet burning. An analytical model based on an assumption of combined quasi-steady and transient behavior of the process is presented to exemplify the unsteady, spherically-symmetric single droplet combustion under microgravity. The modeling approach especially focuses on predicting; the variations of droplet and flame diameters with burning time, the effect of vaporization enthalpy on burning behavior, the average burning rates and the effect of change in ambient oxygen concentration on flame structure. The droplet combustion model has been successfully implemented for description of devolatilization of a coal particle where more restrictive assumptions were made. The model describes the heat and mass transfer mechanisms among the particle, the flame, and the external environment. The volatile diffusive transport has been explained with quasi-steady state behavior unlike unsteady diffusive transport of oxidant. Moreover, the data incongruity existing in estimation of kinetic coefficients for gasification of coke by CO_2 has shown a need to perform experimental investigation. This work includes experimental targets for re-estimation of kinetic rate coefficient of Boudouard reaction, which depends on the type of coke. A new set of activation energies and pre exponential factors differs mostly from the values available in the literature. Moreover, theoretical analyses are reported to describe the importance of Boudouard reaction during those combustion processes where the value of excess air number is approximately 1. Both the experimental and computational results reported in the present study suggest that Boudouard reaction has a great influence on process (air excess number ≤ 1) and shows dependence on a type of coal used in the process. Simulations of single particle combustion have been conducted using a steady state model that includes a detailed description of transport phenomenon coupled with chemical reactions. The results of simulations are compared with experimental data available in the literature.

Chapter 1

Introduction

1.1 Coal: Utilization

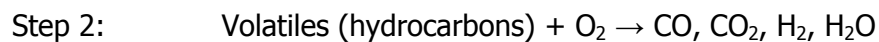
The combustion of solid fuels has a history stretching over many millennia. Coal is a naturally occurring hydrocarbon that consists of the fossilized remains of buried plant debris that have undergone progressive physical and chemical alteration, called coalification, in the course of geologic time. Coal utilization covers a wide area of applications, but in terms of classes it involves domestic and commercial heating, industrial applications, and power station or utility applications. A number of energy prediction scenarios have suggested that bioenergy might account for 10%–33% of the primary energy supply by 2050 [*IEA World Energy Outlook, Shell International*], but modern biomass utilization techniques based on commercial fuels will provide much less than this. Coal utilization will, however, remain the dominant commercial solid fuel source until at least 2020, and the International Energy Agency estimates [*IEA World Energy Outlook*] indicate that coal, together with combustible renewables, will form 28% of the traded fuels by 2020, compared with 24% in 1998. Gasification, which is a mean to convert fossil fuels, biomass and wastes into either a combustible gas or a synthesis gas for subsequent utilization, offers the potential both for clean power and chemicals production. Some 20% of the gasification plants throughout the world that use coal as the feedstock produce electric power [*USDoE and Gasification Technology Council*]. Coal gasification can produce a gas used for synthesis, or as a source of hydrogen for the manufacture of ammonia or hydrogenation applications in refineries,

and many of the technologies have been developed by petroleum companies with these applications in mind.

1.2 Coal: Past, Present and Future

The early technologies involved methods for the combustion of fuels such as wood logs or lump coal, generally in fixed beds with an uncontrolled inflow of undergrate and secondary air supplies. The industrial revolution was largely based on this technology but had the inevitable inefficient combustion and high pollution levels [*Lowry*]. Over the years, combustion efficiency increased by the introduction of controlled airflows and better boiler design, but combustion intensity, being fundamentally a quantity dependant on combustion temperature and coal particle surface area, remained attracted extensive research activity and has developed technologically as a result. Fluidized-bed combustion, particularly pressurized circulating-bed combustion, offered even higher efficiencies [*Grace et al.*], but so far, this has not been greatly favored by industry. The amount of CO₂ in the atmosphere has risen by over 30% since 1750, and if no action is taken, it will double its pre-industrial value during the second half of the twenty-first century. This is associated with adverse climatic effects. Most of it is due to the use of fossil fuels, especially coal.

The general processes that take place in coal combustion are shown in **Fig. 1.1**. The main processes of coal combustion, namely, coal devolatilization and char burn-out, are usually simplified to the following reactions:



Nitrogen is released from the coal, as shown in Fig. 1.1, and forms nitrogen oxides. The inorganic materials decompose to form ash and then slag. Sulfur is released, forming sulfur oxides together with some toxic metals; these aspects of combustion are not dealt with here, nor is slag formation.

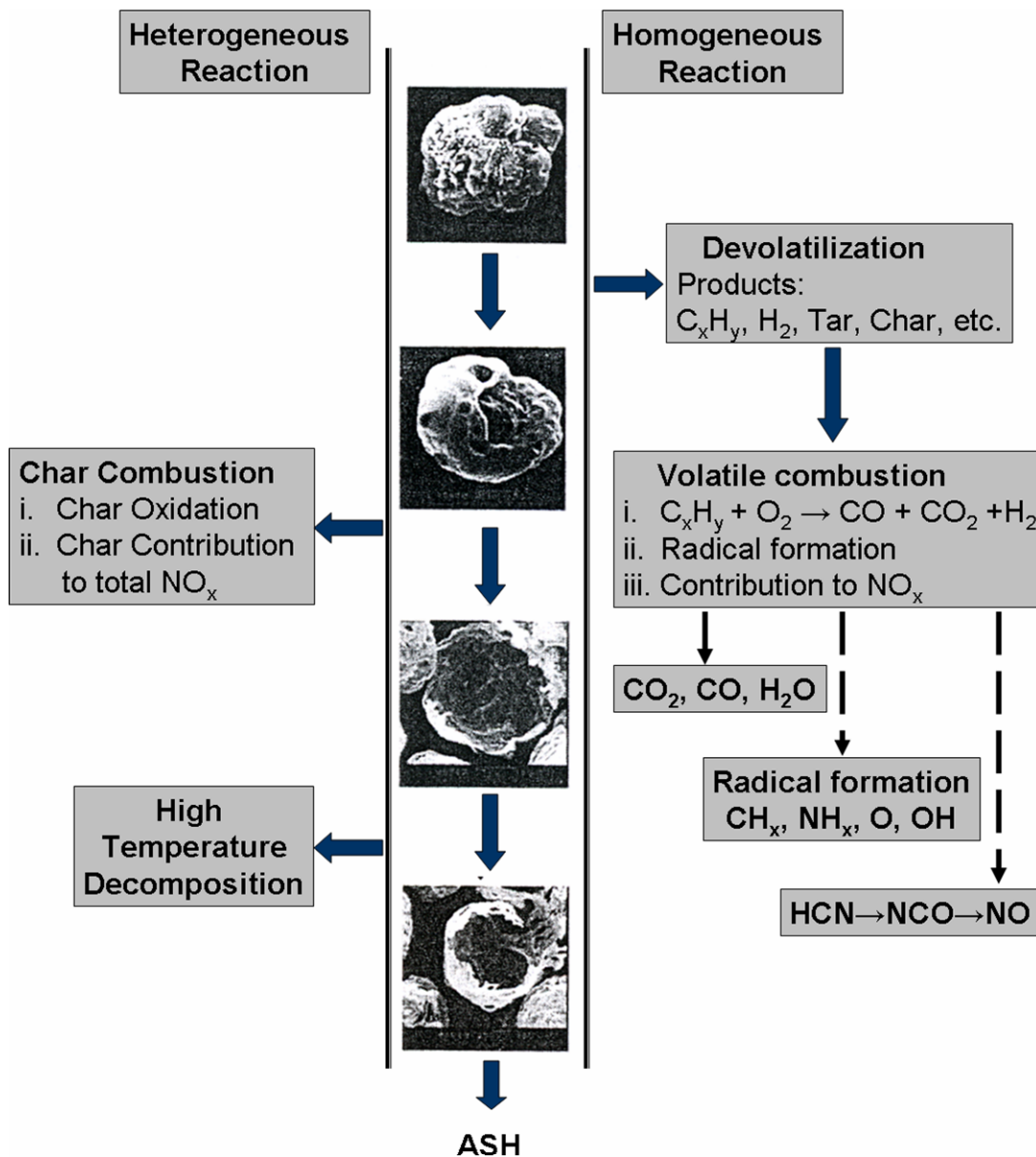


Figure 1.1: Diagram showing the combustion process of a single coal particle. The left-hand side shows the heterogeneous steps, and the homogeneous reactions are shown on the right-hand side.

Coal is generally classified by rank which is a broad measure based on the average carbon content of the particular coal. Within each coal particle there are variations in composition within its constituent macerals, and the mineral matter may vary in type and extent. However, the macerals units are geometrically small, typically 2-5 μm in diameter, so that individual pulverized coal particles are effectively pseudo-homogeneous. Larger coal particles may have a banded structure so that the properties are clearly anisotropic, for instance, they are susceptible to fracture and fragmentation along these bands. Many coal combustion models are linked to an average coal

property, and this is particularly the case with most devolatilization and char combustion models. However, the advent of combustion models based on molecular modeling has opened a vast amount of information for the combustion researchers.

Coal combustion research has often concentrated on understanding combustion behavior in two distinctively different processes, namely, devolatilization and char combustion. Most devolatilization studies have dealt with thermal decomposition in an inert atmosphere, while char studies have used nonvolatile char or carbon particles. This kind of ideal situation may not be encountered in practical applications such as in a furnace. In an oxidizing environment coal particle heat-up and devolatilization can progress simultaneously or sequentially. The complexities involved in the phenomena seem to hinder more direct approaches.

The mathematical equation used to represent the heating-up of particles in pulverized coal models may be truncated and therefore can differ from model to model, with some stressing the influence of radiant flux and others convective heat transfer. In most cases, this will not make a significant difference in theoretical predictions in pulverized coal flames. However, it becomes an important factor with larger particle sizes in fixed or fluidized-bed combustion.

In pulverized coal combustion, numerous studies suggest that devolatilization can result in particle rotation. Theoretical calculations show [*Unsworth et al., Sorensen et al.*] that for an ideal sphere, convective heating-up times (99% final T) are 5 ms for 25 μm particles, 35 ms for 80 μm particles, and 75 ms for 120 μm particles; and for all these particles, the Biot number is such that the internal temperature profile is essentially uniform. However, important factors are the characteristic times for radiation and convection, internal conduction, and the reaction rate in circumstances where gases are starting to emit from the surface. In this case, convective heat transfer is lower than the ideal theoretical case, so that in fact, radiative heating is of paramount importance. Thus, low NO_x burners with lower flame temperatures and a lower radiative flux result in particles being heated at a much lower rate than in "conventional" burners. Likewise, larger particles are heated at rates approximately proportional to the diameter, and the resultant slower and more uneven heating leads to fragmentation. Computational fluid dynamics (CFD) computational methods applied to combustion have made considerable advances over the last few years.

Coal gasification has a wide range of applications that are set out in **Fig. 1.2**. However, one of the main current interests is in the application of gasified product in electricity generation. The conversion of coal to electricity, via such an intermediate gaseous

product stage, can be achieved by employing the integrated gasification combined cycle (IGCC) technology.

The feedstocks include coal, natural gas (for reforming applications) [Geertsema, Morita] refinery residues [Graaf, Pena FG] and biomass/wastes in combination with coal [Hirato et al.], etc. Although the large majority of gasification projects to date are based upon the use of fuels other than coal, much R & D attention has been focused on using coal as the primary feedstock. All coal types can be gasified. However, on economic grounds, low ash content coals are preferred.

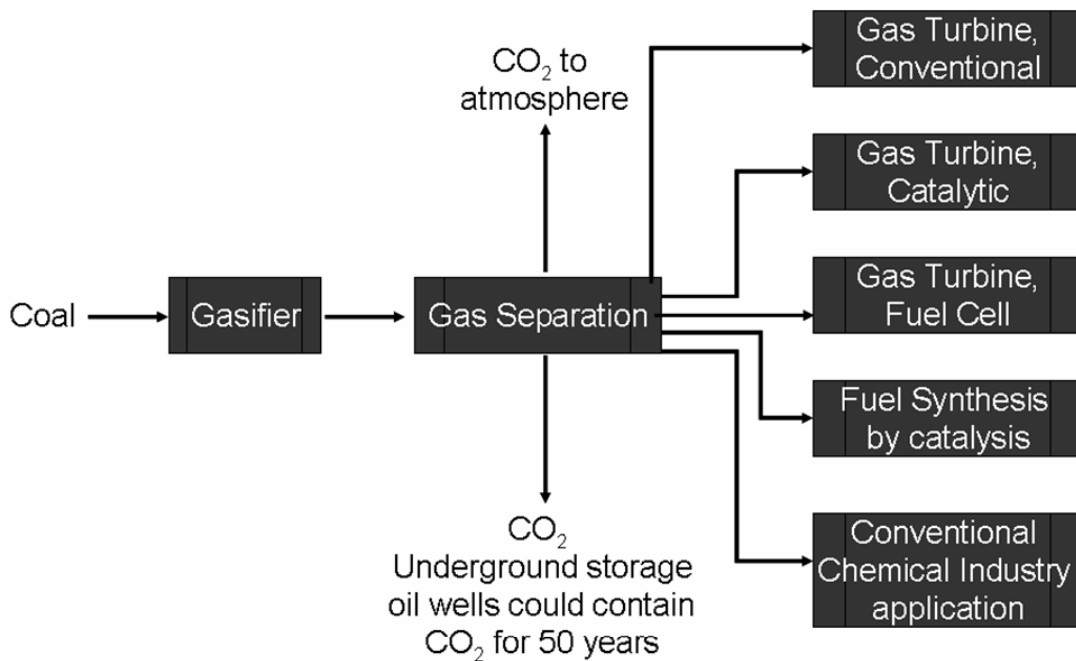


Figure 1.2: Application of gasification and possible future role.

On a worldwide basis, there are some 160 modern, gasification plants in operation and a further 35 at the planning stage. The majority of these plants are located either in Europe or in the USA, of which those plants that either currently are in operation or are planning to produce electricity are shown in **Tables 1.1**.

In the EU, many companies have actively been developing IGCC technology. The following 'commercial' power projects are either in operation or under development.

- *Buggenum, Netherlands*, firing coal only (plus some part biomass trials). This is a 283 MW electric power plant that uses Shell gasification technology. It has been in operation since 1994 [Sendin et al., Ploeg].
- *Puertollano, Spain*, a 335 MW e IGCC demonstration plant firing a 50:50 blend of petroleum coke and coal. The project received a subsidy from European Commission's Thermie program with a grant of 50 million ECUs (~\$60 m). The

project uses a PRENFLO entrained-flow system with dry feeding, supplied by Krupp Uhde [*Schellberg, Schellberg, Green, Mendez et al., Mendes, Elcogas*].

Country	Plant Name	Type	Feedstock	Products	Year
Australia	Whytess gully waste to energy plant	Unknown	Biomass	Electricity	1999
Austria	Zeltweg gasification plant	Unknown	RFD	Electricity	1997
Canada	MSW plant	Thermogenics, Inc.	Biomass	Electricity	2000
Canada	Toronto MSW plant	Thermogenics, Inc.	Municipal waste	Electricity	2000
China	Beijing town gas plant	Texaco	Coal	Town gas and electricity	1995
Czech Rep.	Vresova IGCC plant	Lurgi dry ash	Lignite	Electricity and steam	1996
Finland	Kymijärvi ACFBG plant	FW ACFBG	Biofuels	Electricity and district heat	1998
Germany	Schwarze pumpe town gas plant	Lurgi dry ash	Municipal waste	Electricity and methanol	1964
Germany	Leuna methanol Anlage	Shell	Visbreaker residue	H ₂ , methanol and electricity	1985
Germany	Slurry/oil gasification	Lurgi MPG	Oil and slurry	Electricity and methanol	1968
Germany	Schwarze pumpe power/methanol plant	BGL	Household waste and Bit. coal	Electricity and methanol	1999
Germany	Schwarze pumpe gasification plant	GSP	Municipal waste	Electricity and methanol	1992
Germany	Fondotoce gasification plant	ThermoSelect	MSW	Electricity	1999
India	Sanghi IGCC plant GTI (IGT)	U-GAS	Lignite	Electricity and steam	2002
Italy	Project	Texaco	ROSE asphalt	Electricity, H ₂ and steam	2000
Italy	SARLUX GCC/H ₂ plant	Texaco	Visbreaker residue	Electricity, H ₂ and steam	2001
Netherlands	Pernis Shell gasif. hydrogen plant	Shell	Visbreaker residue	H ₂ and electricity	1997
Netherlands	Buggenum IGCC plant	Shell	Bit. Coal	Electricity	1994
Netherlands	Americentrale fuel gas plant	Lurgi CFB	Demolition wood	Electricity	2000
Singapore	Chawan IGCC plant	Texaco	Residual oil	Electricity, H ₂ and steam	2001
Spain	Puertollano GCC plant	PRENFLO	Coal and petcoke	Electricity	1997
Taiwan	Kaohsiung syngas plant	Texaco	Bitumen	H ₂ , CO and methanol SG	1984
USA	Wabash River Energy Ltd	E-GAS (Destec/Dow)	Petcoke	Electricity	1995
USA	Delaware clean energy Cogen. Project	Texaco	Fluid petcoke	Electricity and steam	2001
USA	Polk County IGCC Project	Texaco	Coal	Electricity	1996
USA	Commercial Demonstration Facility	Brightstar Env. Ltd	Biomass	Electricity	1996
USA	New Bern gasification plant	Chemrec	Black liquor	Electricity	1997
USA	McNeil IGCC Project	Fut. ener. resources	Forest residue	Electricity	1997
U S A	El Dorado IGCC Plant	Texaco	Petcoke, Ref. Waste & Nat. gas	Electricity & HP steam	1996

Table 1.1: Major electricity producing gasification plants by country. **Source:** Derived from the World Gasification Database, US DoE and Gasification Technology Council [*USDoE and Gasification Technology Council*].

- *Shell Pernis Refinery, Netherlands.* This project uses Shell gasification technology to convert vacuum cracked residue and asphalt to electricity. It has a total capacity of 1650 T/d residue and produces 130 MW of electricity [*Graaf*].
- *Sarlux, Italy.* This project gasifies 3424 T/d (3771 short-t/d) of visbreaker residue to produce steam, 550 MW of power, and hydrogen in a Texaco gasifier at the Saras refinery in Sarroch, Cagliari [*Collod*].
- *ISAB, Italy,* uses a Texaco quench gasifier to convert 130 T/h of de-asphalter bottoms from the ISAB refinery in Priolo Gargallo, Siracusa, Sicily, to produce a nominal 510 MW of power [*Collod*].
- *API, Italy.* This project uses a Texaco gasifier to gasify 1335 t/d (1470 short-t/d) of visbreaker residue from the API refinery in Falconara to produce steam and 280 MW of power [*Spence*].

- *Schwarze Pumpe, Germany*, converts a mix of 450, 000 T/annum of solid waste, and 50,000 T/annum of liquid wastes into electricity, steam, and methanol feedstock using four solid-bed gasifiers made by a variety of manufacturers, and firing visbreaker residue [*Buttker et al.*].
- *Sulcis, Italy*, in development for a 450 MW e coal-based power plant using the Shell gasification technology. The plant will be in operation in 2005 [*Cavalli et al.*].
- *Agip, Italy*, in development for use of high-viscous bottom tar from a visbreaking unit and produce clean syngas for a power generation unit, where it will be co-fired with natural gas. The plant will use Shell gasification technology and is planned to be in operation in 2004.
- *Piensa, Spain*, commissioning for 2004/2005 is planned for this IGCC complex that will use refinery heavy stocks to produce 784 MW of net power, hydrogen, sulphur and metals concentrate using Texaco gasification technology [*Ubis et al., Bressan et al.*].

In Europe, for example, the projections suggest that in the EU alone over the period to 2030, some 550 GW of new generation plant will have to be installed, to meet new demand, and to replace ageing power stations. The prevailing view is that the future energy needs of the enlarged EU will be so significant that the full range of available fuels (including renewables, nuclear, natural gas and coal) will have to be utilized to meet the demand. This presents two problems:

1. The new plant that is to be built will itself have a lifetime of about 40 years and so will be operating during the onset of the transition away from oil and gas, and with the associated price increases that will inevitably occur;
2. The scale of operations, costs, and the need for reliability in the new plant, will make it difficult to accommodate the large-scale introduction of new, unproven and essentially small-scale energy technologies such as biomass, wave or tidal power.

Consequently, a very large proportion of this new and replacement plant will have to be coal fired. However, such plant will need to achieve a much higher environmental performance than existing units in order to meet future EU environmental standards. At the same time, if the need to achieve near zero emissions is factored into the deliberations then by, say, 2020 it will be necessary to have available coal fired technologies with integrated CO₂ removal processes. This suggests that the prime need is to ensure that combustion technology can achieve high efficiency with proven

reliability at acceptable capital cost. This thesis is largely concerned with the fundamentals of the processes involved in the combustion and devolatilization of coal and how they can be beneficial in modeling industrial combustors.

1.3 Motivation and Scope of this Work

In few last decades, extensive research has been carried out in development of comprehensive computer models for better performance of coal in many industrial applications. However, the processes occurring during coal combustion and their interaction, especially in devolatilization, are scarcely understood. Although, as mentioned in section 1.1, the ideal situations of either nonvolatile char combustion or devolatilization in an inert atmosphere are inconsistent with practical situation, there has been only few research works in this field. The objective of this work has been to systematically analyze coal devolatilization, the radiation and convection effect over combustion, internal conduction within coal particle, and the reaction rates in circumstances where highly reactive gases are starting to come in contact with coal particle. Special emphasis has been placed on modeling and understanding the physical and chemical processes and their interaction which dominate the burning phenomenon. The modeling concept is similar to that of liquid droplet combustion except that volatiles emitted from the coal particle which has a constant diameter during devolatilization unlike droplet burning. Moreover, the data incongruity existing in estimation of kinetic coefficients for gasification of coke by CO_2 has shown a need to perform experimental investigation.

The thesis is structured into four main parts:

- [1] An analytical study of droplet combustion under microgravity (chapter 2)
- [2] Modeling coal particle behavior under devolatilization (chapter 3)
- [3] Coke gasification in an environment of CO_2 (chapter 4)
- [4] Modeling coal combustion (chapter 5)

In **chapter 2**, an analytical model based on an assumption of combined quasi-steady and transient behavior of the process is presented to exemplify the unsteady, spherically-symmetric single droplet combustion under microgravity. The model based on an alternative approach of describing the droplet combustion as a process where the diffusion of fuel vapor residing inside the region between the droplet surface and the flame interface experiences quasi-steadiness while the diffusion of oxidizer inside the region between the flame interface and the ambient surrounding experiences

unsteadiness. The modeling approach especially focuses on predicting; the variations of droplet and flame diameters with burning time, the effect of vaporization enthalpy on burning behavior, the average burning rates and the effect of change in ambient oxygen concentration on flame structure. The modeling results are compared with a wide range of experimental data available in the literature.

The model described in chapter 2 has also been successfully implemented for devolatilization of a coal particle, where more restrictive assumptions were made. A quasi-steady-transient model has been developed to describe a coal particle undergoing devolatilization. **Chapter 3** presents an in-depth analysis of the principle phenomena occurring in during devolatilization. The modeling concept is similar to that of liquid droplet combustion except that volatiles emitted from the constant diameter coal particle. The model describes the heat and mass transfer mechanisms among the particle, the flame, and the external environment. The volatile diffusive transport has been explained with quasi-steady state behavior unlike unsteady diffusive transport of oxidant.

Various reaction kinetic descriptions have been formulated and have been discriminated for gasification of coke with CO₂ on experimental as well as modeling spectra. The occurrence of data incongruity among kinetics parameters is shown as an indicator for experimental investigation, which is described in **chapter 4**. Extensive experimental work has been carried out to calculate intrinsic and apparent reaction coefficients with a new set of activation energy.

Chapter 5 presents the modeling of single coal particle combustion in atmosphere of O₂. Model is able to qualitatively and quantitatively describe the steady-state behavior of the coal combustion. It includes homogeneous and heterogeneous chemical processes in the gas phase and in the solid phase respectively. Moreover, a mathematical analysis is also described to model a special case of combustion where oxygen concentration (air excess number ≤ 1) is restricted.

Chapter 2

An Analytical Study of Droplet Combustion under Microgravity

2.1 Introduction

One of the main objectives in combustion research is the development of comprehensive computer models to give a better understanding of spray combustion in many practical applications e.g. gas-turbine engine, diesel engine, oil fired boilers, process heater, etc. An isolated droplet combustion study under microgravity conditions serves as an ideal platform in providing a basis for enhancing the existing understanding of burning process, and gives proper explication of the process which is important for economical use of fuels and for reducing the production of pollutants. Microgravity condition is necessary not only for the spherically-symmetric droplet combustion in quiescent atmosphere, but also for the resulting one dimensional solution approach of combustion.

A great number of modeling studies for better understanding of vaporization and combustion of a fuel droplet under microgravity conditions have been reported for nearly five decades. Godsave and Spalding derived the classical d^2 -law, which yields relatively good estimates of the gasification rate. Kumagai et al. successfully performed the first droplet combustion experiments in microgravity conditions to validate d^2 -law. They showed that droplet gasification rate was constant over time which is one of the most important features of d^2 -law. Most of the existing models are based on the assumption of process dynamics: models taking into account the quasi-steady nature of

the process, and models which are based on transient assumption. The quasi-steady character of spherically-symmetric combustion of a droplet has been extensively studied, analytically as well as numerically [Godsmith *et al.*, Kassooy *et al.*, Williams *et al.*, Puri *et al.*, Filho]. Most of these models were reported taking into account the temperature dependence of transport properties, kinetics effects and the transport mechanisms. Puri and Libby proposed a numerical model for steady state droplet combustion with a proper description of gas-phase transport mechanism. Model predictions for gasification rate and flame location showed a good agreement with experimental data. Filho presented an analytical, steady state, droplet combustion model with considerations of temperature dependence of transport coefficients and non-unity Lewis number. Although the model considers temperature dependence of transport coefficients, the results do not have good agreement with the experimental results.

Based on several experimental studies [Kumagai *et al.*, Okajima *et al.*, Hara *et al.*, Choi *et al.*, Yang *et al.*], it was found that the predictions of d^2 -law for flame stand-off ratio are not in accordance with the experimental observations. Experiments have shown that the flame stand-off ratio continues to increase while the gasification rate follows a steady state behavior shortly after the ignition period. However, a better explanation of pure liquid droplet combustion can be given by considering unsteady effects as well. Theoretical studies regarding the unsteadiness of the droplet combustion has been described in detail elsewhere [Law, Cho *et al.*, Marchese *et al.*, Cho *et al.*]. Law and Faeth presented their review papers for detail discussion of fuel droplet combustion. Recently, King briefly reviewed the previous transient droplet combustion literature. The complete modeling of droplet combustion is quite complicated because of the involvement of low temperature auto ignition, radiative heat transfer, complex reaction kinetics, and of non-linear transport/thermophysical properties. As a result, droplet combustion modeling deals with either quasi-steady approach or the transient approach which is more complex and requires a lot of numerical computations.

In this chapter, a mathematical model is presented for single fuel droplet combustion under microgravity conditions. The present mathematical analysis is based on an alternative approach, according to which the simplicity in describing the droplet combustion is based on the fact that this process is controlled by both the quasi-steady behavior for the region between the droplet surface and the flame interface, and the transient behavior for the region between the flame interface and the ambient surrounding. The main purpose of this work is to demonstrate that even simplified quasi-steady transient approach towards droplet combustion yields behavior similar to

the classical droplet combustion. The modeling results of variations of flame diameter and droplet diameter-squared are compared against a variety of experimental data available in the literature for isolated droplet combustion.

2.2 Model Formulation

The mathematical model used to depict the combustion phenomenon of isolated pure fuel droplet under microgravity condition is briefly described here. Consider an isolated spherical droplet of pure fuel, initially at temperature T_0 , immersed in a quiescent environment at temperature T_∞ (**Fig. 2.1**). The liquid droplet is surrounded by fuel vapor that diffuses outward from the droplet surface to the flame interface (region-I) while oxidizer diffuses radially inward from the ambience towards the flame interface (region-II). Modeling was performed using an alternative approach that the diffusive transport of oxygen towards the flame interface is unsteady. In general, it is found that a typical value of air demand for complete combustion of droplet is 14 (kg of air/kg of oil). On this basis, we calculate the diameter of spherical volume of air associated to the fuel droplet with the density of air estimated at an average temperature of ~ 1200 K which is more often in the vicinity of the flame interface (region-II). This comes about 30 times of the droplet diameter, which is less than the distance needed for steady-state profile for the oxygen diffusion. As a consequence, the stored amount of oxygen in this range can not be neglected against the diffusive mass transport. With such a huge amount of oxidizer associated with fuel droplet, the assumption of quasi-steadiness for disappearance of oxygen can not be taken into consideration for the droplet combustion. Thus, a better description of oxygen diffusion in region-II can be accomplished only with an assumption of unsteadiness. The unsteady-state diffusion of oxygen in region-II is similar to the case of diffusion inside semi-infinite bodies, as shown in Fig. 2.1. Moreover, the total amount of liquid residing within region-I is much more than the amount of fuel vapor accumulated in the same region. Therefore, the condition of quasi steadiness for diffusive transport of fuel vapor from the droplet surface to the flame interface exists for region-I.

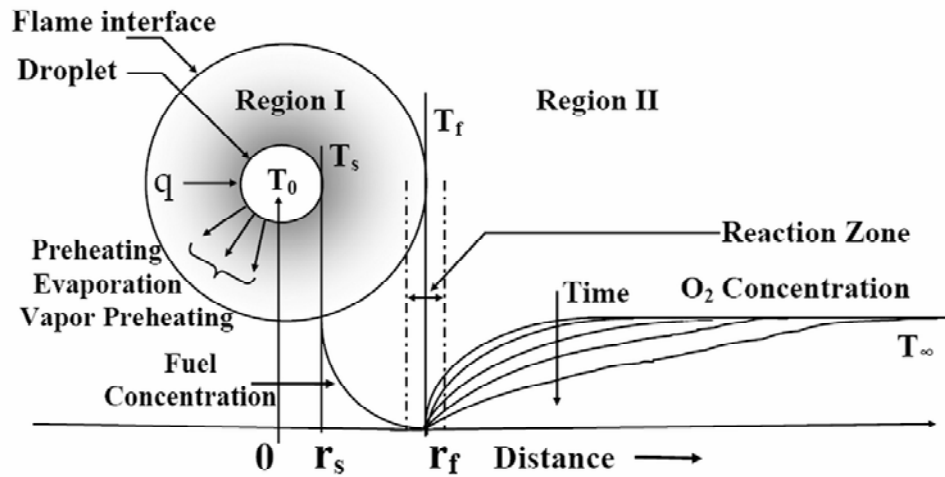


Figure 2.1: Schematic diagram of a droplet combustion process.

This model deals with many assumptions including a few from the classical quasi-steady droplet combustion model, which is described in detail elsewhere [Spalding, Godsave]. The main assumptions are as follows:

- (1) Lewis number in the gas phase is equal to unity;
- (2) all thermophysical properties including the heat of vaporization remain constant with temperature and their average values are taken for computation;
- (3) the combustion products do not affect the process;
- (4) the reaction zone at flame interface is restricted only to a narrow region i.e. infinite-rate kinetics;
- (5) heat loss due to radiation is negligible;
- (6) initially, the droplet is assumed to be at room temperature.

The droplet is considered to be in a quiescent atmosphere, so that all processes in the gas phase will have spherical symmetry. Note that on the basis of different studies [Abramzon *et al.*], it has been found that the Lewis number is not constant and changes during the process of vaporization. Furthermore, because of the existence of high temperature difference between the droplet and the flame interface, the use of average values of the thermophysical properties may cause small errors. Despite the violation of the assumptions of the classical model in many cases, it is widely used in comprehensive modeling of evaporation and combustion process of sprays [Sirignano, Faeth].

2.2.1 Droplet Combustion Time

The mechanism of heat transfer in region-I is quite complicated as it involves the preheating of the droplet, the fuel evaporation and the heating of the fuel vapor diffusing from the droplet surface to the flame interface. The analytical models described earlier did not take into account the heat absorbed by the diffusing fuel vapor. Since the preheating of the droplet depends on time, the combustion process of a droplet initially involves more preheating rather than vaporization. On the basis that the amount of heat absorbed by the fuel vapor is much more than both the heat required for evaporation and the heat necessary for preheating of the droplet, the effect of change of T_0 is neglected. For analytical solution of the problem, the amount of heat required for preheating of the droplet is taken to be constant. Based on the assumption that heat loss due to radiation is zero, the total amount of heat transferred from the flame interface to the droplet surface is used only for these three different kinds of heat consumption.

The total amount of heat transferred due to gas phase conduction between the flame interface and the droplet surface can be calculated analytically by,

$$q = 4\pi\lambda_g \frac{T_f - T_s}{\left(\frac{1}{r_s} - \frac{1}{r_f}\right)} \quad (1a)$$

where q is the amount of heat transferred from the flame interface to the droplet, T_f and T_s are the temperatures at the flame interface and the droplet surface respectively, and r_s and r_f are the values of radius of the droplet and the flame respectively. The value of gas phase thermal conductivity λ_g is averaged between the flame interface and the droplet surface. The heat gained by the vaporizing droplet can be calculated by the following equation,

$$q = M_v \left(cp_l (T_s - T_0) + \Delta H_v + cp_g (T_f - T_s) \right) \quad (1b)$$

where M_v is the mass flow rate of the vapor, ΔH_v the heat of vaporization, T_0 the initial droplet temperature, and cp_l and cp_g the specific heats of the liquid phase and the gas phase respectively. Equation (1b) takes into account the amount of heat required for droplet preheating, vaporization, and heating up the fuel vapor.

The time variant radius of the fuel droplet undergoing combustion can be found from the equation,

$$M_v = \frac{dm_d}{dt} = \rho_l 4\pi r_s^2 \frac{dr_s}{dt} \quad (2)$$

here m_d is the mass of the droplet and ρ_l is the density of the liquid fuel. Total time taken for complete combustion of the droplet can easily be calculated by integrating Eq. (2). The value of vapor mass flow rate can be obtained by considering Eqs. (1a) and (1b). While calculating combustion time using Eq. (2), the value of the ratio of r_s/r_f is excluded from the expression because its value being very less as compared to unity. Further, the integration of Eq. (2) yields,

$$d_t^2 = d_o^2 - Kt \quad (3)$$

where t is the time, d_o the initial droplet diameter, d_t the time dependent droplet diameter, and K the gasification rate. Equation (3) corresponds to behavior similar to the classical d^2 law with a value of gasification rate given by,

$$K = 8 \frac{\lambda_g}{\rho_l} \frac{(T_f - T_s)}{(cp_l(T_s - T_o) + \Delta H_v + cp_g(T_f - T_s))}. \quad (4)$$

2.2.2 Flame Dynamics

The flame dynamics of spherically-symmetric droplet combustion involves a set of conservation equations of species and energy in region-I & II. At liquid-gas interface, the vapor and liquid are assumed to be in equilibrium. The continuous droplet evaporation rate can be calculated by applying Fick's law of diffusion through a hollow sphere (region-I),

$$N_v = \frac{4\pi D_{f,g} P}{RT_{df} (1/r_s - 1/r_f)} \ln \left(1 - \frac{P_{v,s}}{P} \right) \quad (5)$$

$$P_{v,s} = A \exp(-B/T_s) \quad (6)$$

where $P_{v,s}$ denotes the vapor pressure of pure liquid, P the total pressure, R the universal gas constant, T_{df} the average temperature between the droplet surface and the flame interface, $D_{f,g}$ the diffusion coefficient of the fuel vapor, and N_v the molar flow rate of the fuel vapor. The values of constants A and B used to calculate vapor pressure of pure liquid depend on the kind of fuel.

The unsteady mass transfer of oxygen in region-II can be determined by the following equations taken from Carslaw and Jaeger,

$$N_{O_2} = \frac{8\pi D_{O_2}^{3/2} C_\infty}{(\sqrt{\pi} - N_f)} \sqrt{t} \exp(-\eta_f^2) \quad (7)$$

$$\eta_f = \frac{r_f}{2\sqrt{D_{O_2}}} t^{-1/2} \quad (8)$$

$$N_f = \left(\frac{e^{-\eta_f^2}}{\eta_f} \right) + \sqrt{\pi} \operatorname{erf}(\eta_f) \quad (9)$$

where t is the time, C_∞ the concentration of oxygen at infinite distance, D_{O_2} the diffusion coefficient of oxygen, and N_{O_2} the molar flow rate of oxygen.

In the region-II, oxygen is diffusing radially inward towards the flame interface while the fuel vapor (region-I) is transported radially outward from the droplet surface to the flame interface. It is considered that for each unit of fuel consumed, ν units of oxygen are used up. At the flame interface, the stoichiometric relationship between oxygen and fuel can be explained as follows [Turns],

$$N_{O_2} = -\nu N_v \quad (10)$$

where ν is the stoichiometric ratio. The molar flow rates of the fuel vapor (M_v/m^*) and oxygen at the flame interface can be calculated using Eqs. (1a), (1b) and (7); where m^* is the molecular weight of the fuel. But the solution of these equations involves the values of the droplet surface temperature and the flame interface temperature, which are required to calculate the values of physical parameters e.g. diffusivity, vapor pressure, etc. These values of temperature can be calculated by comparing Eqs. (1a), (1b) and (5). Taking into account our assumption of Lewis number equal to unity, we can get the following equation,

$$\left| \ln \left(1 - P_{v,s} / P \right) \left(c p_l (T_s - T_0) + \Delta H_v + c p_g (T_f - T_s) \right) \right| = \left| c p_g (T_f - T_s) \right|. \quad (11)$$

It can be seen from the above equation that the value of T_s remains constant during the burning. The unknown value of flame radius can be calculated by using Eq. (10). Thus, this analytical model is also capable of estimating the variations of both the droplet radius and the flame radius with time via Eqs. (3) and (10) respectively.

2.3 Simulation Results

The model described in the previous sections was applied to study the spherically symmetric combustion process of a single pure fuel droplet in quiescent environment. Simulation were carried out to generate a set of data consisting of; the variations of droplet diameter and flame diameter with time, the gasification rate, the effect of vaporization enthalpy on burning behavior, the variations of flame stand-off ratio with time and the effect of the ambient oxygen concentration on flame structure. A time

interval of 0.05 sec was used to solve the system of nonlinear algebraic equations of the model on discrete basis. The physical properties of the liquid and gas are taken from Reid et al. and Perry and Green. Simulation predictions for two fuels i.e. n-heptane and ethanol, are compared with experimental data available in several literature sources.

2.3.1 Droplet and Flame Structure Characteristics

Figure 2.2 compares the model predictions with the experimental data of Kumagai et al. for n-heptane droplets of different diameters. The model predicts a value of 356 K for n-heptane droplet surface temperature. The model predictions are in good agreement with experimental measurements for both droplet and flame diameters as functions of burning time, even though the model slightly overestimates the values of flame diameter during the early period of burning, and the flame diameter decreases substantially over droplet burning time henceforth. It is readily seen from these plots that as the droplet diameter increases, the flame diameter also increases since the flame diameter depends primarily on the evaporated mass of fuel droplet, and secondarily on the diffusion process. Results shown in Fig. 2.2 neglect the influence of radiation because the small droplet sizes with respect to volume of gases result in small view factor so the influence of radiative heat loss can be neglected. Although the model predictions yield the total time of complete droplet burning that is less than the experimental measurements for droplets with diameters of 0.836 mm and 0.92 mm, it predicts well for higher diameter droplet of 0.98 mm. This behavior is believed to be caused by the constant higher values of gasification rate, which is independent of initial droplet diameters. Nonetheless, the model appears to give a good description of the data in terms of the general trend of d^2-t curve.

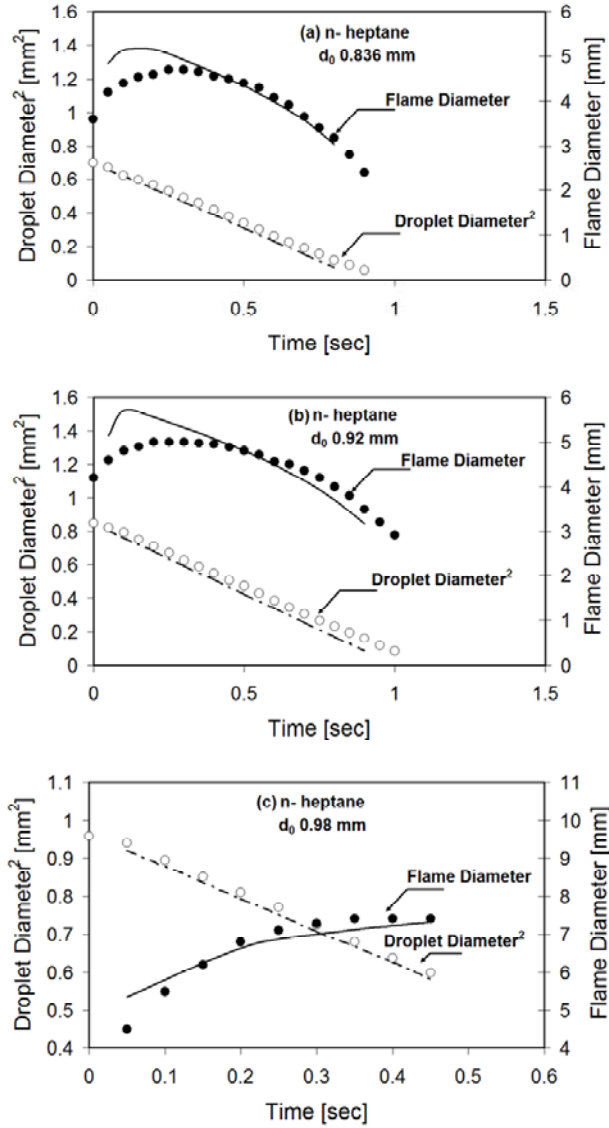


Figure 2.2: Comparison between experimental [Kumagai *et al.*] (points) and predicted (lines) data of the droplet diameter and the flame diameter variations with time. Initial conditions: n-heptane; drop diameters, (a) 0.836 mm, (b) 0.92 mm, (c) 0.98 mm; ambient temperature, 298 K; atmosphere, air at 1 atm pressure.

Figure 2.3 compares the simulation results with the experimental data of Kumagai *et al.* for ethanol droplet at atmospheric pressure. The agreement between the simulation results and experimental results is excellent. However, the model slightly overestimates the values of flame diameter during the early period of burning, and the flame diameter decreases substantially over droplet burning time henceforth. The classical trends of flame dynamics and droplet combustion can easily be seen for the case of ethanol as well.

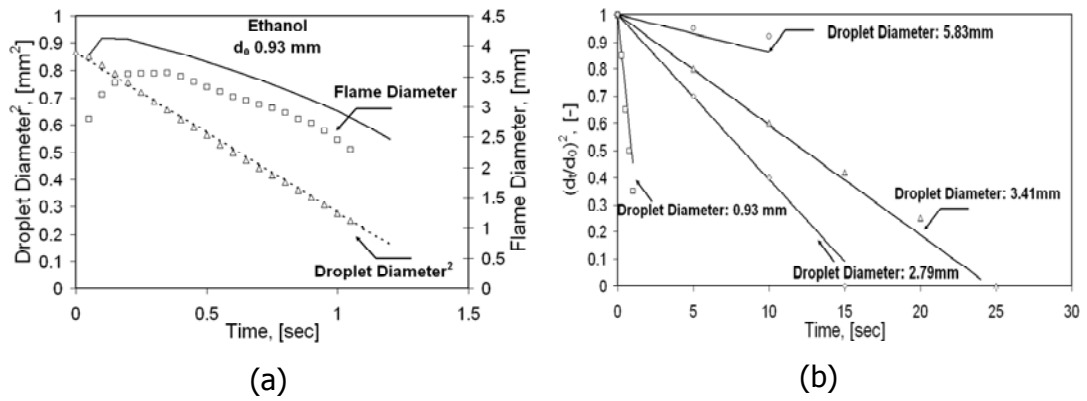


Figure 2.3: Comparison between experimental [Kumagai *et al.*] (points) and predicted (lines) data of the droplet diameter and the flame diameter variations with time. Initial conditions: ethanol; (a) droplet diameter, 0.93 mm; ambient temperature, 298 K; atmosphere, air at 1 atm pressure; (b) droplet diameter, 0.93 mm, 2.79 mm, 3.41 mm, 5.83 mm; ambient temperature, 298 K; atmosphere, air at 1 atm pressure;

2.3.2 Estimation of Gasification Rate

Figure 2.4 shows comparison of model predictions with the experimental results obtained by Kumagai *et al.* [Okajima, *et al.*, Hara *et al.*] for the evolution of gasification rate for n-heptane and ethanol droplets of different sizes. A constant value $0.84 \text{ mm}^2 \cdot \text{s}^{-1}$ for gasification rate of the n-heptane droplets was found. As shown in Fig. 2.4, the possible reason for the discrepancy of the model predictions from the experimental measurements is that the model predicts the gasification rates with an assumption that the flame interface temperature equals the adiabatic flame temperature. However, under real experimental conditions an amount of heat transferred from flame interface to the ambient surroundings might cause the flame temperature to attain a value lesser than the adiabatic flame temperature. Results of model predictions of the gasification rate for the ethanol droplets are in good agreement with experimental data. Model predicts a constant value $0.58 \text{ mm}^2 \cdot \text{s}^{-1}$ for the gasification rate for the ethanol droplets of different sizes. Figure 2.4 also shows the predictions of the models of Puri and Libby and Filho for the ethanol droplets. Model predictions match with those predicted by Puri and Libby.

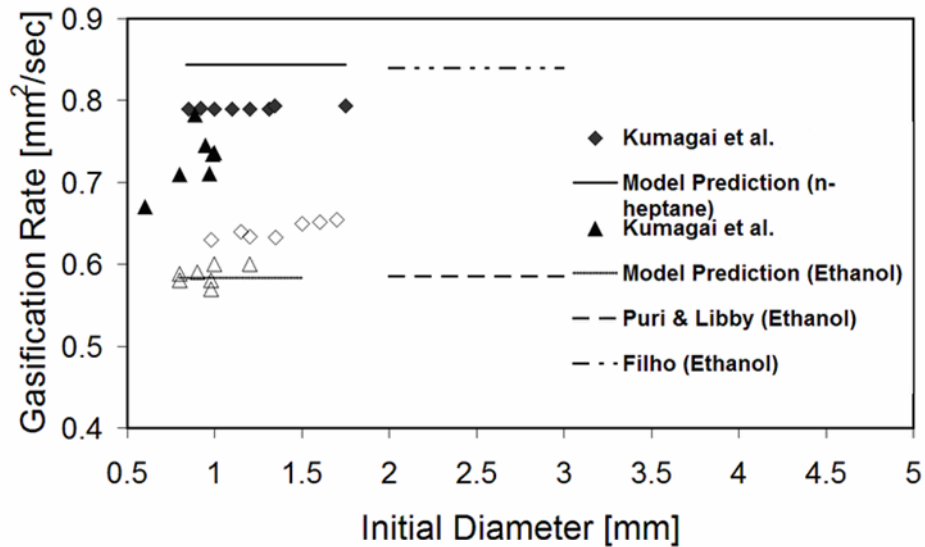


Figure 2.4: Comparison of calculated gasification rate (solid lines) with the experimental results (points) of Kumagai et al. and the model predictions (dotted lines) of Puri and Filho. Points: solid points for n-heptane; empty points for ethanol.

2.3.3 Influence of Vaporization Enthalpy on Burning Behavior

Figure 2.5 presents the variation of droplet diameter-squared with time for the n-heptane and ethanol droplets burned in air at pressure of 1 atm. The heat of evaporation of ethanol is more than the vaporization enthalpy of n-heptane. For the 0.93 mm initial diameter ethanol droplet the model predictions are in good agreement with the experiments while in the case of n-heptane with an initial diameter of 0.92 mm the model predicts a complete burnout of the droplet earlier than experimental observation, as discussed previously. On the basis of comparison between the model predictions for these two liquids, it should be noted that the results show the effect of change of vaporization enthalpy over burning behavior.

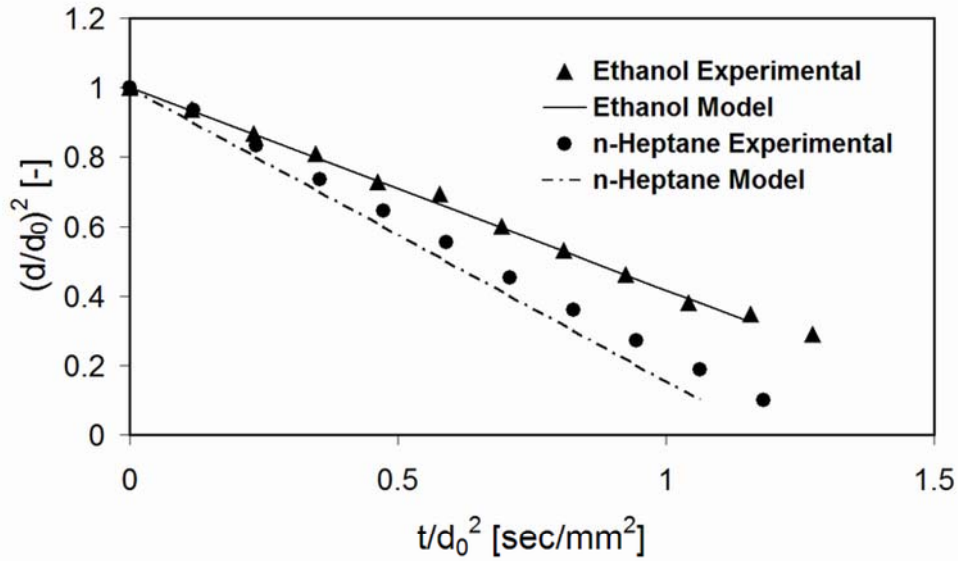


Figure 2.5: Calculated and measured droplet diameter-squared of Kumagai *et al.* for n-heptane and ethanol droplets in an air at 1 atm. Initial droplet diameter: n-heptane- 0.92 mm; ethanol- 0.93 mm.

2.3.4. Flame Stand-off Ratio

Figure 2.6 compares the model predictions for flame stand-off ratio with experimental data of Kumagai et al. for the n-heptane droplets with initial diameters of 0.836 mm and 0.92 mm.

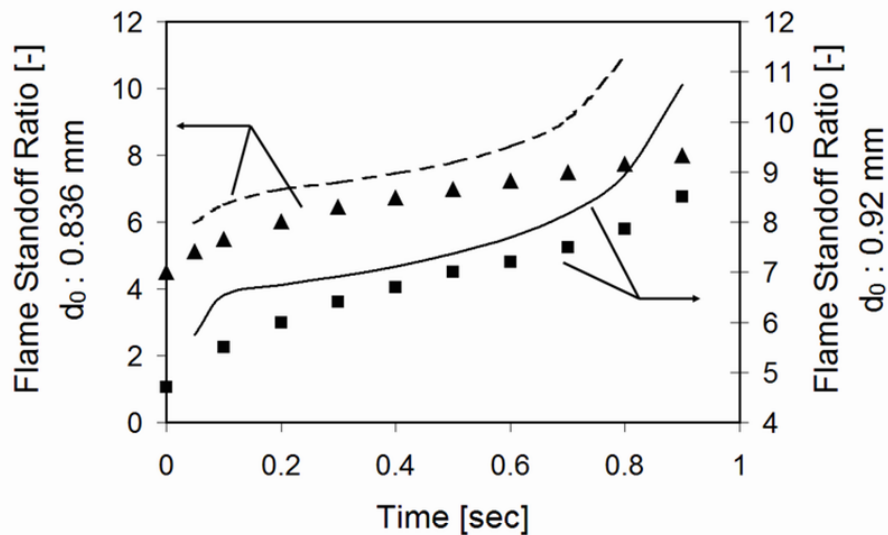


Figure 2.6: Variation in flame stand-off ratio for the n-heptane droplets with time. Comparison between experimental [11] (points) and predicted (lines) data for n-heptane droplets burning in atmospheric pressure air.

Although the flame extinction occurs earlier than the experimental observations, the model predictions show qualitatively similar behavior to the experiments. However, the

flame stand-off ratio increases continuously for both diameters until burn-out and there is no evidence of its constant values for any finite time interval during burning. Thus, the model predictions support the unsteadiness of the droplet burning.

2.3.5 Influence of Ambient Oxygen Concentration on Flame Structure

Figure 2.7 describes the variations of flame diameter with burning time for different ambient oxygen concentrations for the n-heptane droplets having initial droplet diameter of 0.836 mm. Maximum flame diameter in 21% oxygen concentration is 5.15 mm while it reduces to 4.33 mm at 30% oxygen concentration. Model Eq. 7 accounts for this reason with involvement of ambient oxygen concentration C_{∞} . The classical d^2 -law also demonstrates the influence of ambient oxygen concentration on the flame diameter. For low concentration of ambient oxygen, the large quantity of fuel vapor accumulated near the droplet surface will create a flame front at a distance far away from the droplet surface. However, an increase in oxygen concentration reduces the flame front location significantly.

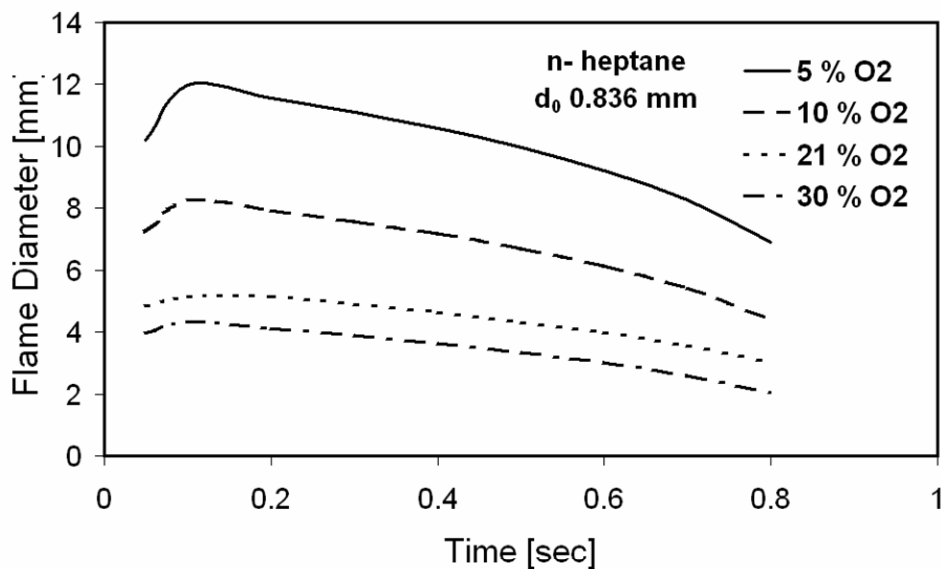


Figure 2.7: Calculated variations in flame diameter with time for various oxygen concentrations for 0.836 mm n-heptane droplets.

2.4 Concluding Remark

An analytical, spherically-symmetric model of an isolated droplet in microgravity, taking into account both the quasi-steady and the transient behavior of droplet combustion, has

been described here. In this study, the consideration of unsteady behavior of oxidizer diffusion in addition to quasi steadiness for fuel vapor diffusion yields good estimations for various droplet combustion characteristics such as droplet diameter-squared, flame diameter, flame stand-off ratio, gasification rate and influence of ambient oxygen concentration on flame structure. The analytical formulae are derived for heat and mass fluxes in the vicinity of evaporating droplet. The comparisons of modeling results with experimental data available in literature demonstrate the validity of the model. Although the model predicts the little bit higher values of flame diameter for n-heptane, the classical trend of flame diameter to increase and decrease from its maximum value with burning time is observed. Furthermore, the behavior of d^2-t curve is similar with experimental observations for both n-heptane and ethanol. Although the model calculates $\sim 7\%$ higher value of gasification rate for n-heptane, it is shown that the predicted burning rates for both fuels are consistent with the reported measurements for small droplet sizes with no radiation effect. Finally, the effect of ambient oxygen concentration on flame structure is well described by the model. The presented analytical quasi-steady transient model is sufficient enough to describe the fundamental characteristics of single droplet combustion. However, the assumption of quasi-steady behavior for fuel vapor diffusion and transient behavior for oxygen diffusion serves as a basis for subsequent development of analytical models to accommodate the effects of radiation, non-unity Lewis number and possibility of different chemical reactions during the combustion process. In the following chapter, the successful implementation of droplet combustion model under micro-gravity to the process of devolatilization of coal is elaborated in detail.

Chapter 3

Modeling Coal Particle Behavior under Devolatilization

3.1 Introduction

For the proper understanding of fixed and fluidized-bed coal combustors and gasifiers, it is necessary to have the detailed knowledge of the devolatilization and combustion characteristics of coal particles. Both of these properties are involved functions of the nature of coal, particle size, temperature, pressure, heating rates, environmental conditions (inert, oxidizing or reducing) etc. The decomposition products of coal obtained on heating depend upon the rank of coal [*Idris*]. Coal contains certain occluded gases such as carbon dioxide, hydrocarbons and water. On heating the occluded carbon dioxide and hydrocarbons are first driven off, and their removal is almost complete at higher temperature. Chukhanov *et al.* proposes that coal devolatilization takes place in three stages. Carbon oxides and water evolve first, hydrocarbon gases and tar are formed next, and lastly the residue degasifies. Suuberg *et al.* from their work on lignite have suggested that coal devolatilization involves five principal phases. The first phase is associated with moisture evolution. The second phase begins with a large initial evolution of carbon dioxide and a small amount of tar. The third phase involves evolution of chemically formed water and carbon dioxide as the other significant product. The fourth phase involves a final rapid evolution of carbon-containing species such as carbon oxides, tar, hydrogen, and hydrocarbon gases. The fifth phase is the high temperature formation of carbon oxides.

It is well known that increasing the heating rate and final temperature of a particle increases the yield of volatiles from a coal particle [Solomon *et al.*, Kobayashi *et al.*]. From a practical point of view, shorter residence times facilitate the construction of smaller combustors, if only the coal particle can release more volatile matter for homogeneous combustion in the gas phase. Knowledge of the combustion of single particles over a wide range of temperatures and oxygen concentrations is useful in optimizing combustion. Devolatilization is assumed to occur in a thin reaction zone located initially at the surface of the particle and then moving inward toward the center, leaving behind a porous matrix containing fixed carbon and a component of the volatile matter which is relatively slow to evolve [Howard *et al.*]. It is generally assumed that devolatilization and char combustion are successive processes. In an actual system devolatilization and combustion phenomena may interact with each other and thereby may further complicate the capability with which predictions for such systems can be made. Char oxidation may occur simultaneously, if oxygen reaches the particle's surface during devolatilization [Howard *et al.*, Midkiff *et al.*, Saito *et al.*, Gururajan *et al.*, Saastamoinen *et al.*]. In the thin-flame sheet model [Howard *et al.*, Gururajan *et al.*, Saastamoinen *et al.*, Jost *et al.*, Beck *et al.*, Lau *et al.*] oxidizer from the surroundings is not present between the flame sheet and the solid, when the rate of devolatilization is high enough to move the reaction zone away from the particle. In furnace calculations it is commonly assumed that char combustion can only start after devolatilization has ended. The char combustion rates are also usually calculated from a quasi-steady model. Then the temperature of the char particle is calculated from an equilibrium heat balance.

Various qualitative features of devolatilization of different types of coals are described in the literature [Saxena] as well as various mechanisms, phenomenological and chemical models. Single and multi reaction models are also being a topic of discussion in relation to the kinetic expressions for the pyrolysis reactions. Depending on the availability of the oxygen supply, the combustible volatiles react and subsequently release combustion energy. This energy may in turn contribute to the heat up of the particle and enhance volatile release rate, which is known as a strong function of particle temperature. A better explication of coal devolatilization theorizes that much amount of heat released during combustion at flame front is used to heat up the volatile vapor existing in between the region particle surface and flame interface. The conventional method to determine the location of flame front involves a vast computation to solve a number of transient differential equations of mass and energy balances [Sangmin *et al.*, Weibiao *et*

al., Annamalai et al., Veras et al.]. Till date there is no existing analytical model to determine the value of flame radius around the particle.

In this chapter, a mathematical model is presented for devolatilization of a single coal particle. Dynamics of devolatilization of a coal particle is almost similar to droplet combustion under microgravity conditions. However, a change in diameter for devolatilization of coal is restricted to exist.

3.2 Single Coal Particle Devolatilization Modeling

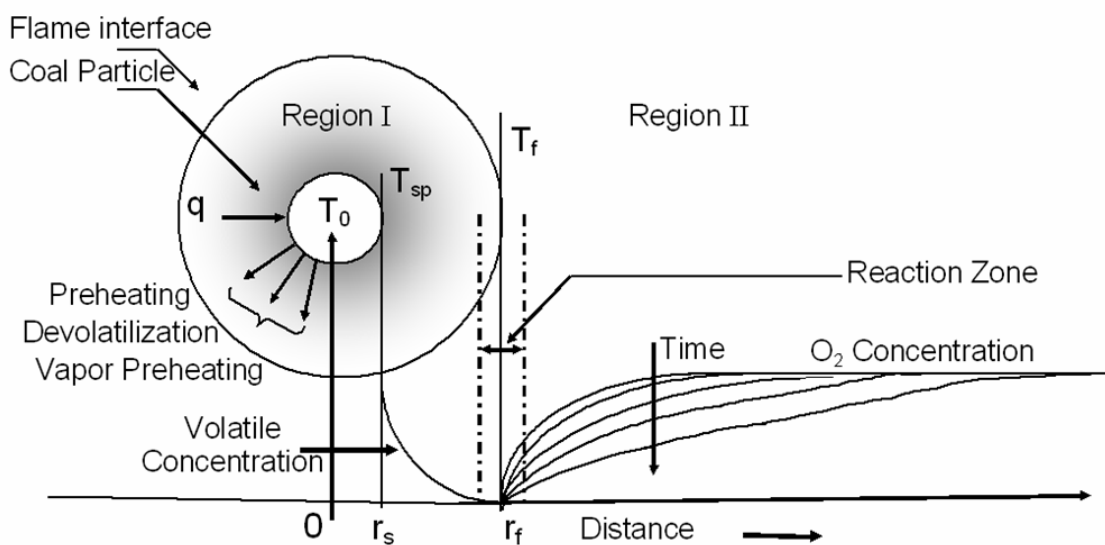


Figure 3.1: Schematic diagram of a single coal particle devolatilization process.

Consider a spherical coal particle, initially at temperature T_0 (**Fig. 3.1**). When it gets heat, the volatile matter present inside the particle starts to come out. The volatile matters diffuses outward from the particle's surface to the flame interface (region-I) while oxidizer diffuses radially inward from the ambience towards the flame interface (region-II). To model the devolatilization of a single coal particle, we need to rearrange a few of terms in previously defined model for the single droplet combustion. Modeling was performed using similar approach that the diffusive transport of oxygen towards the flame interface is unsteady while diffusion of volatile matters outward is quasi-steady state process. In the case of coal devolatilization the particle doesn't shrink like droplet does due to evaporation of liquid fuel. The rate of devolatilization i.e. mass flow rate of volatiles can be calculated using the equation that is similar to Arrhenius

equation where kinetic parameters depend on the type of the coal. Many devolatilization models for coal have been reported till date. However, they cannot be universally applied, since the kinetics parameters used for devolatilization of coal depend on coal type. The simplest description of the kinetics of the devolatilization is to use a first order reaction for total weight loss of the volatiles;

$$\frac{dv}{dt} = (v_{\infty} - v) \cdot K_{v0} \cdot \exp\left(-\frac{E_v}{RT_{sp}}\right) \quad (1)$$

Here v is the total of volatiles evolved up to time t , v_{∞} represents the ultimate yield of volatiles at $t = \infty$ and it is also equal to the total volatile content of coal, T_{sp} is the particle's surface temperature, K_{v0} , E_v are pre-exponential factor and activation energy respectively and R is the universal gas constant. A few of numeric values of K_{v0} , E_v are given below;

Model Type: Single Overall Reaction,

Reaction Science: Coal \rightarrow volatile + char,

Rate Expression:
$$\frac{dv}{dt} = (v_{\infty} - v) \cdot K_{v0} \cdot \exp\left(-\frac{E_v}{RT_{sp}}\right),$$

Kinetic Parameters: $K_{v0} = 5.5 \times 10^5$, $E_v = 78.7 \text{kJ} \cdot \text{mol}^{-1}$, [*Goldberg and Essenhigh*]

$K_{v0} = 1.34 \times 10^5$, $E_v = 74 \text{kJ} \cdot \text{mol}^{-1}$. [*Badzioch and Hawksley*]

The values of K_{v0} , E_v , and v_{∞} are determined experimentally. Details of the different experimental methods are discussed by Anthony and Howard. It is important to point out that in order to obtain accurate kinetic parameters, the experiments must be designed so that the transport limitations are negligible.

Similar to the droplet model, the region between the coal particle surface and the ambience is divided in two sections i.e. the region between the particle surface and flame interface; the region between the flame interface and ambience. The main assumptions are more or less same of the case of droplet combustion those are as following:

- (1) all thermophysical properties including the heat of vaporization remain constant with temperature and their average values are taken for computation;
- (2) the combustion products do not affect the process;
- (3) the reaction zone at flame interface is restricted only to a narrow region i.e. infinite-rate kinetics;

- (4) heat loss due to radiation is negligible;
- (5) initially, the coal particle is assumed to be at room temperature.

From the energy balance between the flame interface and particle surface can be formulated in the following which is heat balance over hollow sphere;

$$q_{f-p} = 4\pi\lambda_g \frac{T_f - T_{sp}}{\left(\frac{1}{r_{sp}} - \frac{1}{r_f}\right)} \quad (2)$$

where q_{f-p} is the amount of heat transferred from the flame interface to the particle surface, λ_g is the thermal conductivity, T_f and T_{sp} are the temperatures of flame interface and particle surface respectively, r_{sp} and r_f are the radius of particle and flame respectively.

The amount of heat taken by the particle is used for; vaporization of volatiles matters, preheating of the volatile vapor in the region between the particle and flame interface and heating of the solid particle. The term responsible for heating of solid particle is new compared to our previous model. Heat consumption can be described mathematically by the following;

$$q_{f-p} = \rho_v \cdot \frac{dv}{dt} \cdot (\Delta H_v + cp_g (T_f - T_{sp})) + m_p \cdot c_p \cdot \frac{dT_{sp}}{dt} \quad (3)$$

where ρ_v is the density of volatile vapor, $\frac{dv}{dt}$ is the rate of devolatilization, ΔH_v is the devolatilization enthalpy, cp_g is the specific heat capacity of the gas, m_p is the mass of the particle, c_p is the specific heat capacity of the coal particle and t is the time. In the equation 3, the heat loss due to radiation is excluded from the analysis. The reason is that in order to calculate the radiative heat loss, we need a value of ambient temperature which can not be generalized for all combustion processes. For example; in case of boiler vessels, a value of ambient temperature can be ~ 300 K while in the case of rotary kilns, this value increases to ~ 1200 K. Consequently, the introduction of radiation term in Eq. 3 makes the mathematical analysis more complicated. Hence, the radiative loss is excluded from this study.

In devolatilization, coal particles are heated to convert most of the organic coal mass, hydrogen, oxygen, nitrogen, and sulfur into gases. Volatiles consist of permanent gases with high heating value, light oils suitable as fuels, and high-boiling tars for subsequent refining. Tar is a mixture of aromatic compounds of molecular weights from 100 to more than 1000 whose chemical structure closely resembles that of the parent coal. A model, similar to Equilibrium Flash Distillation, for the rapid devolatilization of individual coal particles is developed by analogy with a single-stage equilibrium flash distillation

[Stephen]. There exists equilibrium between the liquid phase and the gas phase. A crude correlation for the vapor pressure of high molecular weight condensed-ring aromatics with aliphatic side chains has been suggested by Unger [Unger *et al.*]. The equilibrium existing in between the liquid phase and the gas phase can be described by a correlation given by Unger;

$$P = 5756 \cdot \exp\left(-\frac{255M^{0.586}}{T_{sp}}\right) \quad (4)$$

where M is the molecular weight of the species, P is total pressure and T is the temperature (K). The molar rate of devolatilization N_v can be described by the Eq. 1.

Volatile matters coming from the particle diffuse from its surface toward the flame interface, the rate of diffusion can be expressed mathematically using Fick's law of diffusion;

$$N_v = \frac{4\pi D_{fv} P}{RT_{sf} \left(\frac{1}{r_{sp}} - \frac{1}{r_f}\right)} \cdot \ln\left(1 - \frac{P_{sv}}{P}\right) \quad (5)$$

where D_{fv} is the diffusivity of volatile matter, T_{sf} is the average temperature between the particle and flame interface and P_{sv} is the saturation pressure at the surface temperature of the particle.

The un-steady state diffusion of oxygen from the ambience toward the flame interface is analogous to the case of the droplet and can be expressed as;

$$N_{O_2} = \frac{8\pi D_{O_2}^{3/2} C_\infty}{(\sqrt{\pi} - N_f)} \cdot \sqrt{t} \cdot \exp(-n_f^2) \quad (6)$$

$$\eta_f = \frac{r_f}{2\sqrt{D_{O_2}}} t^{-1/2} \quad (7)$$

$$N_f = \left(\frac{e^{-\eta_f^2}}{\eta_f}\right) + \sqrt{\pi} \operatorname{erf}(\eta_f) \quad (8)$$

$$N_{O_2} = -\nu N_v \quad (9)$$

3.3 Simulation Results

Model consists of a number of coupled algebraic as well as differential equations. A solution strategy is proposed as follows. The unknown value of particle surface temperature can be obtained using Eqs. (1) and (5) where a value of the flame

temperature can be taken equal to adiabatic temperature of the flame. While calculating the value of surface temperature, the value of $\frac{1}{r_f}$ is taken approximately 0 because this value is less compared to $\frac{1}{r_{sp}}$ and can be neglected. With calculated value of the surface temperature of the particle, the total time taken to evaporate 10% of the volatile content present in the particle can be obtained using Eq. (1). Flame radius around the particle can be obtained using Eqs. (5), (6) and (9). A comparison of Eq. (2) with Eq. (3) can be used to determine a new value of the surface temperature of the particle. Furthermore, a set of new values of particle surface temperature, flame radius and amount of volatile content can be generated till the pre-assumed amount of the volatile content inside the particle doesn't evaporate. Simulation results are generated for the particles with different radius. The results mainly consist of discussion over surface temperature variation and flame dynamics with time.

3.3.1 Particle's Surface Temperature

Figure 3.2 describes the variation of the surface temperature of the particle with time for a particle radius of 10mm with changing volatile concentration inside the particle from 10 to 50%. It is shown by simulation results that the temperature of the particle goes on increasing with time which was expected because of loss of volatile matters and utilization of heat coming from the exothermic reaction at the flame interface to heat the particle. It can be seen from the Fig. 3.2, an increase in the amount of volatile matter inside the particle increases the maximum value of temperature attain by the particle. For lower values of volatile matter concentration inside the particle, the particle attains a lesser value than the required value needed for the combustion of the particle. Simulation results fit qualitatively to the expected behavior of the particle. Model can describe qualitatively why it is difficult to ignite anthracite coal in cold wall furnace? The reason is the less amount of volatile matter inside the particle. Consequently, the particle is not able to reach a surface temperature value required for the combustion. Anthracite coal can only be ignited in the furnace which has its wall at higher temperature so that the particle can get enough heat from the walls and get ignited.

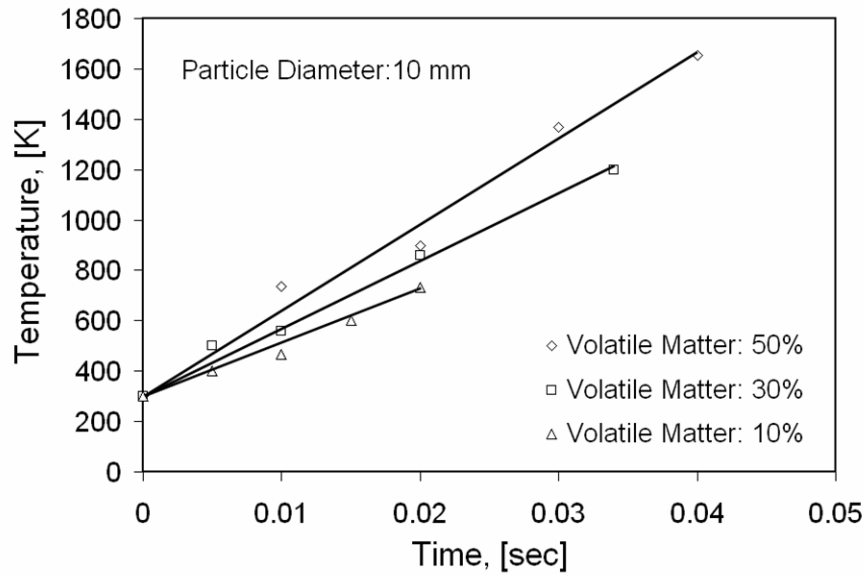


Figure 3.2: Calculated variations in surface temperature of the particle with time: particle diameter: 10mm; volatile matter content: 10, 30 and 50%.

3.3.2. Flame Dynamics

Figure 3.3 illustrates variations of the ratio of the diameter of flame to particle with time for particle radius of 1, 5 and 10 mm. For all particle radiuses, it has been found that flame radius decreases with time. This trend of flame radius variation to decrease from its maximum value in the beginning to its minimum is due to expected decrease of volatile content in the particle. Due to non-availability of experimental results for the flame radius for a coal particle, the simulation results can not be compared with any experimental result in the literature. However, from the practical experience it's found the value of flame radius decreases with the radius of the particle and especially for smaller particle diameter e.g. pulverized coal; it is restricted to the particle surface only. From the Fig. 3.3, it can easily be seen that for a particle radius 1 mm, the maximum value of diameter ratio is approximately 2 which goes to ~ 1 at the end. It has also been shown by Gurgel *et al.* that the diameter ratio value can have a value in the range of 2 to 8.

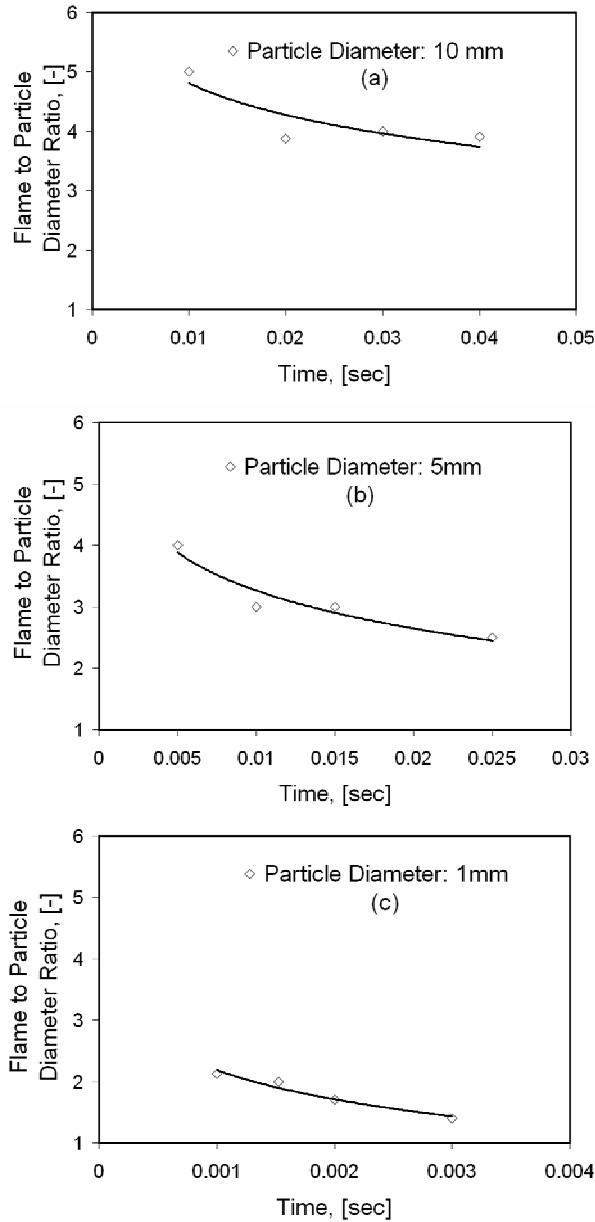


Figure 3.3: Profile of flame to particle diameter ratio for an amount of volatile matter of 50%: particle diameter: (a) 10 mm, (b) 5mm and (c) 10mm.

3.4 Concluding Remark

Analogical approach, based on the modeling of the liquid droplet combustion, to model the coal devolatilization is found to give a better reproduction of the dynamics of the process. The analytical model to describe the devolatilization of a coal particle consists of a few more restrictive assumptions compared to the droplet combustion. The inheritance between the solid coal particle devolatilization and sphero-symmetric droplet combustion in microgravity has been shown to be successfully implemented. Though

model predictions are not compared with the experimental data due to non-availability in the literature, the qualitative analysis gives a good explanation of the process dynamics. The temperature of the particle keeps on increasing till the entire volatile matter lasts before the combustion starts. Model predictions show that during the devolatilization the particle temperature increase to a value which is required for the combustion to take place. It has also shown by model predictions that with an increase in amount of volatile matter inside the particle, it is possible to ignite the coal particle easily. Model can successfully give the reason why it is difficult to ignite anthracite coal inside the furnace with no external heating. The reason is the less amount of volatile matter in anthracite coal which is incapable to take the particle to a temperature value which is needed for the ignition. The flame radius increases with an increase in particle radius. The values of flame radius calculated using the presented model are in the range of the values described by Gurgel *et al.* for the modeling of devolatilization of small coal particles. The process parameters e.g. amount of volatile matter, kinetic parameters for devolatilization, etc. used in modeling can not be generalize as these values are dependent on the type of the coal used for simulation purpose.

Chapter 4

Coke Gasification in an Environment of CO₂

4.1 Introduction

Gasification has emerged as a clean and effective way for the production of gas which can be used for power or heat generation or as a synthesis precursor. A good understanding of the char reactivity makes it possible to improve gasifier design and efficiency. A distinction of the factors affecting the gasification process can be made on according to whether they are only related to the intrinsic chemical characteristics of the specimen, or if they can be related to the physical structure of the specimen or to the environment in which it goes through the chemical reactions. Reactivity of coke gasification with CO₂ has extensively been studied in this section. The reaction between C and CO₂ known as Boudouard reaction ($C + CO_2 \rightarrow 2CO$) has always been a subject of study because of its scientific as well as technological importance. Being highly endothermic and consuming carbon directly from the coke in many metallurgical and industrial processes, this reaction has gained much importance. For example, the blast furnace process to reduce iron ore [*Grabke et al.*, *Cheng et al.*], the cupola furnace process for melting iron scrap, the shaft kiln process to produce lime and dolomite ($CaCO_3 \rightarrow CaO + CO_2$), the production process of manganese and chromium alloy [*Kaczorowski et al.*], the production of micro-porous materials of valuable properties from carbonaceous surfaces [*Montoya et al.*], etc. Modeling of a process involving the influence of Boudouard reaction can not be described mathematically without

knowledge of reaction kinetic parameters and their dependence on type of coke. For example; in metallurgy industry, the equilibrium relationship [curve (1)] of Boudouard reaction to reduce iron ore can be better expressed by **Fig. 4.1**.

When the concentration of CO is below this curve (1), the reaction proceeds in the direction for forming CO, this being called the carbon solution reaction or solution-loss reaction. In the neighborhood of 1200 K, CO₂ that has been formed by the reduction of iron oxide is changed into CO by Boudouard reaction. Consequently, the gas concentration of CO in this region goes above curve (1) and a carbon deposition reaction occurs according to equilibrium theory; that is, CO is dissociated into CO₂ and carbon, and carbon is deposited. However, due to its extremely slow speed, this reaction does not practically proceed at lower temperatures and low CO concentrations. Carbon deposition actually occurs in the region where metallic iron coexists to provide strong catalytic action, and in the region of higher temperature and high CO concentration.

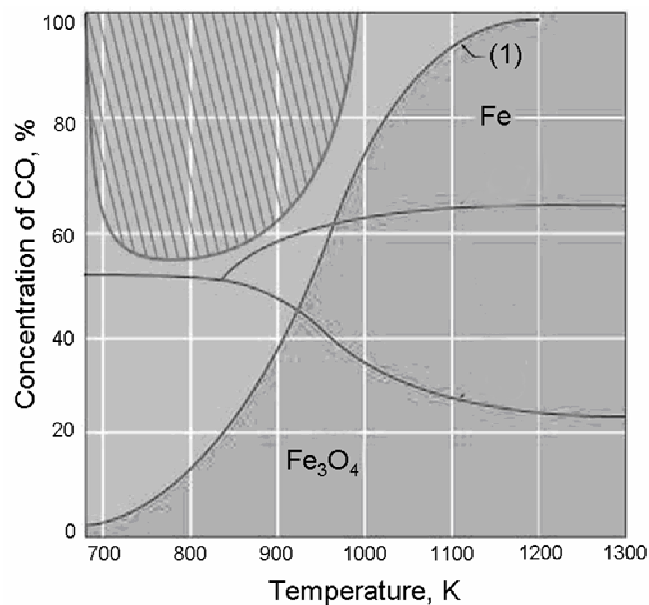


Figure 4.1: Equilibrium relationship of Boudouard reaction during reduction of iron ore.

Examination of the foregoing equilibrium theory makes it possible to decide whether a desirable reaction is possible and which conditions need to be met to obtain such a reaction. For practical control of a reaction, however, the mechanism that controls the reaction rate should be clarified and the heat and mass transfer should be analyzed on the basis of reaction rate theory and transport phenomena.

The intrinsic as well as apparent char reactivity have been recognized as the important

factors. A great number of modeling as well as experimental studies for better understanding of reaction mechanism and determination of reaction coefficient have been reported for a span of a few last decades. Consequently, it has been found that the values of kinetic parameters are dependent on the types of coke used for the process and influenced by the porous nature of the specimen. Moreover, the effects of temperature, pressure and gaseous environment on the reaction rate have also been comprehensively investigated by various investigators. The reaction rates of the most previous studies were measured by changes of mass or evolved gas analysis, and hence were the total rates over all active sites. However, a considerable discrepancy has been reported among the values of activation energy of this reaction, ranging from 200 to 400 $\text{kJ}\cdot\text{mol}^{-1}$. **Table 4.1** summarizes the previous studies done on the carbon-carbon dioxide system by different investigators. It also includes the values of activation energy reported by these studies.

Reference	Activation Energy ($\text{kJ}\cdot\text{mol}^{-1}$)	Reference	Activation Energy ($\text{kJ}\cdot\text{mol}^{-1}$)
Baldea, Niac	100-150	Walker, Foresti, Wright	201
Agrawal, Sears	223	Austin, Walker	226.8
Beyer, Pückeroff, Ulrich	227	Fuchs, Yovorsky	228
Overholser, Blakely	230	Ergun	247
Dutta, Wen, Belt	248	Blackwood	252-273
Moormann	255	Ballal, Zygourakis	257
Yoshida, Kunni	259	Visser	260
Turkdogan, Vinters	306.6	Rao, Jalan	333
Strange, Walker	414		

Table 4.1. Summary of activation energies of carbon-carbon dioxide reaction.

Great differences in the char reactivity imply that it is necessary to understand the char reactivity more precisely. Moreover, on the other hand, the pore structure of porous char is the critical physical property that affects char combustion. The total accessible surface area of pores and pore volume dominate the char combustion rate. In the diffusion controlled regime, the reaction rate is controlled by the gas diffusion through the rough pore surface, whereas, in the kinetic controlled regime, it is limited by the total internal surface area. It has been reported that the specific surface area would increase to a maximum and then decreases as the fractional char conversion increases from 0 to 1.

In addition, most of the models published in the literature do not explicitly account the importance of Boudouard reaction for certain reasons i.e. Boudouard reaction has lower reaction rate even for temperature value of 900°C and the rate of C-O₂ reaction is several order of magnitude faster than the rate of C-CO₂ reaction. But for the cases, where oxygen concentration (air excess number ~1) is restricted e.g. the combustion chamber to control NO emissions and coal fired burners; the effect of Boudouard reaction on process can not be excluded from modeling. During these processes, O₂ concentration keeps on decreasing because of combustion and it is counterbalanced by the production of CO₂. At higher conversion, the particle is exposed to the high concentration of CO₂ and it might be the only possible reason that there is always 100% conversion of particle even for non-existent concentration of O₂ at the end of the process.

The main purpose of the chapter is to investigate experimentally the gasification reactivity of pure carbon and determine the apparent kinetic parameters for various char. Moreover, the effects of process parameters are also illustrated. The prescript to above tasks includes the definition of rate coefficients and the kinetic analysis.

4.2 Langmuir-Hinshelwood Semi Global Kinetics

The following Langmuir-Hinshelwood rate equation has been found to give better interpretation of the experimental data for carbon-carbon dioxide reaction,

$$n_{rc} = \frac{K_B \cdot P_{CO_2}}{(1 + K_{CO_2} \cdot P_{CO_2} + K_{CO} \cdot P_{CO}) R \cdot T} \quad (1)$$

where n_{rc} is net rate of the reaction, K_B is the surface related reaction coefficient of Boudouard reaction, P_{CO_2} is the partial pressure of CO₂, K_{CO_2} is the sorption coefficient of CO₂, K_{CO} is the sorption coefficient of CO, P_{CO} is the partial pressure of CO, R is universal gas constant and T is the temperature. No attempt is made to define the precise stoichiometry of the steps or complexes, and the simplest forms of the rate laws are used, in which the reactions are assumed to be all first order (rather than second order). The detailed reaction mechanism is described in this section which is absolutely necessary to interpret precisely the experimental results. Furthermore, the different definitions of the reaction coefficients are also discussed in this section.

The typical reaction mechanism follows a traditional manner for carbon dioxide to get absorbed at the reactive surface before it reacts with carbon to produce carbon mono-

oxide and later the carbon mono-oxide desorbed from the surface. This process of adsorption-desorption according to Langmuir-Hinshelwood deals with a few of assumptions described next;

- the surface has a uniform activity and can be evenly occupied,
- a monolayer forms,
- there is no interaction between the adsorbed active sites,
- the adsorption and desorption are in equilibrium with each other.

The rate of CO₂ adsorption which is proportional to the molecular partial density of CO₂ and the total number of free sites available for the reaction at the surface can be calculated as,

$$\bar{n}_{ad_1} = K_{ad_1} \cdot \rho_1 \cdot (1 - \theta_1 - \theta_2), \quad (2)$$

the rate of CO₂ desorption is proportional to the surface covered by the gas and given by,

$$\bar{n}_{de_1} = K_{de_1} \cdot \theta_1, \quad (3)$$

similarly, the rate of adsorption of CO is given by the following equation,

$$\bar{n}_{ad_2} = K_{ad_2} \cdot \rho_2 \cdot (1 - \theta_1 - \theta_2), \quad (4)$$

and the rate of desorption follows,

$$\bar{n}_{de_2} = K_{de_2} \cdot \theta_2, \quad (5)$$

where \bar{n}_{ad_j} is the rate of adsorption of j^{th} species, \bar{n}_{de_j} is the rate of desorption of j^{th} species, K_{ad_j} is the adsorption coefficient of j^{th} species, K_{de_j} is the desorption coefficient of j^{th} species, ρ_j is the partial molar density of j^{th} species, θ_j is the fraction of the surface covered by j^{th} species, j is 1 for CO₂ & 2 for CO.

According to one of the assumptions made in the beginning, the rate of adsorption can be compared with rate of desorption for both of the species,

$$\bar{n}_{ad_1} = \bar{n}_{de_1} \quad (6)$$

and

$$\bar{n}_{ad_2} = \bar{n}_{de_2}. \quad (7)$$

The fractions of area covered by each of gases can be calculated using the equations (2) to (7). Here, we introduce the definitions of some coefficients as follows,

$$\bar{K}_1 = \frac{K_{ad_1}}{K_{de_1}} \quad (8)$$

and

$$\bar{K}_2 = \frac{K_{ad_2}}{K_{de_2}}. \quad (9)$$

Consequently, the fractions of area covered by each of gases can be given by the following equations,

$$\theta_1 = \frac{\bar{K}_1 \cdot \rho_1}{1 + \bar{K}_1 \cdot \rho_1 + \bar{K}_2 \cdot \rho_2} \quad (10)$$

and

$$\theta_2 = \frac{\bar{K}_2 \cdot \rho_2}{1 + \bar{K}_1 \cdot \rho_1 + \bar{K}_2 \cdot \rho_2} \quad (11)$$

The rate of forward reaction i.e. $C+CO_2 \rightarrow 2CO$ can be described in term of surface area covered by CO_2 as follows,

$$\vec{n} = \vec{K} \cdot \theta_1, \quad (12)$$

while on the other hand the rate of backward reaction i.e. $2CO \rightarrow C+CO_2$ can be given by the following equation,

$$\overleftarrow{n} = \overleftarrow{K} \cdot (1 - \theta_1 - \theta_2), \quad (13)$$

where \vec{K} is the reaction coefficient of the forward reaction, \overleftarrow{K} is the reaction coefficient of the backward reaction, \vec{n} is the rate of forward reaction, \overleftarrow{n} is the rate of backward reaction.

For the condition of equilibrium, the both rates i.e. forward and backward reaction rates should be equal to each other,

$$\vec{n} = \overleftarrow{n} \quad (14)$$

Using Eqs. 10, 11 and 14, we can find a relationship among the different coefficients as follows,

$$\overleftarrow{K} = \vec{K} \cdot \bar{K}_1 \cdot \rho_{1i}, \quad (15)$$

where ρ_{1i} is the equilibrium molar density of CO_2 in the gas. Net rate of the reaction is given by,

$$n_{rc} = \vec{n} - \overleftarrow{n} \quad (16)$$

and we get,

$$n_{rc} = \frac{\vec{K} \cdot \overleftarrow{K}_1 \cdot (\rho_1 - \rho_{1i})}{1 + \overleftarrow{K}_1 \cdot \rho_1 + \overleftarrow{K}_2 \cdot \rho_2} \quad (17)$$

Equation 17 is the Langmuir Hinselwood formulation. The partial molar densities of both gases can be expressed in terms of partial pressures and Eq. 17 can be rewritten using the new definitions of the coefficients,

$$K_B = \vec{K} \cdot \overleftarrow{K}_1, \quad (19)$$

$$K_{CO_2} = \frac{\overleftarrow{K}_1}{R.T}, \quad (20)$$

and

$$K_{CO} = \frac{\overleftarrow{K}_2}{R.T}. \quad (21)$$

Thus Eq. 17 can be illustrated as follows,

$$n_{rc} = \frac{K_B \cdot (P_{CO_2} - P_{CO_2i})}{(1 + K_{CO_2} \cdot P_{CO_2} + K_{CO} \cdot P_{CO}) \cdot R.T} \quad (22)$$

Some of the authors [*Grabke*] proposed other reaction mechanisms, however, which were not able to give proper explication of reaction behavior. At higher values of temperature the equilibrium pressure P_{CO_2i} has a very lower value that can be neglected compared to CO_2 partial pressure. Note that for the temperature values less than ~ 900 °C, it is no longer possible to neglect the value of CO_2 equilibrium pressure. Moreover for higher values of CO partial pressures, it is possible for CO_2 equilibrium pressure to be higher than the CO_2 partial pressure. In such cases, the Boudouard reaction can no longer proceed in forward direction i.e. carbon deposition reaction. For high temperature processes with no CO enrichment, Eq. 22 can be simplified as follows;

$$n_{rc} = \frac{K_B \cdot P_{CO_2}}{(1 + K_{CO_2} \cdot P_{CO_2} + K_{CO} \cdot P_{CO}) \cdot R.T} \quad (23)$$

Based on number of studies [*Agrawal et al., Adchiri et al., Molina et al.*] it has been found that internal surface area changes with conversion of the particle. Consequently, to evaluate the value of reaction coefficient on the basis of mass loss vs. time plot is not a better option because the change in number of active sites due to reduced mass during the reaction may yield inappropriate results. **Figure 4.2** illustrates a comparison

of mass-related reaction coefficient found by different investigators.

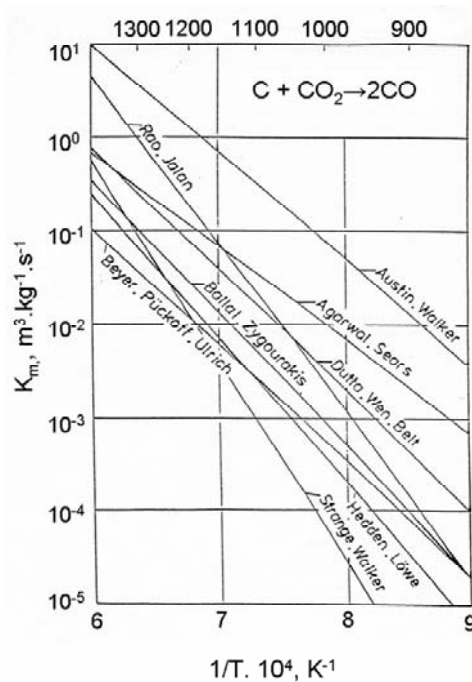


Figure 4.2: Comparison of various mass-related reaction coefficients of Boudouard reaction

From Fig. 4.2 it can be seen that the values of reaction coefficient differ from one another by a factor more than 100. Most of previous investigations were based on powdered sample because of its suitability to determine the activation energy and the effect of gas composition over the conversion and, therefore, also the governing reaction mechanism. Furthermore, the reactivity of different types of coke can also be compared. In addition, it is also possible to investigate the catalytic effect of different foreign substances or impurities. Nevertheless, the difficulty of determining the reactive surface that depends on the particle size distribution is one of the disadvantages. Moreover, the process could also be influenced by the diffusive transport of reactant. The inhomogeneous character of the sample used can be considered to be a substantial reason for data incongruity of the values of reaction coefficients.

Nevertheless, the converted mass of the carbon can be related to the surface of the specimen used and the values obtained are the surface-related reaction coefficients. Moreover, the relationship between the mass and surface-related coefficients can be obtained on the basis of the following analysis.

Molecular flow density, described previously by Eq. 23, can be related to mass flow rate of the carbon by the following equation,

$$n_C = \frac{\dot{M}_C}{A \cdot \bar{M}_C}, \quad (24)$$

in Eq. 23 the rate coefficient that defines the reaction rate of the carbon gasification has a unit $\text{m}\cdot\text{s}^{-1}$, however, the rate of carbon gasification can also be related to the mass as follows,

$$\frac{1}{M_C} \cdot \frac{dM_C}{dt} = \frac{K_{Bm} \cdot \rho_{CO_2}}{(1 + K_{CO_2} \cdot P_{CO_2} + K_{CO} \cdot P_{CO})}, \quad (25)$$

where the reaction coefficient K_{Bm} is the mass related reaction coefficient, n_C is the molar flow rate of the carbon, \dot{M}_i is the mass flow rate of i^{th} species, \bar{M}_i is the molecular mass of i^{th} species, M_i is the total mass of i^{th} species and A is the surface.

Using Eqs. 23 to 25, the correlation between the mass and surface related coefficient can be derived as follows,

$$\dot{M}_C = \bar{M}_C \cdot A \cdot \frac{K_B}{R.T} \cdot \frac{P_{CO_2}}{1 + K_{CO_2} \cdot P_{CO_2} + K_{CO} \cdot P_{CO}} \quad (26)$$

and Eq. 25 gives,

$$\dot{M}_C = M_C \cdot \frac{K_{Bm}}{R.T} \cdot \frac{P_{CO_2} \cdot \bar{M}_{CO_2}}{1 + K_{CO_2} \cdot P_{CO_2} + K_{CO} \cdot P_{CO}}. \quad (27)$$

With a definition of specific internal surface area,

$$A_{in} = \frac{A}{M_C} \quad (28)$$

the Eqs. 26 & 27 yield to a relationship between these two coefficients as follows,

$$K_B = \frac{\bar{M}_{CO_2}}{\bar{M}_C} \cdot \frac{K_{Bm}}{A_{in}} \quad (29)$$

On the basis of above relationship, the calculated values of surface related reaction coefficient using the mass related coefficient values with known internal surface area show more data incongruity among the different results shown in Fig. 4.2. It leads to the conclusion that internal surface area changes with conversion of the particle. Wherefore, Eq. 29 can not be used to convert the mass-related values to the surface-related values.

4.3 Experiments

The experimental investigation for re-estimation of kinetic rate constants of Boudouard reaction, which also depends on the type of coke, has been carried out under a wide condition range (900-1200 °C). While making the experiments, precautions must be taken in removing the traces of oxygen and the inert carrier gas. The ratio of the overall rates, as measured by TGA or evolved gas analysis for the oxygen/carbon dioxide reactions, is approximately 10^5 under the conditions usually reported in the literature [Walker *et al.*]. Thus, the gasification rate by 1ppm of O₂ is approximately same as the rate by 0.1 atm of CO₂; most of the commercial grades of the inert gases e.g. N₂, Ar and CO₂ contain more than 1ppm of O₂. In this experimental investigation is carried out in the flowing stream of pure CO₂ with a minimum purity of 99.99% at atmospheric pressure. This investigation will also help us to find the relationship, if any, between the reactivity and the physical characteristic of the sample.

4.3.1 Experimental Setup and Materials used

The experiments were performed in the apparatus, illustrated in **Fig. 4.3**. Experiments were conducted inside a tube furnace having a diameter of 0.089 m and a height of 1.2 m, using an environment of CO₂-CO-N₂ gaseous mixture at 1 bar under a wide temperature range of 900 to 1200 °C. The reaction rate can be either kinetic controlled or diffusion controlled. As one of the main aims of performing the experiments, the reaction rate should only be kinetics-controlled. The experimental targets also include investigations of mass transfer to assure that the process is mainly influenced by the chemical reaction only.

A variety of cokes (Graphite, Poland coke, Czech coke, Anthracite coal) with different properties were taken for the experiments. The specimens used here have fixed geometry of a cylinder; with a diameter of 20 mm and a height of 50 mm, and of a plate; with a length of 90 mm, a width of 50mm and a thickness of 10 mm. **Figure 4.4** describes the geometries of the sample used during the experiments. Figure 4.4 also includes geometry of aluminum plate which was used to perform the experiments related to mass transfer calculations. The majority of authors carried out their investigations using powdered sample.

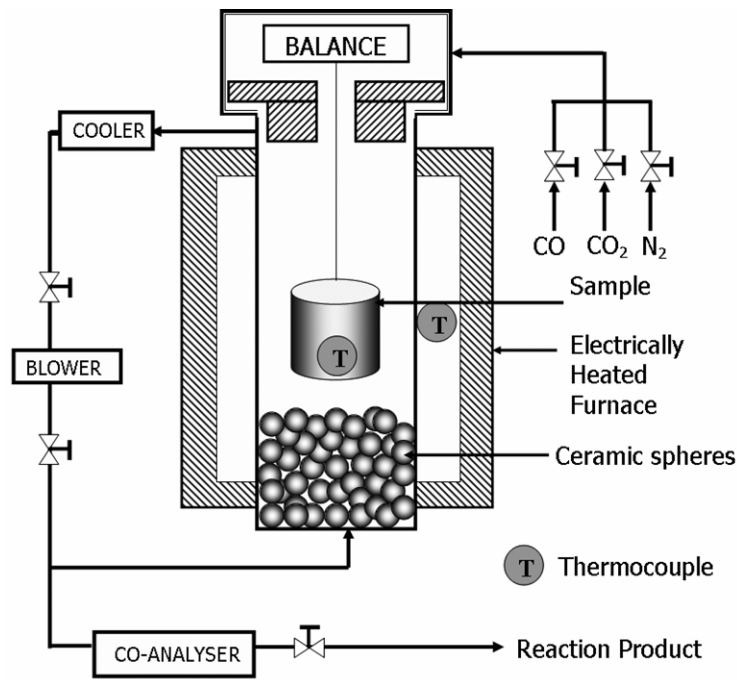


Figure 4.3: Schematic diagram of the experimental setup.

However, the difficulty of measurement of the reactive surface area along the progress of reaction as well as the effect of diffusive transport point out towards the use of fixed geometry. Furthermore, to compare the reaction behavior of different coke samples, the fixed geometry of specimens is required for the experiments. During experiments, the samples were placed on a balance which continuously measured the converted mass of specimen with time. Meanwhile the temperature of the sample was measured using thermocouple situated at the center. The experiments also covered the measurements of mass transfer coefficient.

The influence of mass transfer was reduced by adjusting the gas flow-rate and specimen dimensions. Consequently, it gives the true values of reaction coefficients for a kinetic controlled process. The higher gas flow rates require the gas to be circulated in a closed circuit as shown in the Fig. 4.3. However, a part of the circulating gas is being taken off continuously to avoid high concentration of CO so that the carbon deposition reaction should not take place at higher temperatures. An IR-analyzer was used to control continually the CO content in the gas. The purged gas was replaced by make-up gas which was being produced according to the required compositions of CO₂-CO-N₂. The supply of make-up gas through the balance assembly keeps it to be cooled constantly and also confines its exposure to the hot gas coming from the conduit just below it. Moreover, an increase in gas velocity was limited to 1 m.s⁻¹ so that the mass loss from specimen surface, which is caused by removal of small particles due to high

gas flow rate, could be prevented. We have run a few of experiments to see how a sample is influenced by higher values of the flow rate and found that there was a severe effect especially at the lower part of the sample where it is directly being hit by hot reactant gas coming from the lower part of the furnace.



Figure 4.4: Specimens used in the experiments. Geometry (from left to right): cylindrical specimen of coke, plate of graphite, plate of aluminum

Figure 4.5 shows a comparison of two samples before and after the experiment and it can easily be seen that sample thickness varies from its bottom to upper section and there is a big loss of sample mass due to higher gas velocity. Consequently, our assumption of constant surface area seems to be inconsistent. Hence an optimized gas velocity of $1 \text{ m}\cdot\text{s}^{-1}$ is used for experimental runs. In the lower section of the furnace, the gas flows through a fixed bed of inert ceramic spheres to attain a homogeneous flow over the cross section as well as temperature equal to that of the furnace wall temperature.

With graphite slabs having a porosity of 1.2%, the diffusive transport of the reactant into the pores of a sample can be considered negligible. Thus, the outer surface of the graphite specimen can be assumed as the reaction surface and the value of reaction coefficient obtained can be taken as the true value. After a short reaction time, however, the initially smooth surface of the specimen becomes rough. Although due to the roughness of the specimen surface the actual reaction surface might become larger than the geometric surface, the effect of difference between these two surfaces over the reaction is not included in this study as it was difficult to measure during the progress of the reaction.

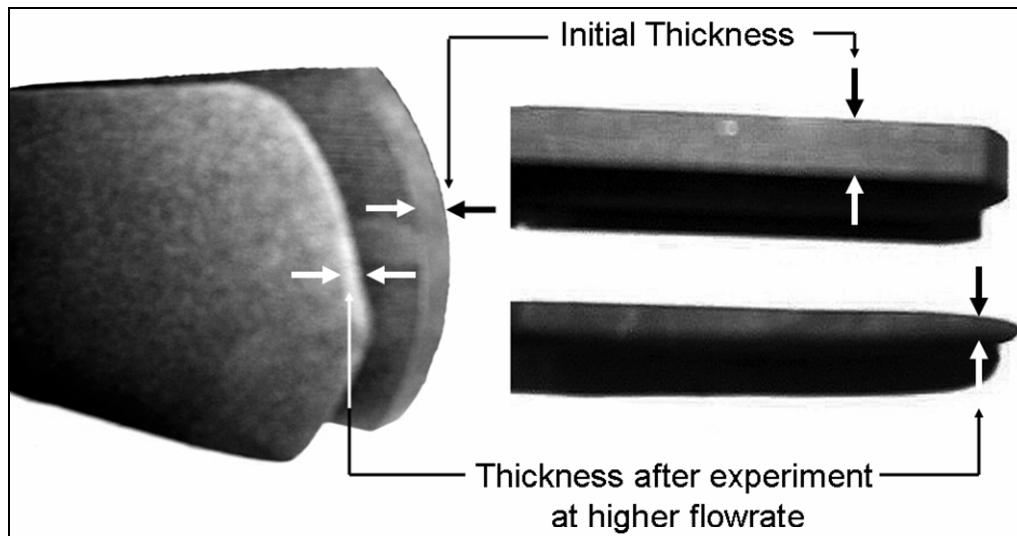


Figure 4.5: Comparison of sample thickness before and after the experiment: influence of higher flow rate of CO_2

Figure 4.6 shows the samples before and after the completion of the experiment. It can easily be seen that the surface of the sample is become rough with small contours over the surface. Furthermore, we have also performed a number of experiments using cokes to describe the influence of porous nature on the reaction rate. These experimental investigations give the values of apparent reaction parameters which involves the influence of the change in internal surface area, particle porosity and density.

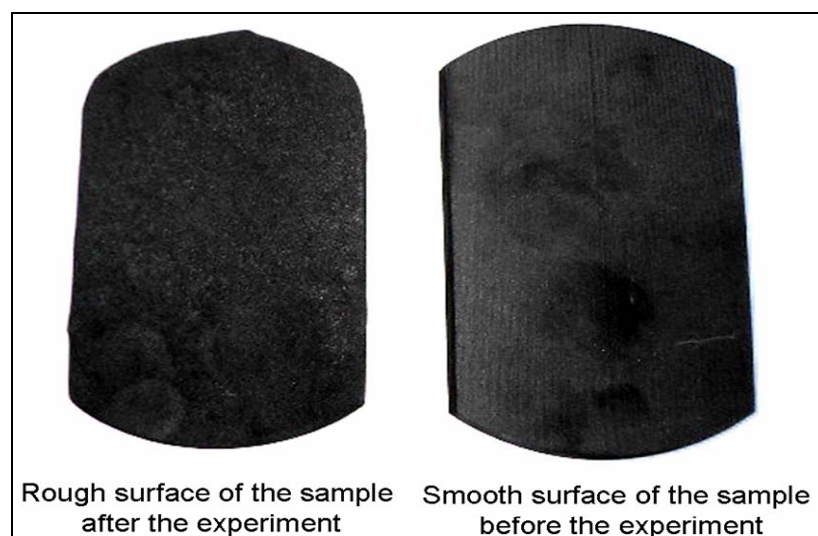


Figure 4.6: Comparison of sample surface before and after the experiment at a temperature $1000\text{ }^\circ\text{C}$: influence of chemical reaction

4.3.2 Mass Transfer Calculations

The effect of the bulk diffusion of the reactant gas is probed here. In general, the reaction rate expression includes the reaction kinetics and diffusional resistance on to the external surface of the particle. During this study, however, the sample geometry and the flow rate of the reactant gas are optimized in such a manner that the process is mainly influenced by the chemical reaction only. Therefore, Eq. 23 is capable to describe the reaction rate with no influence of diffusive transport. Calculation of the values of mass transfer coefficient is based on the analogy between the heat and mass transfer. Specimen of aluminum plate was chosen to confirm that there is no influence of reaction as it would be in the case of graphite slab. Aluminum plate with a length of 90 mm, a width of 50 mm and a thickness of 10mm was used to measure the convective heat transfer rate from the hot plate surface to the CO₂ gas flowing at a lower temperature.

Based on the assumption of lumped parameter model i.e. the temperature of the whole body is same as the core temperature, the core temperature of the body was measured continually.

According to lumped parameter model;

$$m.c_p \cdot \frac{dT}{dt} = h.A_p.(T_p - T_g). \quad (30)$$

Integration of Eq. 30 yields the following equation;

$$\ln(T_p - T_g) = \frac{h.A_p}{m.c_p} .t + c \quad (31)$$

where m is the mass of the aluminum plate, c_p is the specific heat capacity, h is the heat transfer coefficient, t is the time, T_p is the temperature at center of the plate, T_g is the gas temperature and A_p is the surface area of the plate.

Experiments have been carried out to calculate the variation of the plate core temperature with time. A plot of $\ln(T_p - T_g)$ vs. t for the various flow-rates of CO₂ can be constructed based on Eq. 31. The experimental analysis gives the value of heat transfer coefficient for each experimental run with a particular value of the CO₂ flow-rate. According to analogy between the heat and mass transfer, the values of the mass transfer coefficient can be calculated as follows;

$$\beta = \frac{h.D_{CO_2}}{\lambda}, \quad (32)$$

where β is the mass transfer coefficient, D_{CO_2} is the diffusivity of CO_2 and λ is the thermal conductivity.

4.4 Experimental Results

4.4.1 Measurement of Mass Transfer Coefficient

Analogy between the heat and mass transfer based on the experimental findings using aluminum specimen is used to calculate the values of mass transfer coefficient. **Figure 4.7** shows the measured temperature-time plots of the core of aluminum plate for CO_2 flow rates of 3 and 4 $m^3 \cdot hr^{-1}$. The specimens were kept at various initial temperatures in the range from 192 to 313 $^{\circ}C$. It can be seen from Fig 4.7 that there is continuous decrease in specimen temperature due to convective heat loss from the hot metal surface to the cold gas flowing at higher flow rate. The results plotted in the Fig. 4.7 are further used to generate the plots between $\ln(T_p - T_g)$ and t which is necessary for calculation of the values of the heat transfer coefficient at various flow rates of CO_2 .

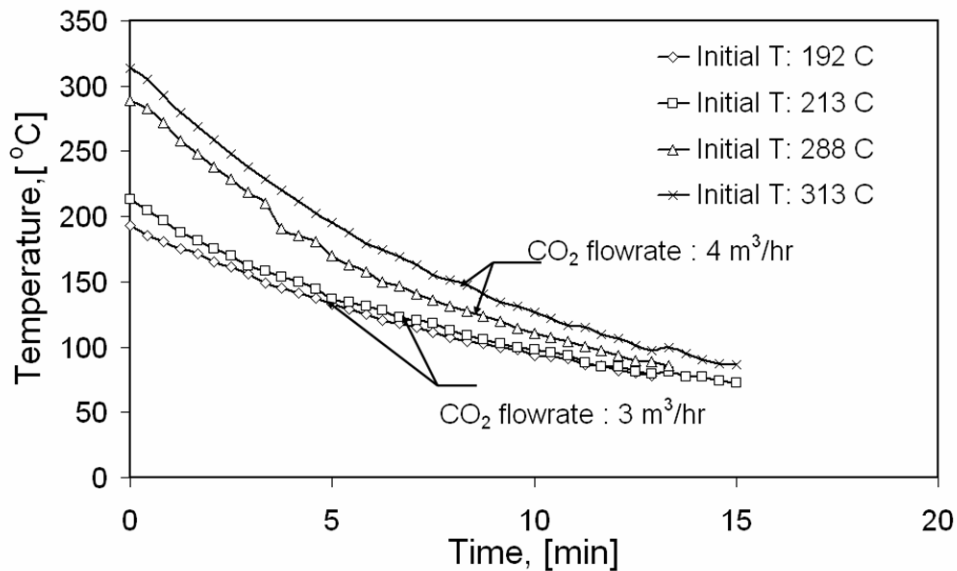


Figure 4.7: Temperature-time plot of aluminum plate at different volumetric flow rates of CO_2 .

These $\ln(T_p - T_g)$ and t plots are illustrated in **Fig. 4.8**. The linearity of all plots in Fig. 4.8 confirms the fidelity of the experiments, and later the values of heat transfer coefficient are calculated using equation 31.

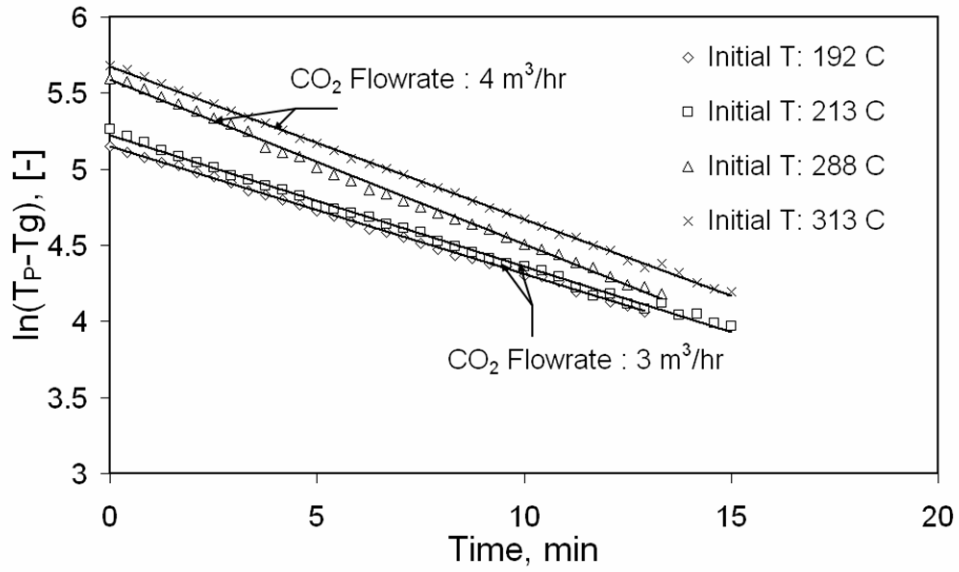


Figure 4.8: Experimental $\ln(T_p - T_g)$ vs. t plot at different volumetric flow rates of CO₂.

Using Eq. 32, the values of mass transfer coefficients were calculated based on the measured values of heat transfer coefficients (Fig. 4.8).

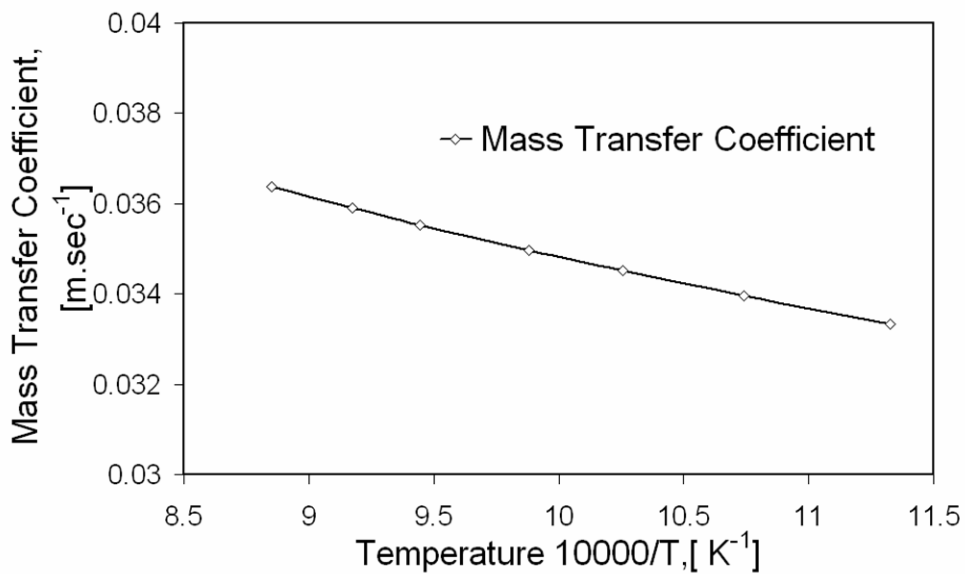


Figure 4.9: Plot of variation of mass transfer coefficient with temperature.

Figure 4.9 describes the variation of mass transfer coefficient with temperature. Experimentally found values of mass transfer coefficient confirm that there is no significant influence of mass transfer on the process as the resistance to mass transfer has very less value compared to the resistance caused by the reaction. Hence, the process is mainly influenced by reaction only. Moreover, it is further investigated by

changing the value of flow rate at a particular temperature and it has been found that the influence of mass transfer on the process is not significant.

4.4.2 Intrinsic Kinetic Parameters for Coke Gasification in CO₂ Environment

Graphite slab with dimensions described previously (**section 4.3.1**) has been used to calculate the true value of the reaction coefficient. Since graphite has porosity of 1.2 %, it is assumed that there is no significant contribution of pore diffusion over the process. On this basis, we can assume that the loss in specimen weight is only because of reaction taking place at the outer surface. Note that it has already been confirmed, on the basis of the experiments described in the previous **section 4.4.1**, that mass diffusion resistance is negligible compared to the reaction. The pure CO₂ was used for these experimental runs at different temperatures in the range of 900 to 1200 °C. The sample weight is plotted against reaction time at different temperatures in **Fig. 4.10**. Figure 4.10 describes the summary of only three experiments carried out at temperatures 900, 1000 and 1100 °C.

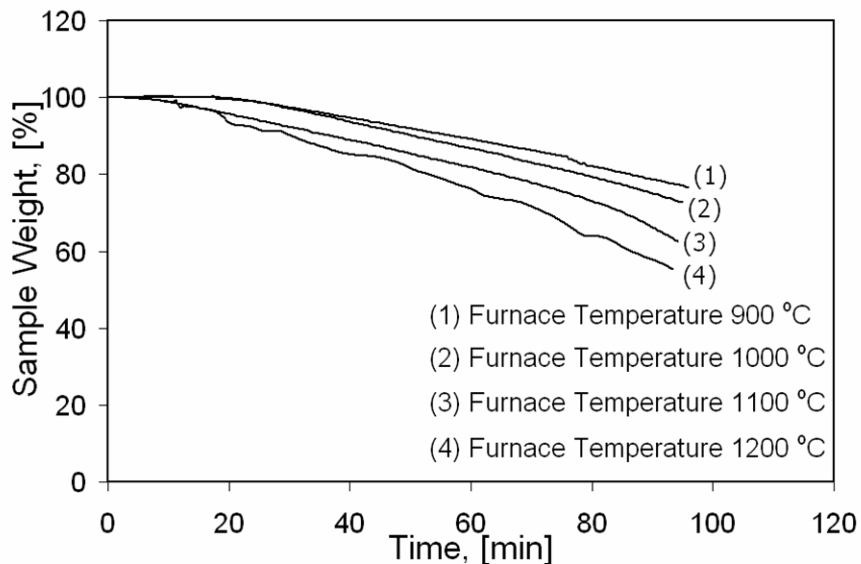


Figure 4.10: Plot of sample weight vs. time: graphite specimen at atmospheric pressure and temperatures 900, 1000, 1100 and 1200 °C.

In the beginning of the process, specimen loses its weight slowly with time since during this time interval all the moisture present inside the specimen goes off and particle attains a temperature equal to the desired reaction temperature which is approximately equal to the furnace temperature. Afterward, it has been found that a linear variation of

weight loss with time exists (Fig. 4.10).

Before we discuss the results in context to the reaction coefficient, the experimental evidence about the endothermic nature of the Boudouard reaction is shown in **Fig. 4.11**. Figure 4.11 describes a number of experimental runs for three temperatures i.e. furnace temperature, gas temperature and specimen temperature. Although at lower values of the furnace temperature the specimen reaches to a temperature which is approximately same as the furnace temperature, the influence of endothermic reaction is clearly visible for the higher values of furnace temperature. Moreover, the gas reaches to a temperature which is approximately same as the furnace temperature.

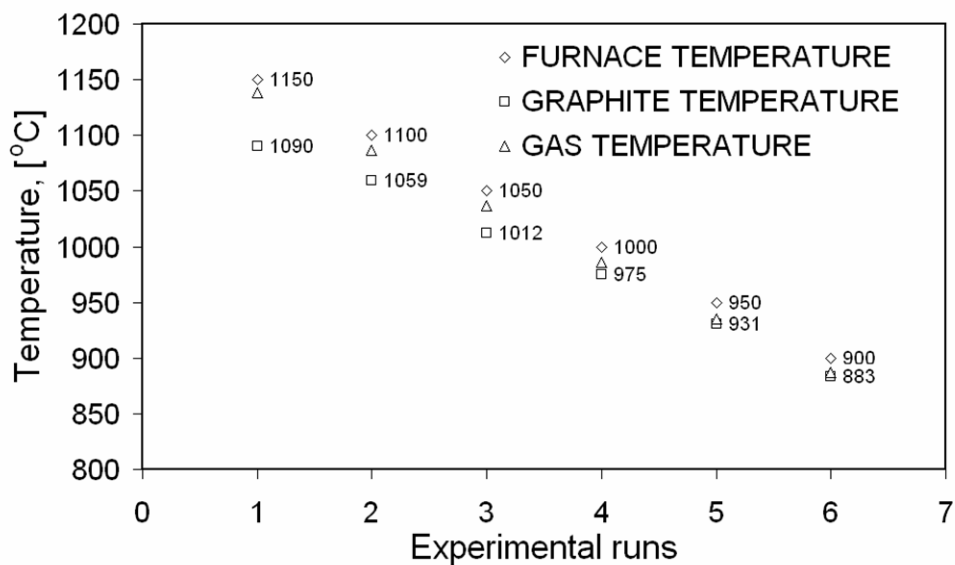


Figure 4.11: Experimental history of specimen temperature to describe the influence of endothermic Boudouard reaction.

To calculate the value of reaction rate at a particular temperature, we have chosen the linear part of the curve (Fig. 4.10) when specimen is at the reaction temperature and experiences the weight loss due to highly endothermic Boudouard reaction. We have run a number of experiments at various temperatures lies in between temperatures 900 and 1200 °C. **Figure 4.12** illustrates a summary of the experiments.

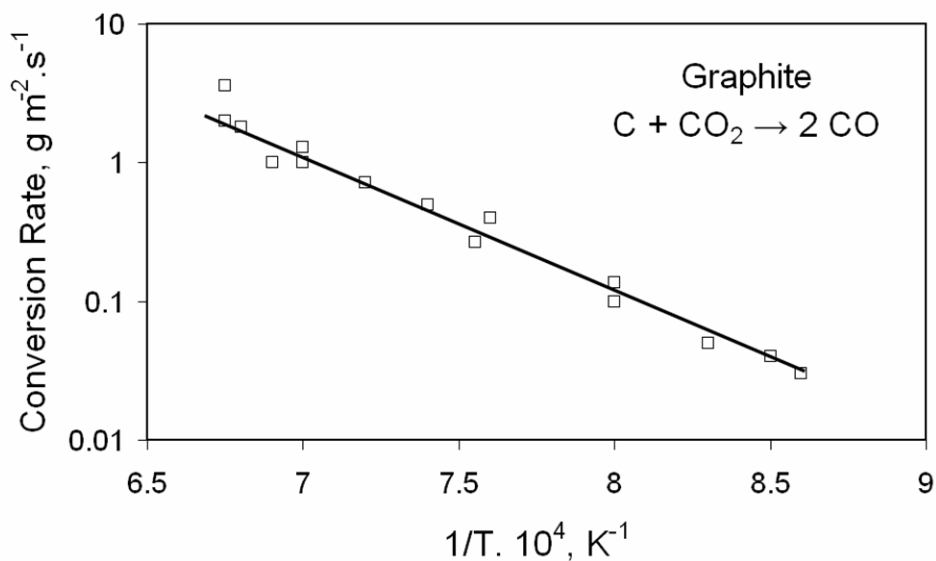


Figure 4.12: Conversion rate of graphite as a function of the temperature in an environment of CO₂. The values of reaction coefficient at different temperatures can be easily calculated from the slope of linear weight loss vs. time plot. As thin slabs of graphite were taken as specimens, whereby the area that accounts for the sides is less in comparison to the total area, the outer surface decreases only slightly during the experiments. The experimental points were fitted to Arrhenius relation. In this study, the values of pre-exponential factor and activation energy of reaction were found to be 5.42×10^6 and $222 \text{ kJ} \cdot \text{mol}^{-1}$ respectively. The values of activation energy given in the literature cover a range from 113 to $414 \text{ kJ} \cdot \text{mol}^{-1}$ and most of them have a value between 201 and $260 \text{ kJ} \cdot \text{mol}^{-1}$ (**Table 4.1**). The experimental value of activation energy found in this study falls in lower third of the values given in the literature.

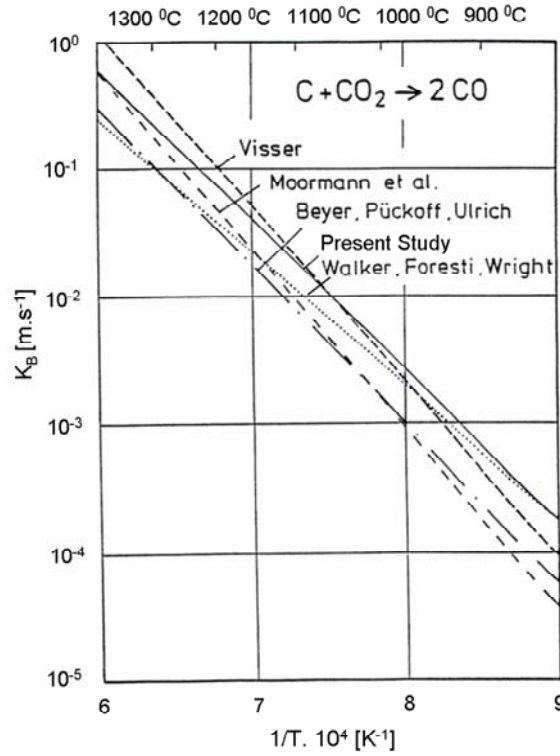


Figure 4.13: Comparison of experimentally found reaction coefficient with the values available in the literature: Arrhenius plot.

Arrhenius equation can be rewritten as follows,

$$K_B = 5.42 \times 10^6 \cdot \exp\left(-\frac{222 \text{ kJ/mol}}{RT}\right), \text{ m.s}^{-1}. \quad (33)$$

Only a few values of the surface related reaction coefficient are available in published work, which are compared with present value of reaction coefficient in **Fig. 4.13**. It can be seen that the deviation among the surface related values is much smaller compared to the mass related values (Fig. 4.2).

4.4.3 Determination of Sorption Coefficient of CO₂

Equation 23 can be rewritten while assuming the value of P_{CO} equal to zero,

$$\frac{\bar{M}_C}{RT} \cdot \frac{P_{CO_2}}{m_C} = \frac{1}{K_B} + \frac{K_{CO_2}}{K_B} \cdot P_{CO_2}. \quad (34)$$

The influence of CO₂ partial pressure on the rate of Boudouard reaction is shown in **Fig. 4.14**. During the experiments, the specimens were brought into contact with a mixture of CO₂ and N₂. Furthermore, the temperature was varied while maintaining the gas composition constant. Illustration of Eq. 34 in Fig. 4.14 is used to calculate the value of CO₂-sorption coefficient using the gradient of each of plots. Moreover, the dependency

of the sorption coefficient on the temperature is shown in **Fig. 4.15**. The value of sorption coefficient was found to be $\sim 2.4 \text{ bar}^{-1}$. In the range of investigated temperature, however, no significant dependency of the coefficient on temperature was established.

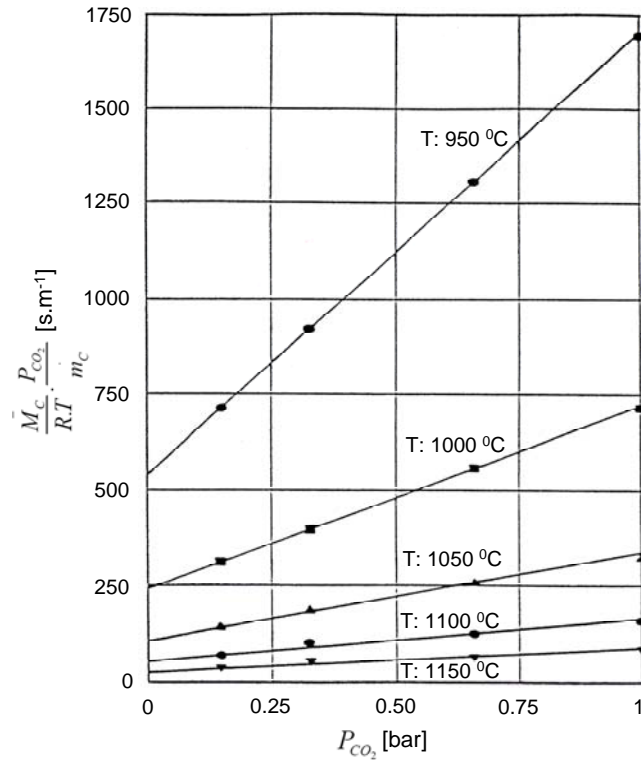


Figure 4.14: Illustrations of the experimental runs with partial pressures of CO_2 at different temperatures.

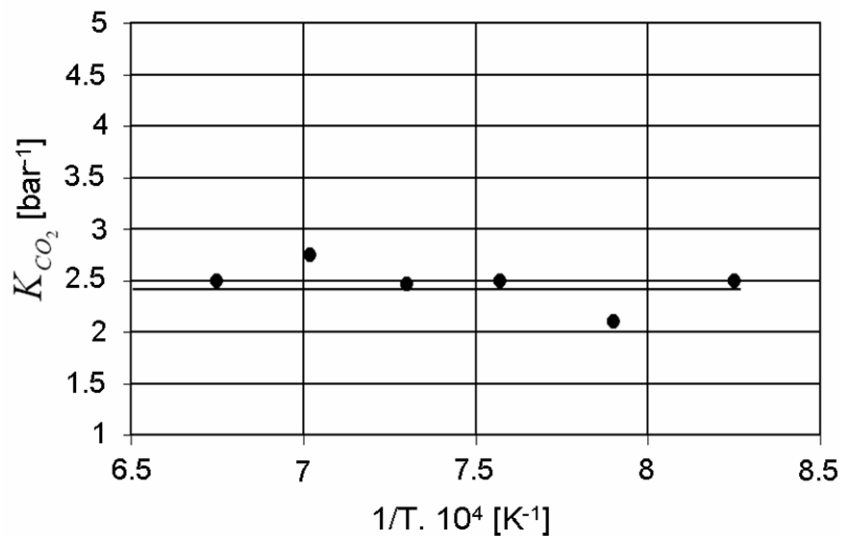


Figure 4.15: Temperature dependency of CO_2 -sorption coefficient on temperature.

Figure 4.16 shows a comparison of our experimental results with the values available in the literature. It can be seen in Fig. 4.16 that the values differ sometimes

considerably. The main reason is the value of the reaction coefficient of Boudouard reaction in Eq. 34.

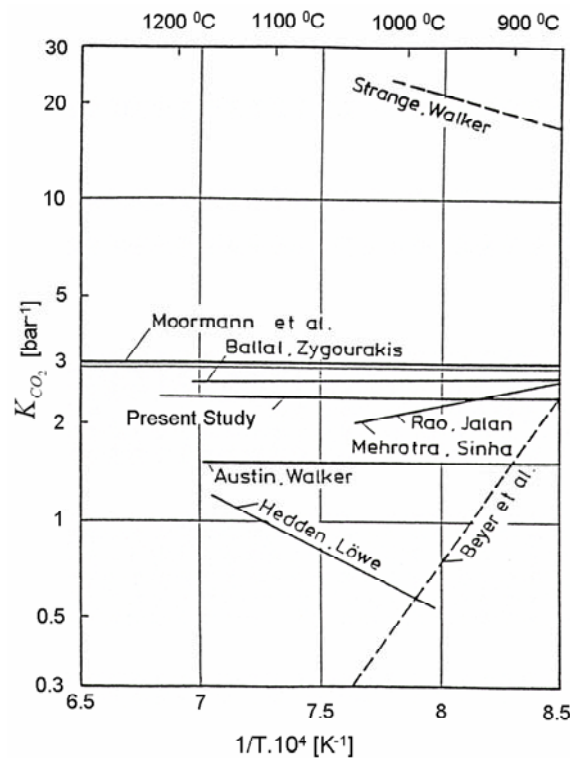


Figure 4.16: Comparison of CO₂ sorption coefficient with the values available in the literature.

As numerically the reciprocal value of K_B is significantly higher than K_{CO_2} , a slight change in the value of K_B influences K_{CO_2} considerably. Assuming an average value of CO₂ sorption coefficient equal to 2 for all values of CO₂ partial pressure < 0.2 bar, however, the product of $K_{CO_2} \times P_{CO_2}$ becomes small compared to 1. This might be a possible reason why the investigators who investigated Boudouard reaction for lower values of CO₂ partial pressure, were failed to confirm the Langmuir-Hinshelwood formulation.

4.4.4 Determination of Sorption Coefficient of CO

The experiments were carried out under the two conditions: the gas composition of the mixture of CO₂-CO-N₂ remained constant while the temperature was varied; the gas composition was varied at constant temperature. **Figure 4.17** illustrates the influence of CO-partial pressure on the conversion rate. However, these measurements were taken using CO-CO₂ mixture only.

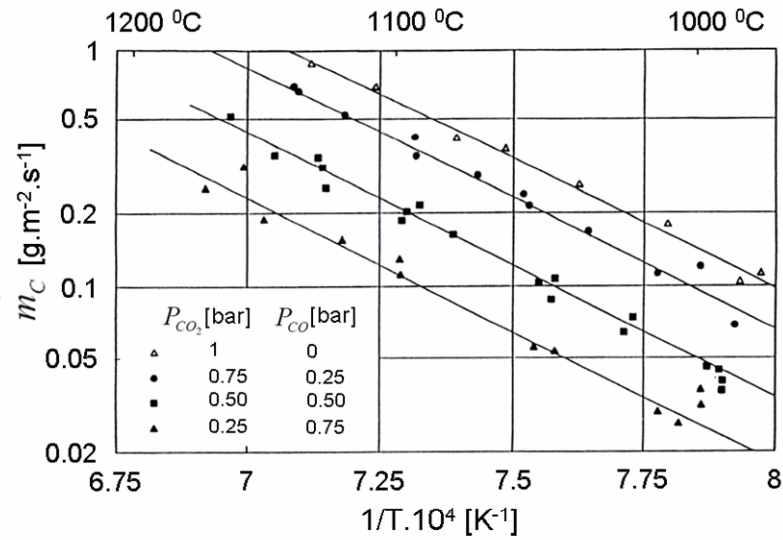


Figure 4.17: Influence of CO-partial pressure over the conversion rate.

The sorption coefficient of CO can be determined by transforming the Eq. 23 as follows,

$$\frac{\bar{M}_C}{RT} \cdot \frac{K_B \cdot P_{CO_2}}{m_C} - 1 - K_{CO_2} \cdot P_{CO_2} = K_{CO} \cdot P_{CO} \quad (35)$$

This relation is depicted in Fig. 4.18 for three temperatures. Although the measured values increase with a decrease in temperature for all values of CO-partial pressure, the resulting temperature dependency of sorption coefficient is weak.

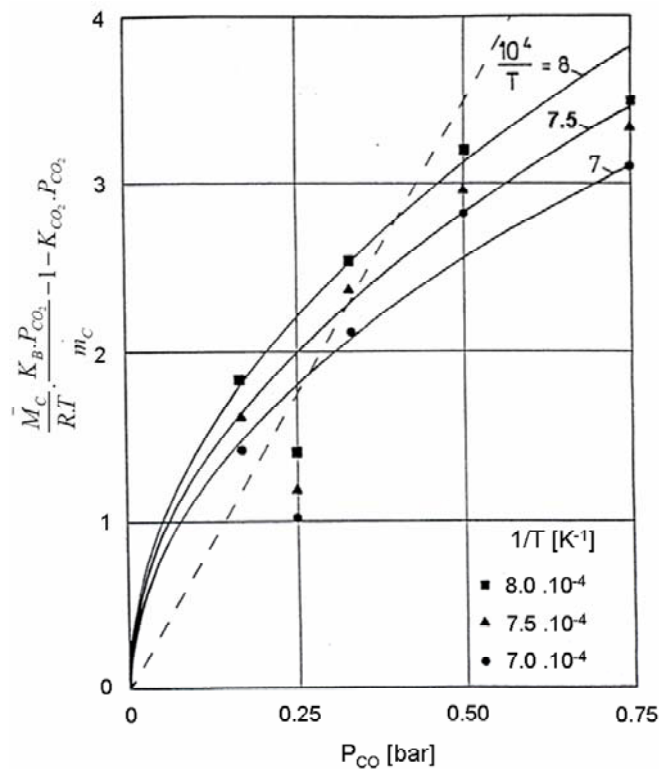


Figure 4.18: Illustrations of the experimental runs with partial pressures of CO at different temperatures.

If the Langmuir-Hinshelwood formulation is valid, the individual points would have lied on the straight line. However a regression line can be drawn on the figure to calculate the value of the CO-sorption coefficient. This value was found to be 7.0 bar^{-1} . The temperature dependency can be neglected compared to the deviation of individual points from the linear curve. It is possible, however, to use a parabolic expression for better approximation of the experimental points as shown in the Fig. 4.18. On the basis of experimental findings, the sorption coefficient can be related to the temperature as follows,

$$K_{CO} = 0.86 \cdot \exp\left(\frac{17 \text{ kJ} \cdot \text{mol}^{-1}}{R \cdot T}\right), \text{bar}^{-1/2}. \quad (36)$$

Consequently, the rate expression of carbon-carbon dioxide reaction can be better expressed by using the following formulation,

$$\dot{m}_C = \frac{\bar{M}_C}{R \cdot T} \cdot \frac{K_B \cdot P_{CO_2}}{1 + K_{CO_2} \cdot P_{CO_2} + K_{CO} \cdot \sqrt{P_{CO}}} \quad (37)$$

where the partial pressure of CO appears with an exponent $1/2$ in place of unity.

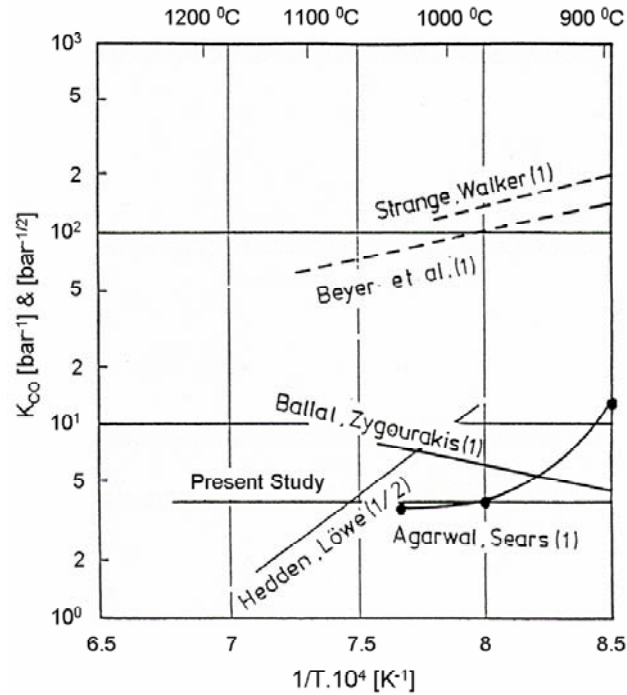


Figure 4.19: Comparison of sorption coefficient with the values available in the literature.

The values given in the literature for the sorption coefficient of CO are compared with present results in **Fig. 4.19**. It includes both the investigations stating the exponent of CO partial pressure in kinetic rate expression equal to 1 and other stating the exponent equal to 1/2. Note that the parabolic influence of CO partial pressure could only be noticeable if the higher values of partial pressure are investigated. As shown in Fig. 4.18, however, for lower values of partial pressure it is possible to approximate the influence of the CO by considering its exponent equal to 1.

4.4.5 Apparent Kinetic Parameters for Coke Gasification in CO₂ Environment

In the previous section the intrinsic reactivity, depending on the external surface area of the specimen with no influence of porous characteristics, is determined for a given pure carbon specimen. Furthermore, this section attempts to review the experimental investigations made to determine the effect of porous nature of different coke samples over the reactivity. Nevertheless, the determination kinetic parameters is the primary task so that the reaction rates can be computed taking into account several factors, such as: temperature, pressure, composition of the atmospheric surrounding of coke, etc.

A number of gas-solid reaction models in the category of volume reaction model have been proposed. According to these models, the reaction takes place uniformly throughout the interior of the solid phase. Theoretically, the reactivity of the carbon defined in terms of conversion rate can be calculated by the following expression,

$$R_A = \frac{1}{1-x} \cdot \frac{dx}{dt}, \quad (38)$$

where x is the conversion of the sample and can be defined as,

$$x = \frac{W_o - W}{W_o}. \quad (39)$$

The reactivity depends on the temperature and CO₂ partial pressure. At fixed total pressure, the reactivity can be determined as follows,

$$R_A = K_{A0} \cdot \exp\left(-\frac{E_A}{R.T}\right) \cdot P_{CO_2}^n, \quad (36)$$

where n is the order of reaction, K_{A0} and E_A are the apparent pre-exponential factor and apparent activation energy respectively. The apparent values take into account the

transport of reactant inside the particle, the change in internal surface and particle density etc. The reaction order for the reaction between the carbon and CO₂ is taken as unity. The apparent reaction coefficient can be described by the following equation,

$$K_A = \sqrt{K_{in} \cdot O_m \cdot \rho_c \cdot D_{eff}} . \quad (40)$$

Taking logarithms and differentiating with respect to temperature and noting that both the intrinsic reaction coefficient and to a lesser extent the diffusional process are temperature dependent gives,

$$\frac{d(\ln(K_A))}{dT} = \frac{1}{2} \left[\frac{d(\ln(K_{in}))}{dT} + \frac{d(\ln(D_{eff}))}{dT} \right], \quad (41)$$

note that the dependencies of internal surface area and carbon density are neglected compared to the other parameters. With Arrhenius temperature dependencies for both reaction and diffusion we have,

$$K_A = K_{A0} \cdot \exp\left(-\frac{E_A}{R.T}\right), \quad (42)$$

$$K_{in} = K_{in0} \cdot \exp\left(-\frac{E_{in}}{R.T}\right), \quad (43)$$

and

$$D_{eff} = D_{eff0} \cdot \exp\left(-\frac{E_D}{R.T}\right). \quad (44)$$

Using Eqs. (41-44), we can simply calculate that the apparent activation energy is the combined effect of both chemical reaction and diffusion of the reactant inside the porous structure of the specimen. Solution of Eq. 41 yields,

$$E_A = \frac{E_{in} + E_D}{2} . \quad (45)$$

Several experimental runs were carried out in a wide range of temperature from 900 to 1100 °C. During the experiments, three different types of porous specimens have been used with different properties e.g. Poland coke, Czech coke and Anthracite coal.

The samples were heated in CO₂ environment to the final desired reaction temperature and weighed continuously during burn-off. The experiments were aimed to calculate the variations of the sample temperature and weight with gasification time. **Figure 4.20** describes the summary of one experiment for Poland coke sample at 1100 °C to show how the weight and temperature of the specimen vary with burning time. As shown in Fig. 4.20, there exists a preheating zone during which all moisture and inorganic matters present inside the particle come out of the particle. Henceforth, the sample

attains the maximum required temperature for reaction to take place. Experimental result illustrates that the particle temperature remain constant inside the particle, though it has a temperature value less than the furnace temperature due to endothermic nature of Boudouard reaction. During the experimental run, specimen weight continuously decreases and follows a linear variation with time at reaction temperature.

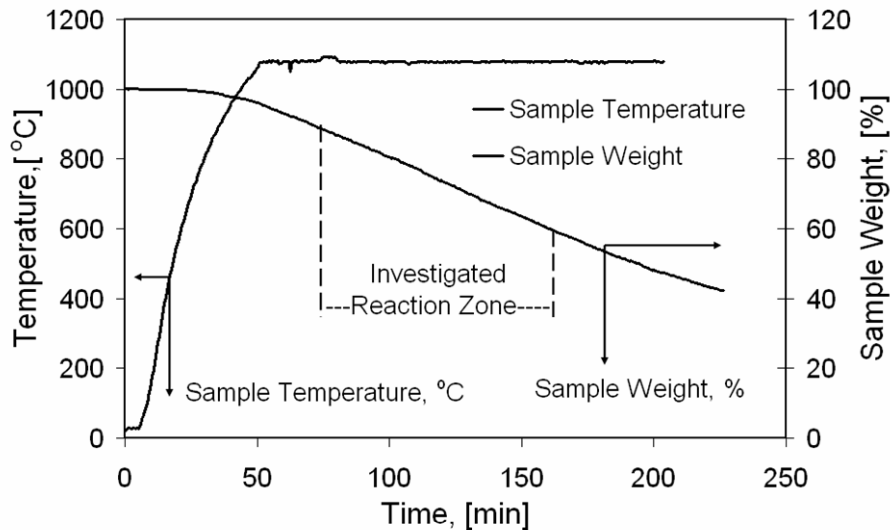


Figure 4.20: Particle temperature and weight variations with time at 1100 °C. Specimen used: Poland coke. However, in the beginning of the experiment the particle weight goes down slowly because the loss in sample weight is mainly due to vaporization of moisture content inside and is very less compared to the total mass of the sample. Therefore, this section is excluded from investigation. A section of the plot where the sample weight follows a linear decrease until the end of the experiment is considered for the investigation.

Figure 4.21 describes an experimental run using Czech coke specimen where the temperature of the furnace increase continuously from initial room temperature to the maximum temperature i.e. 1100 °C. It is shown in Fig. 4.21 the plot of weight loss vs. time changes its slope to show the effect of the reaction with an increase in temperature.

As it has already been described in previous discussion so far that the internal surface area of the given coke sample changes with degree of conversion i.e. it reaches to its maximum and decreases with total conversion of the particle henceforth. Adanez *et al.* did not find any variation in surface area as reaction advances.

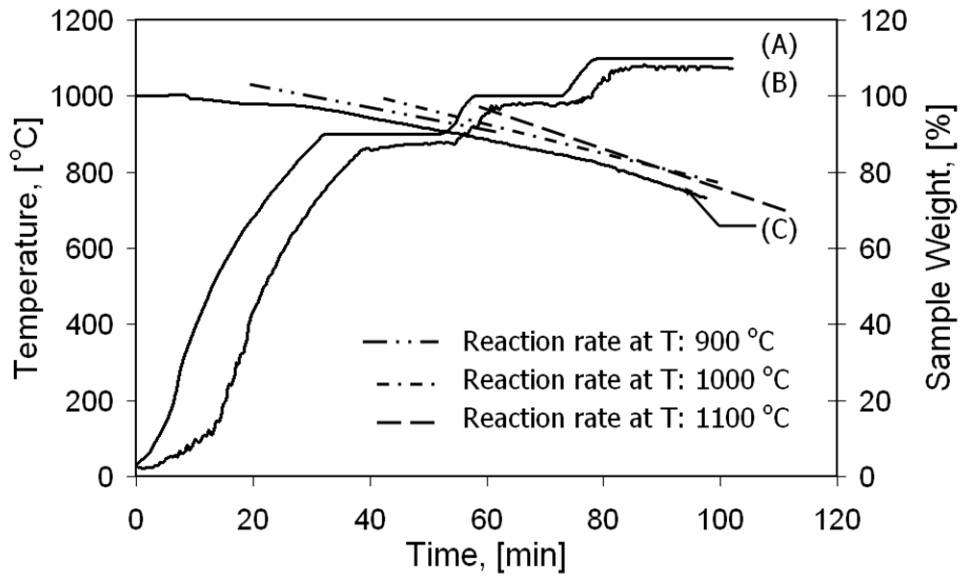


Figure 4.21: Temperature and weight loss histories of Czech coke at atmospheric pressure. Curve (A) is the profile of furnace temperature, curve (B) is the profile of sample's temperature and curve (C) is the profile of sample weight loss with time.

On the other hand, Adshiri *et al.* considered that the gasification rate is proportional to the surface area during gasification. However, the most common result is that surface area presents a maximum value, as does the reaction rate, for conversions between 20 and 60%. **Figure 4.22** describes the variation of the surface area with reaction progress.

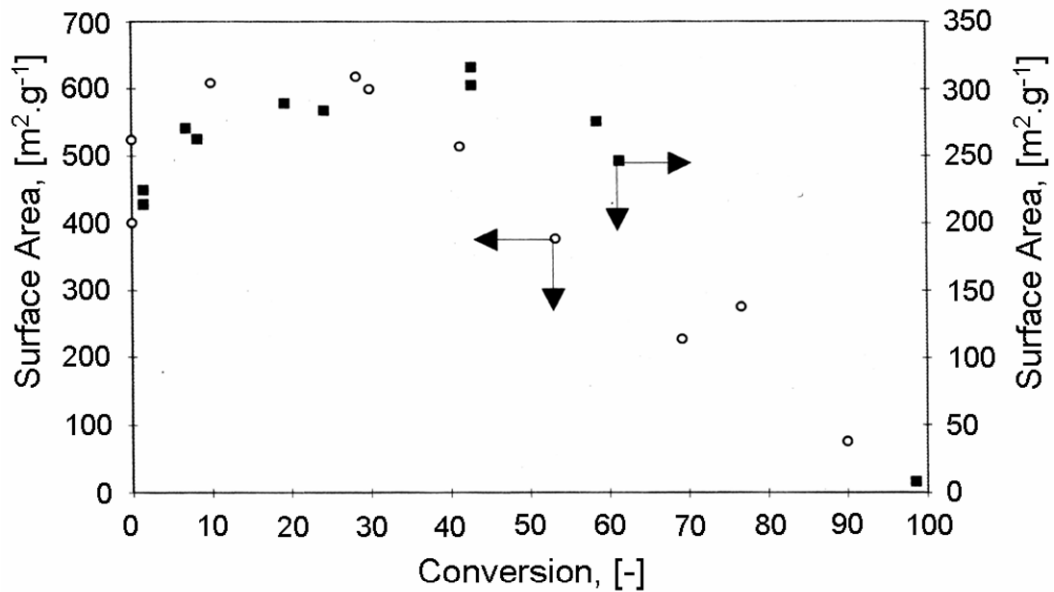


Figure 4.22: Surface area variation during the gasification with CO_2 . Empty circle points: Adschiri *et al.*, Solid rectangular points: Agarwal *et al.*

Figure 4.23 describes a qualitative comparison of the experimental results of Poland coke and Czech coke with the results found in the literature. The main purpose here is to show that during the experiment, the particle exhibits a variation of the conversion rate along the progress of the reaction and also shows a few of maximum values for a range of conversion. As shown in the Figure 4.23, Poland coke exhibits its maximum value at 20 % while the results from the literature show the maximum value at ~55% conversion.

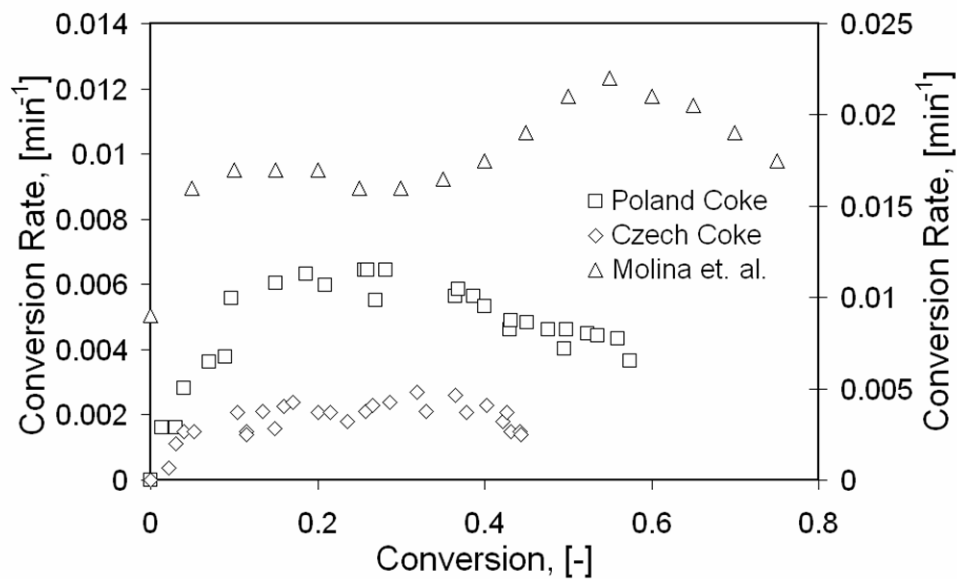


Figure 4.23: Plot of conversion rate vs. conversion. Experimental results: solid rectangles, Poland coke (left ordinate), Czech coke (left ordinate), Solid triangles (right ordinate): Molina *et al.*

While in a case of Czech coke, the conversion rate doesn't show much influence of the reaction progress. In all cases, however, the increase of the conversion rate with reaction progress to reach a maximum value and henceforth, to decrease to its minimum is qualitatively varied. Finally, some studies [Kovacik *et al.*, Matsui *et al.*, Adanez *et al.*, Schmal *et al.*] regarding coal reactivity during gasification do not consider gasification rate variation with conversion and only report the gasification rate at a specific value of conversion. Although the relationship between reaction rate and surface area has been widely studied, [Agrawal *et al.*, Dutta *et al.*, Yang *et al.*, Alvarez *et al.*, Kasaoka *et al.*, Kuo *et al.*, Hashimoto *et al.*] there is no general agreement. Chin *et al.* and Adshiri *et al.* state that reaction rate is proportional to surface area. However, most of the studies [Agrawal *et al.*, Dutta *et al.*, Yang *et al.*, Alvarez *et al.*, Kasaoka *et*

al., Kuo et al., Hashimoto et al.] found that surface area and reaction rate are not proportional.

According to new theories of gasification reaction, proportionality is rather found between reaction rate and other parameters such as active surface area [*Molina et al., Alvarez et al.*] or the total micropore volume [*Alvarez et al., Kasaoka et al.*]. However, it was not possible to measure the active surface area as well the micropore volume during the scope of this study.

Figure 4.24 illustrates a summary of the experiments carried out in the range of temperature from 900 to 1100 °C. As shown in the Fig. 4.24, there is no great influence of coke type over the reaction rate for the temperature about 900 °C.

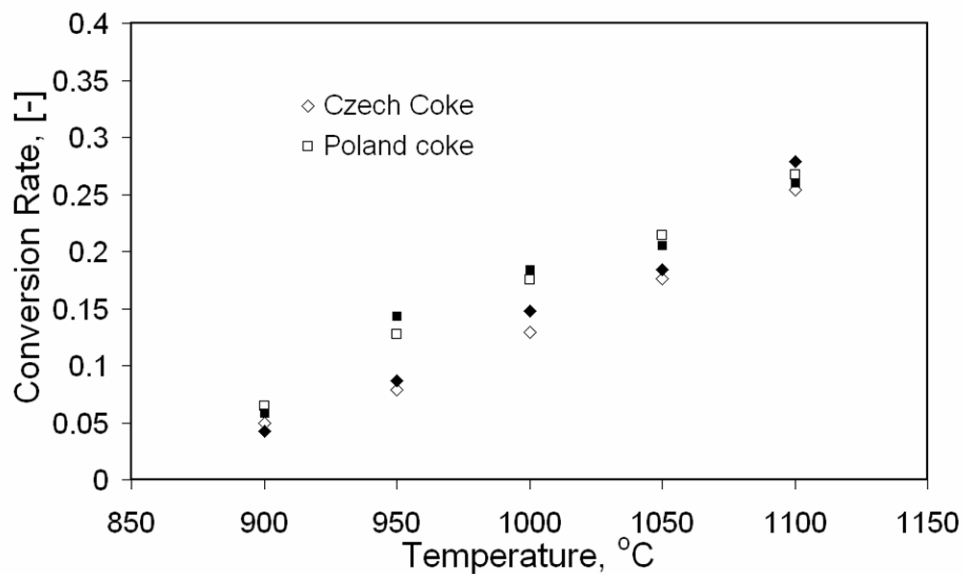


Figure 4.24: Plot of conversion rate variation with temperature. Poland and Czech coke at atmospheric pressure in an environment of CO₂. Empty and filled points correspond to two sets of experiments.

The possible reason is very slow reaction for such value of the temperature. However, with an increase in temperature also leads to an increase in reaction rate. Moreover, the difference between the values for two cokes is significant for temperature range from 950 to 1050 °C. The possible reason is the behavior of coke to react against temperature that includes that change in porous structure, total number of active sites, etc. Nevertheless for the higher values of the temperature ≥ 1100 °C the rate of gasification is too high and reaction takes place only at the surface of the particle. It can also be verified from the experimental results shown in Fig. 4.24, at temperature 1100 °C the values of reaction rate are almost same for both cokes and there is no

evidence of coke type i.e. porous structure over the reaction rate. For the temperature regime over 1100 °C, the gasification process is mass-diffusion controlled.

Figure 4.25 shows a summary of pictures of the samples taken after completion of the experiments. It can easily be visualized from surface of each sample that each of cokes and anthracite coal have their own way to behave against CO₂. At temperature 900 °C, reaction rate is too slow and can easily be visualized from smooth external surface of samples. However, with an increase in temperature, the roughness over the surface of the sample also increases.



Figure 4.25: Specimen after completion of experiments. 'A' row: 900 °C, 'B' row: 1000 °C and 'C' row: 1100 °C.

Table 4.2 illustrates a summary of apparent as well as true values of activation energies. It describes the dependence of Boudouard reaction on different types of coke. During the gasification process, the internal surface area changes and it is very difficult to measure the value of internal surface area along the progress of the reaction. As one of the experimental results, however, it has been found that the apparent values are much lower than the true value of activation energy and exhibit a lower temperature

dependency. Equation 45 is also the theoretical proof of the above statement.

$C + CO_2 \rightarrow 2CO$	
Coal Type	Activation Energy (kJ.mol ⁻¹)
Graphite	226
Poland coke	166
Czech coke	141

Table 4.2: Apparent (Poland and Czech coke) and true activation energy (Graphite) of Boudouard reaction.

4.5 Concluding Remark

The kinetic analysis based on experiments provides the values of activation energy, the pre-exponential factor of the reaction and the sorption coefficients of CO₂ and CO. The new set of activation energies, pre exponential factor and particle conversion are compared against a variety of data available in the literature. Gasification was carried out in a tubular furnace over a temperature range from 900 to 1200 °C show that except at low CO partial pressures, a nonlinear influence of CO partial pressure over the reaction rate can be recommended. Moreover, the influence of CO₂ partial pressure over the process is better described by linear approximation. Although no significant influence of temperature on the sorption coefficients of CO₂ could be observed, a weak dependency of CO sorption coefficient on the temperature was found. Furthermore, the good compatibility of results for surface related reaction coefficients has been observed for a broad range of parameter values. And finally, an approximate formula with a modification in Langmuir-Hinshelwood formulation is proposed. The new value of reaction coefficient for the Boudouard reaction will be used in the modeling of the combustion of a single coal particle which is described in the following chapters.

Chapter 5

Modeling Coal Combustion

5.1 Introduction

One of the major objectives of coal combustion research is the development of comprehensive computer models to help design combustors and gasifiers for the clean utilization of coal usually in complex burners and combustion chambers. Coal combustion is the process of combination of different processes which proceed at different rates and mutually interdependent of one-another (**Fig. 5.1**).

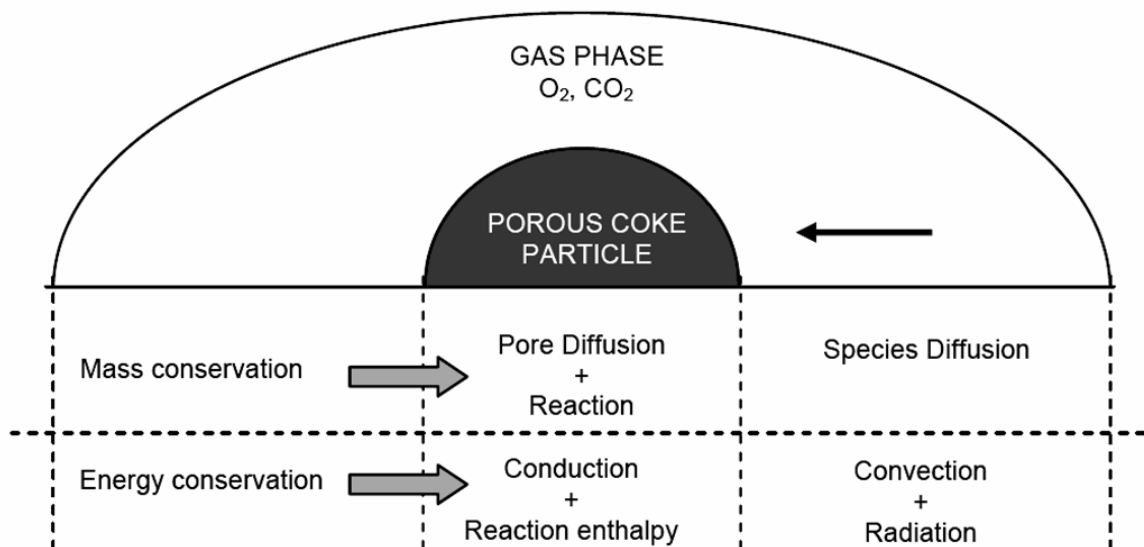


Figure 5.1: Schematic presentation of a typical combustion process of a single coal particle.

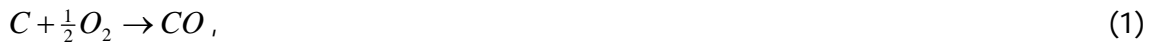
A few qualitative remarks about the combustion of coal particles are made in the previous chapters. This aspect will now be dealt with in a more general fashion following the mathematical analysis and several other significant works. In order to adequately describe the combustion of coal in a fixed or fluidized-bed or in other industrial applications, it is essential that the mechanism which governs the combustion of a single coal particle is well understood. Only limited effort has been made to resolve this problem and such mechanistic models will be detailed in this section.

First, a brief discussion will be presented of the general features and main issues which have made it difficult or even impossible to unambiguously describe the coal particle combustion phenomenon. Bywater has presented an order of magnitude time scale for the different physical and chemical operations that occur in a fluidized-bed combustor. On the other hand gas may take a relatively much shorter time around 1 sec to pass through the bed. As explained in the earlier sections, the volatiles may take typically 1-10sec to be released from the coal but may burn much faster in less than 1 sec. Borghi *et al.* found that the burn out time of char is two orders of magnitude longer than the time for the combustion of volatiles. Consequently the former controls the burning of coal in a fluidized-bed combustor. The burning of the devolatilized coal particles involves the conversion of the fixed carbon of coal into CO and CO₂. A quantitative description of this process involves complete resolution of many involved issues and these are elaborated elsewhere [Basu].

The burning rate of a char particle is controlled by the diffusion of gas from the surroundings to the char surface and is referred to as external transport. The process is characterized by the value of an effective diffusion coefficient. The actual value of effective diffusion coefficient amongst other factors will depend upon porosity and tortuosity of the voids inside the particle. The diffusion of gas through the pores inside the char and the chemical reaction on the pore walls is referred to as intrinsic reactivity. For low intrinsic reactivity the oxygen is able to travel into the interior of the char particle. For such a case, the particle size stays constant during combustion but its density decreases. On the other hand if the reaction rate is very fast, all the oxygen is consumed as it reaches the particle surface. For such a case, the density of the particle stays constant while the particle size changes.

Several workers have attempted to identify the nature of products formed at the particle surface on the basis of what is now known as the two-film model [Hougen *et al.*] or continuous film model a part of the present work. It is assumed that the oxygen

from air diffuses to the surface of the particle and reacts with the carbon of the coal to form CO and CO₂. The chemical reactions are represented in the **Figure 5.2**.



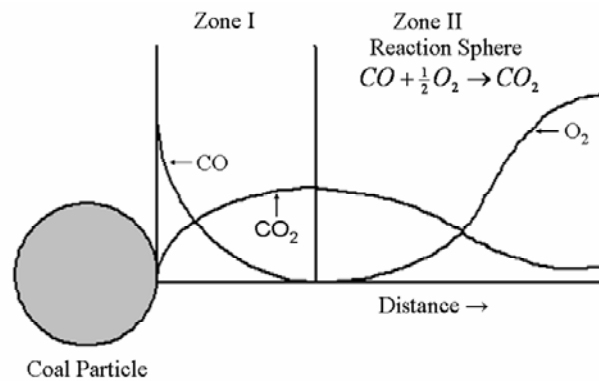
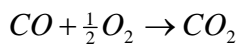
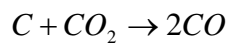
$$\Delta H = -396kJ.mole^{-1}$$



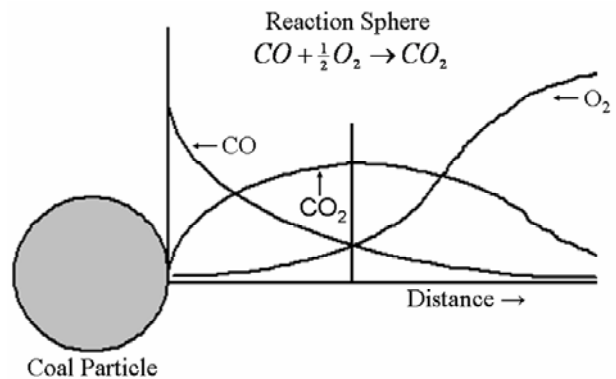
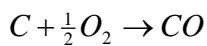
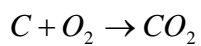
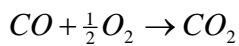
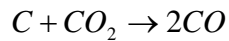
$$\Delta H = 113kJ.mole^{-1}.$$

One can conclude that the extent to which the second reaction occurs at the particle surface is negligible and predominantly the first reaction takes place.

Two Film Model:



Continuous Film Model:



	Within Particle	Particle Surface	Gas	Enthalpy
--	-----------------	------------------	-----	----------

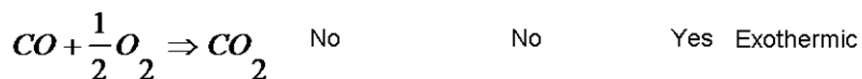


Figure 5.2: Combustion model for the burning of a coal particle: concentration profiles of different species.

CO thus formed at the interface diffuses outwards into the air stream where it reacts with the incoming oxygen to form carbon dioxide in the homogeneous gas-phase reactions,



$$\Delta H = -281kJ.mole^{-1}.$$

The burning of CO is catalyzed by the presence of traces of water vapor and, thus, its chances to escape in the gas stream are rather scarce. The burning of CO in a diffusion flame and the existence of the reaction zone has been experimentally demonstrated. Carbon di-oxide thus formed diffuses back to the particle surface to undergo the heterogeneous reduction reaction at the particle surface,



$$\Delta H = 172.5KJ.mole^{-1}.$$

CO thus generated diffuses outwards and combines with the incoming oxygen to form CO₂. The rest of the cycle repeats again and goes on and on to sustain continuous combustion. The above mentioned qualitative mechanisms of the burning of a coal particle are shown in Figure 5.2.

According to the two-film model, it is claimed that the controlling mechanism for carbon combustion will have the reactions of carbon with carbon dioxide and of carbon monoxide with oxygen which is fast enough. Under this condition, hardly any oxygen will reach to the surface of the coal particle so that the mechanism for the carbon combustion based on the stipulation of the direct oxidation of carbon will not be possible. Avedesian and Davidson developed a quantitative mathematical model for char combustion in a fluidized bed based on the above qualitative description of char particle combustion. Many researchers have argued that when the oxygen of air comes in contact with the carbon of the particle, both CO and CO₂ are produced. However, if the temperature is greater than about 923 K (the ignition temperature of CO), the CO burns in a reaction zone surrounding the particle (direct oxidation model [*Basu et al.*]). If the particle temperature is above 1373 K, CO₂ is reduced to CO on the particle's surface. *Basu et al.* mention that the direct oxidation model is relatively more valid for char combustion than the two-film model under conditions which are characterized by low particle Reynolds number and high temperatures in the range 1173-1573 K.

In order to establish the combustion mechanism for a given combustion system, it is necessary to ascertain two important facts. First, what are the combustion products on the char particle's surface? Secondly, which of the two gases, oxygen or carbon dioxide,

can preferentially diffuse to the surface? Many workers such as Meyer, Strickland-Constable, Shah, Sihvonen and Arthur have attempted to answer the first question. Arthur on the basis of his experiments on carbon burning from artificial graphite and a coal char concluded that depending upon the states of carbon and oxygen molecules both CO and CO₂ are produced. The effort of Basu *et al.* was motivated by the aim to investigate whether the conclusions drawn by Arthur and others, in connection with relative proportions of CO and CO₂ generated on the carbon particle surface under the gas flowing condition, are also valid when such particles are burned in a fluidized bed or not. Basu *et al.* examined the combustion of 1-3 mm diameter anthracite coal particles in a fluidized bed (129mm diameter) at 1123 K and for air fluidizing velocity in the range 0.2-0.3 m/sec. The experiments indicated that the primary combustion products were both CO and CO₂, and oxygen did diffuse to the carbon surface.

At about 1100 K, the diffusion coefficient of oxygen is slightly larger than that of carbon dioxide. Basu *et al.* comment: "If the oxidation rate of CO is much higher than the diffusion rate of O₂, all CO will be quickly consumed leaving the remaining oxygen to diffuse to the surface." They concluded that further experimentation is required to establish the conditions in terms of the size and temperature for transition from the two film mechanism to continuous film mechanism. Avedesian and Davidson and Campbell and Davidson computed the concentration profiles for the two-film model as shown in Fig. 5.2. They assumed that the oxidation reaction of CO (Eq. (3)) consumed all the oxygen which diffused to the carbon surface. There is contradiction to this hypothesis on two grounds. First, the reaction of Eq. (3) is not infinitely fast; and second, the endothermic reaction of Eq. (4) cannot receive sufficient heat from the reaction zone. It is, therefore, concluded that oxygen diffuses to the particle surface and the entire CO produced on it burns in a reaction zone away from the surface.

In this chapter, a mathematical model to describe the combustion of a single coal particle is presented. Combustion modeling is divided into two section i.e. gas phase modeling and solid phase modeling. An assumption of continuous film oxidation for CO is taken into consideration. In order to model solid phase which consists of a number of pores, the effective values of many physical parameter are taken into consideration. Furthermore, a mathematical model using the new values of the reaction coefficient (chapter 4) to model a special case of combustion where oxygen is not available in excess is illustrated.

5.2 Reaction Mechanism

The mechanism involved in the combustion process contains some exothermic and endothermic reactions with complicated reaction mechanisms. There are mainly three reaction involved in the combustion.

First reaction is an exothermic reaction of carbon oxidation.



First step of reaction mechanism is adsorption of oxygen on active site within the particle. There is possibility of single site as well dual site mechanism.



Second step is surface reaction between adsorbed reactant and carbon to produce adsorbed carbon mono-oxide.



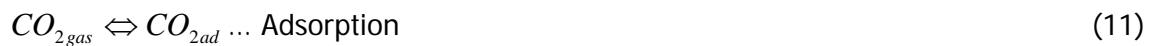
Last step is desorption of adsorbed product to ambient condition.



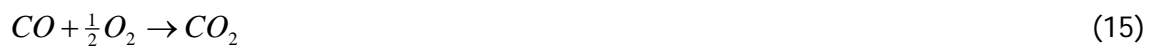
Second reaction is the endothermic reaction between carbon dioxide and carbon to produce carbon mono-oxide.



The reaction mechanism involves adsorption process followed by surface reaction and desorption respectively. This reaction takes place at particle surface due which particle surface temperature is always less than the gas temperature near the surface. The reaction mechanism as follows,



Finally, there is a homogeneous exothermic reaction of CO oxidation to produce high value of temperature.



Certain features of the kinetics of CO oxidation are reasonably well understood, but qualitatively knowledge is less than adequate for the prediction of the time required for

complete combustion. The uncertainty is particularly serious at relatively low temperatures, such as those often encountered in two stage combustion system and in automobile exhaust reactors. The effect of temperature and concentration and approach to equilibrium are in approximate agreement with a mechanism based on rate control by the forward reaction and reserve steps of reaction,



equilibrium of the reactions follows,



5.3 Gas Phase Modeling

Several mathematical models have been developed based on mechanistic details for the combustion of a coal char particle. The present mathematical model considers simultaneously the species diffusion and the reaction. According to the model, CO oxidation takes place over the whole gas boundary with non-zero concentrations of species e.g. CO, CO₂, O₂ at the surface of the particle. Model consists of mass and energy balances for these three species.

From mass balance, we can get;

$$\frac{d^2C_{O_2}}{dr^2} + \frac{2}{r} \cdot \frac{dC_{O_2}}{dr} - \left(\frac{K_v \cdot C_{H_2O}^{\frac{1}{2}} \cdot C_{O_2}^{\frac{1}{2}} \cdot C_{CO}}{2 \cdot D_g} \right) = 0 \quad (20)$$

$$\frac{d^2C_{CO}}{dr^2} + \frac{2}{r} \cdot \frac{dC_{CO}}{dr} - \left(\frac{K_v \cdot C_{H_2O}^{\frac{1}{2}} \cdot C_{O_2}^{\frac{1}{2}} \cdot C_{CO}}{D_g} \right) = 0 \quad (21)$$

$$\frac{d^2C_{CO_2}}{dr^2} + \frac{2}{r} \cdot \frac{dC_{CO_2}}{dr} + \left(\frac{K_v \cdot C_{H_2O}^{\frac{1}{2}} \cdot C_{O_2}^{\frac{1}{2}} \cdot C_{CO}}{D_g} \right) = 0 \quad (22)$$

where C_{O_2} , C_{CO_2} , C_{CO} , C_{H_2O} are the concentrations of oxygen, carbon di-oxide, carbon monoxide and water, r is the radial distance from the surface of the particle towards ambience, K_v is the reaction coefficient of homogeneous reaction between CO and O₂, and D_g is the diffusivity of the gas (this mathematical analysis presumes that diffusivity of each gas is equal to another).

Energy balance over the system yields;

$$\frac{d^2T}{dr^2} + \frac{2}{r} \cdot \frac{dT}{dr} - \left(\frac{\Delta h_v}{\rho_g \cdot c_{pg} \cdot D_g} \right) \cdot \left(K_v \cdot C_{H_2O}^{\frac{1}{2}} \cdot C_{O_2}^{\frac{1}{2}} \cdot C_{CO} \right) = 0 \quad (23)$$

where T is the temperature, Δh_v is the reaction enthalpy of exothermic oxidation of CO, ρ_v is the density of the gas and c_{pg} is the specific heat of the gaseous mixture. This mathematical model consists of a number of coupled differential equations as the reaction coefficient K_v is the strong function of temperature,

$$K_v = 1.3 \times 10^{11} \cdot \exp\left(-\frac{125,600}{R.T}\right), \text{ m}^3 \cdot \text{kmol}^{-1} \cdot \text{s}^{-1}.$$

Solution of the above described model requires a number of boundary conditions in the region between the particle's surface and ambience. Boundary conditions used are described as follows,

at particle's surface;

$$C_{O_2,S} = \frac{1}{DaH} \cdot \frac{dC_{O_2}}{dr} \quad (24)$$

$$\frac{dC_{CO}}{dr} = -2 \cdot \left\{ \left(\frac{dC_{CO_2}}{dr} \right) + \left(\frac{dC_{O_2}}{dr} \right) \right\} \quad (25)$$

$$C_{CO_2,S} = \frac{1}{DaB} \cdot \frac{dC_{CO_2}}{dr} \quad (26)$$

$$C_L \cdot \frac{dT}{dr} = - \left(\Delta h_B \cdot \frac{dC_{CO}}{dr} \right) \quad (27)$$

where,

$$DaH = \frac{K_H}{D_g}, \quad (28)$$

K_H is the reaction coefficient of the reaction between C and O₂ and given by,

$$K_H = 7.0 \times 10^5 \cdot \exp\left(-\frac{160,000}{R.T}\right), \text{ m} \cdot \text{s}^{-1} \quad (29)$$

$$DaB = \frac{K_B}{D_g}, \quad (30)$$

K_B is the reaction coefficient of Boudouard reaction between C and CO₂ and given by,

$$K_B = 3.5 \times 10^5 \cdot \exp\left(-\frac{220,000}{R.T}\right), \text{ m} \cdot \text{s}^{-1} \quad (31)$$

$C_L = L_e \cdot \rho_g \cdot c_{pg} \cdot D_g$ with L_e the Lewis number and Δh_B the enthalpy of Boudouard reaction.

At ambience,

$$C_{CO_2} = C_{CO_2\infty}, \quad (32)$$

$$C_{O_2} = C_{O_2\infty}, \quad (33)$$

$$C_{CO} = 0, \quad (34)$$

$$T=298 \text{ K}. \quad (35)$$

5.4 Simulation Results

The above described model requires lots of numerical calculations as it consists of a number of coupled differential equations those are difficult to be solved analytically. In order to solve this set of differential equations Matlab toolbox for differential equation of Boundary Value Problem is used and the solution is generated over a grid where the boundary meets the requirements.

5.4.1 Species Concentration and Gas Phase Temperature Profile

Figure 5.3 describes the profiles of species concentration and gas phase temperature along the radial distance from the particle's surface towards the ambience.

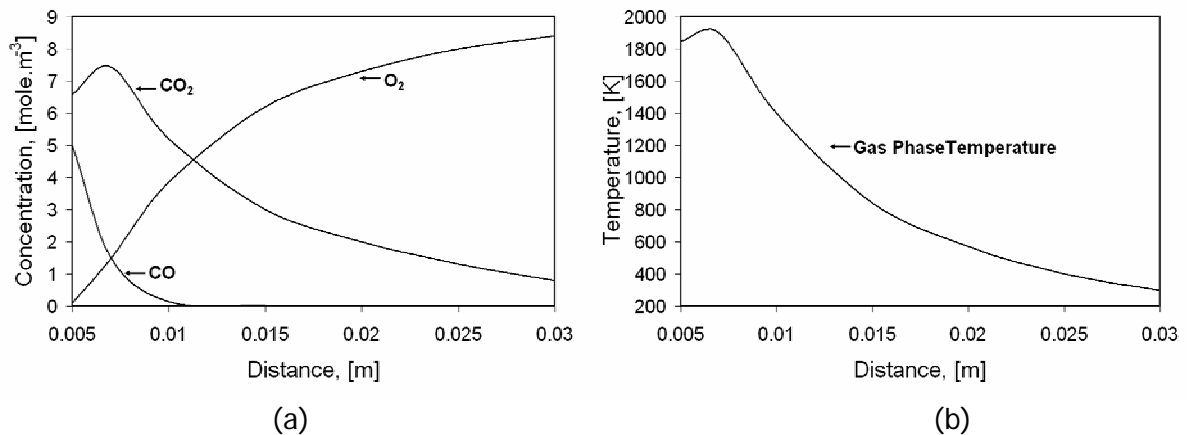


Figure 5.3: (a) Species concentration profiles along the radial distance from the particle's surface towards the ambience. (b) Gas phase temperature profile along the radial distance from the particle's surface towards the ambience.

Carbon mono-oxide has its maximum concentration at the particle surface which is because of the highly exothermic reaction of carbon with oxygen. The produced carbon mono-oxide diffuses towards the ambience and gets oxidized by oxygen to carbon dioxide. In the Fig. 5.3.a, concentration profile of CO₂ has its maximum near to the

surface. CO_2 concentration, passing through its maximum, decreases towards the particle's surface as well as to the ambience. When CO_2 reaches to the particle's surface, it reacts with carbon and produces CO which is also a major share to a maximum value of CO at the particle's surface. The concentration profile of oxygen experiences a continuous decrease towards the particle's surface. On the way towards particle's surface, oxygen experiences diffusive transport coupled with chemical reaction. Figure 5.3.b describes how the temperature of gas phase changes with radial distance from the particle's surface to the ambience. In the Fig. 5.3.b, the temperature profile has its maximum near to the particle's surface and later follows a decrease in both directions i.e. to the particle and to the ambience. In this region, there are basically two important reactions i.e. Boudouard which is highly endothermic reaction and CO oxidation which is an exothermic reaction. The maximum of the temperature near to the particle's surface is because of heat produced from CO oxidation. When CO_2 reacts with carbon i.e. Boudouard reaction, it needs heat which comes from the heat produced during CO oxidation. Simulation results are the theoretical proof of these reactions to be existed in this region where temperature has its maximum near to the particle surface and later it is decreased at the particle's surface because of the Boudouard reaction.

5.5 Solid Phase Modeling

5.5.1 Model Formulation

Combustion of solid phase is the combination of a number of processes which proceed at different rates and mutually interdependent of one-another. A single coal particle can be considered as a porous structure with pores of different size and shapes. These pores are responsible for internal diffusion resistance to the reactant when it diffuses inside the boundary of the particle. There are mainly two resistances for the reactant-resistance due to mass diffusion inside the gas layer over particle surface and internal diffusion resistance due to presence of pores. During combustion, particle surface continuously shrinks because of many heterogeneous reactions among carbon, oxygen, carbon-dioxide etc. and the process temperature changes (**Fig. 5.4**).

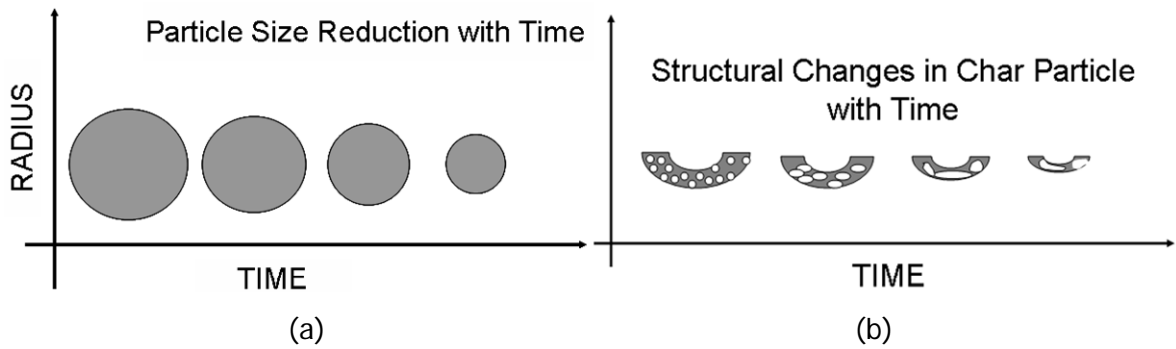


Figure 5.4: Schematic diagram of (a) the particle shrinkage with time. (b) structural change inside the particle geometry.

This results in structural change of porous structure inside the particle. As the reactant first diffuses to macro-pores at particle surface then to micro-pores connected to these macro pores, these structural changes affect the reactivity of process. **Figure 5.5** shows how the internal surface changes with the degree of conversion.

The following mathematical model accounts for the development of concentration and temperature profiles inside the particle, total time taken for complete combustion and particle conversion with time.

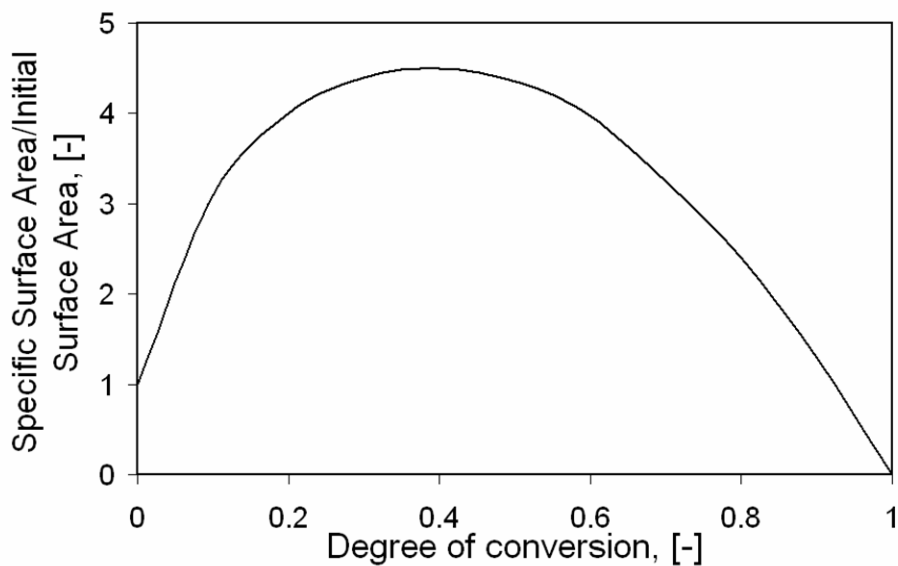


Figure 5.5: Plot: Ratio of Surface area to Initial Surface area vs. Degree of conversion.

The main equations involved are as follows;



Coal particle with spherical geometry is chosen for applying the mass and energy balances over an infinitesimal thickness inside the particle. Mass balance over infinitesimal thickness yields,

$$\frac{1}{r^2} \cdot \frac{d}{dr} \left(D_{eff} \cdot r^2 \cdot \frac{dC_i}{dr} \right) - (-r_A) = \frac{dC_i}{dt}, \quad (38)$$

$$-r_A = K_i \cdot O_m \cdot \rho_C \cdot C_i, \quad (39)$$

$$\frac{1}{D_{eff}} = \frac{1}{D_P} + \frac{1}{\left(\frac{D_G \cdot \varepsilon}{\tau} \right)}, \quad (40)$$

where r is the radial distance inside the particle, i^{th} species CO_2 and O_2 , D_{eff} is the effective diffusivity, C_i is the concentration of i^{th} species, r_A and K_i are the reaction rate and reaction coefficient of a reaction between carbon and i^{th} species, O_m is the internal surface area, ρ_C is the density of coal, ε is the porosity of the coal particle, τ is the tortuosity, D_P is the knudsen diffusivity and D_G is the gas phase diffusivity. For steady state solution of the model, equation 38 can be rewritten as following,

$$\frac{d^2C_i}{dr^2} + \frac{2}{r} \cdot \frac{dC_i}{dr} - \frac{K_i \cdot O_m \cdot \rho_C}{D_{eff}} C_i = 0. \quad (41)$$

Energy balance over this infinitesimal thickness yields,

$$\frac{1}{r^2} \cdot \frac{d}{dr} \left(K_{eff} \cdot r^2 \cdot \frac{dT}{dr} \right) = \sum (-r_A) \Delta H_i + \rho_C \cdot c_p \cdot \frac{dT}{dt}, \quad (42)$$

for steady state solution, $\frac{dT}{dt} = 0$. T is the temperature of the solid, K_{eff} is the effective thermal conductivity, ΔH_i is the enthalpy of the reaction between carbon and i^{th} species and c_p is the specific heat capacity of the coal.

The solution of above described model is bounded with a number of boundary conditions which can be described as follows,

at particle's surface,

$$\frac{dC_i}{dr} = \frac{\beta}{D_{eff}} (C_{i0} - C_i), \quad (43)$$

$$\frac{dT}{dr} = \frac{h}{K_{eff}} (T - T_s) + \frac{e \cdot \sigma \cdot (T - T_s)}{K_{eff}}, \quad (44)$$

at particle's center,

$$\frac{dC_i}{dr} = 0, \quad (45)$$

$$\frac{dT}{dr} = 0, \quad (46)$$

where β is the mass transfer coefficient, h is the heat transfer coefficient, e is the emissivity and σ is the Stefan's constant.

The value of effective thermal conductivity is calculated on basis of both the thermal conductivity of the solid as well as the gas. The mathematical equation used to calculate the value of thermal conductivity is given by,

$$\varepsilon = 0, \quad (47)$$

$$K_{eff} = K_s$$

$$\varepsilon = 0.214,$$

$$\frac{K_{eff}}{K_G} = \frac{\pi}{2\left(\frac{K_G}{K_s} - 1\right)} - \frac{\frac{\pi}{2} - \sin^{-1}\left(\frac{K_G}{K_s} - 1\right)}{\left(\frac{K_G}{K_s} - 1\right)\sqrt{2\frac{K_G}{K_s} - \left(\frac{K_G}{K_s}\right)^2}} \quad (48)$$

$$\varepsilon = 0.475$$

$$\frac{K_{eff}}{K_G} = \frac{\pi}{2\left(\frac{K_G}{K_s} - 1\right)^2} \left[\left(\frac{K_G}{K_s} - 1\right) - \ln\left(\frac{K_G}{K_s}\right) \right] + 1 - \frac{\pi}{4} \quad (49)$$

$$\varepsilon = 1$$

$$K_{eff} = K_G. \quad (50)$$

Particle shrinkage due to mass loss in heterogeneous reaction between carbon, oxygen and carbon di-oxide can easily be formulated as follows,

$$r_t = r_0 - \left(\frac{0.012 \times \sum_{i=2} K_{i,overall} \cdot C_i}{\rho_C} \cdot t \right) \quad (51)$$

particle conversion is given by,

$$X = \left(1 - \left(\frac{r_t}{r_p} \right)^3 \right), \quad (52)$$

where r_t is the instantaneous radius of coal particle, r_p is the particle radius and X is the particle conversion. The process variables used to solve the above model are given in the **Table. 5.1**.

Parameter	Equation	Unit
Reaction coefficient (carbon oxidation)	$K = 7 \times 10^5 \cdot \exp\left(-\frac{160,000}{R.T}\right)$	$\text{m} \cdot \text{s}^{-1}$
Reaction coefficient (Boudouard reaction)	$K = 5.4 \times 10^6 \cdot \exp\left(-\frac{220,000}{R.T}\right)$	$\text{m} \cdot \text{s}^{-1}$
Knudsen diffusivity	$20 \times \exp\left(-\frac{140,000}{R.T}\right)$	$\text{m}^2 \cdot \text{s}^{-1}$
Nusselt number	$Nu = 2 + 1.1 \times Re^{0.50} \times Pr^{0.33}$	[-]
Sherwood number	$Sh = 2 + 0.66 \times Re^{0.50} \times Sc^{0.33}$	[-]
Mass transfer coefficient	$\frac{sh \cdot D_G}{2 \cdot r_p}$	$\text{m} \cdot \text{s}^{-1}$
Heat transfer coefficient	$\frac{Nu \cdot K_G}{2 \cdot r_p}$	$\text{J} \cdot \text{m}^{-2} \cdot \text{K}^{-1} \cdot \text{s}^{-1}$
Overall reaction coefficient	$1 / \left\{ \left(\frac{1}{\beta} \right) + \left(\frac{1}{\sqrt{K_i \cdot \rho_C \cdot O_m}} \right) \right\}$	$\text{m} \cdot \text{s}^{-1}$

Table 5.1: Process variables used in simulation.

5.6 Simulation Results

5.6.1 Total Conversion Time

Figure 5.6 describes fractional conversion of a coal particle with a diameter of 2 cm at temperature values of 900, 1000 and 1100 °C. From the Fig. 5.6, we can easily see that as the temperature increases, the total time take for complete conversion of the coal particle decreases.

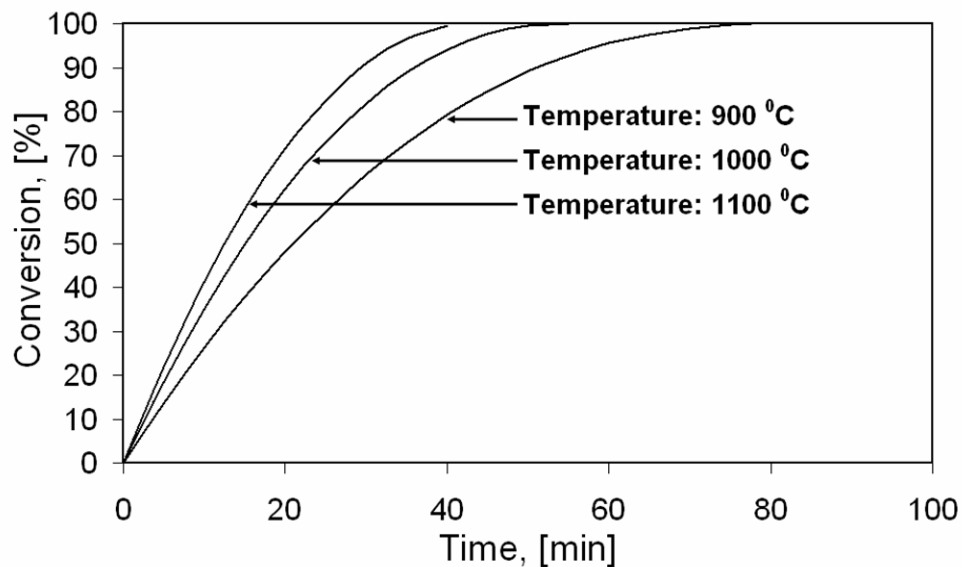


Figure 5.6: Fractional conversion of a coal particle with time. Particle diameter, 2 cm; process temperature, 900, 1000 1100 °C.

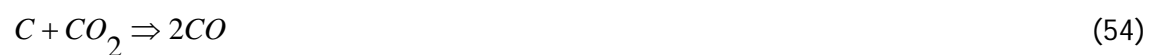
The intensity of carbon oxidation increases with temperature as the reaction coefficients are the strong function of temperature.

5.7 Mathematical Modeling for a Special Case of Combustion with Air Excess Number ≤ 1

In this section, a mathematical model for single coke particle combustion is presented especially for the cases, where oxygen concentration (air excess number ~ 1) is restricted. The model considers simultaneously the effect of both Boudouard reaction and carbon oxidation. The progressive conversion mechanism was considered for modeling, in which the particle does not contain solid components forming an ash layer.

5.7.1 Model Formulation

The single particle model describes the combustion of coke. It can be elucidated on the basis of modeling approach and conditions. It solves for the diffusive heat and mass transport coupled with chemical reaction of reactants and products in a shrinking coke sphere. Effective values of process parameters i.e. diffusivity, thermal conductivity, are used to consider the effect of internal diffusion. The reactant CO_2 and O_2 diffusing inside the particle react with carbon at active sites on the way to their transport. The reaction chemistry of the combustion process can be described by the following heterogeneous reactions:



and one homogeneous reaction



The model does not, however, take into account the homogeneous gas reaction (eq. 55) inside the particle. In this model, it has been considered that the particle is preheated sufficiently so that the moisture content present inside the particle becomes negligible. According to well known mechanism of CO oxidation [Howard *et al.*], it has been found that it is nearly impossible to oxidize CO in the absence of moisture. With a preheated particle it can be considered that CO does not get enough OH radicals to oxidize inside the porous body.

The model is based on following assumptions:

- i. the coke particle is spherically symmetric,
- ii. ash goes off from the particle surface during oxidation,
- iii. pseudo steady state particle combustion.

The governing species mass conservation equations of the particle combustion model are given by the following equation:

$$\frac{1}{r^2} \frac{d}{dr} \left(D_{eff,i} \cdot r^2 \frac{dC_i}{dr} \right) - (k_i \cdot O_m \cdot \rho_c \cdot C_i) = 0 \quad (56)$$

where i stands for both O_2 and CO_2 . In this model we have added an energy balance to take into account particle temperature variation with a possibility of an exothermic and an endothermic reaction. These temperature variations could significantly affect the conversion rates. The heat conservation equations are,

$$\frac{1}{r^2} \frac{d}{dr} \left(\lambda_{eff} \cdot r^2 \frac{dT}{dr} \right) - (k_i \cdot O_m \cdot \rho_c \cdot C_i) \cdot \Delta H_{Ri} = 0. \quad (57)$$

It has been found from experimental work done by many researchers that initially, the internal surface area increases with conversion, because of new pore openings and increase in pore diameter, to reach a maximum value and decreases henceforth. As combustion proceeds, the particle density decreases either due to a new pore opening or a change in pore diameter which leads to an increase in the gas content inside of particle despite of approximately no change in particle diameter. Furthermore, it has been reported [*Wang et al.*] that the porosity of particle has an effect on effective diffusivity i.e. a more porous particle possesses a higher diffusivity of O_2 . The overall diffusivity of O_2 follows a decrease with conversion. As a first approximation to solve these coupled differential equations (eq. 56 & 57), the value of the ratio of product of internal surface and density to effective diffusivity is considered to be a constant.

Solution of the model is bounded with simultaneous diffusive process of CO_2 and O_2 .

The boundary conditions derived from the above consideration are,

$$r = R_p \Big|_{surface}$$

$$\frac{dC_i}{dr} = \frac{\beta_i}{D_{eff,i}} (C_{\infty,i} - C_{s,i}), \quad (58)$$

$$\frac{dT}{dr} = \frac{h}{\lambda_{eff}} (T_{\infty} - T_s) + \frac{e \times \sigma \times (T_{\infty}^4 - T_s^4)}{\lambda_{eff}}, \quad (59)$$

$$r = 0 \Big|_{center}$$

$$\frac{dC_i}{dr} = 0 \quad \& \quad \frac{dT}{dr} = 0. \quad (60)$$

Overall reaction coefficient can be calculated by the following equation, which includes both the mass transfer effect and the reaction,

$$\frac{1}{k_{overall,i}} = \frac{1}{\beta_i} + \frac{1}{\sqrt{k_i \cdot O_m \cdot \rho_c \cdot D_{eff}}}. \quad (61)$$

Particle conversion can be calculated by the following equation,

$$x = \left\{ 1 - \left(\frac{r_i}{r_0} \right)^3 \right\}. \quad (62)$$

Table 5.2 consists of some parameter values used in simulation.

Parameter	Equation
Nusselt number	$Nu = 2 + 1.1 \times Re^{0.50} \times Pr^{0.33}$
Sherwood number	$Sh = 2 + 1.1 \times Re^{0.50} \times Sc^{0.33}$
Effective thermal conductivity	$\lambda_{eff} = 0.23 + 2.44 \cdot 10^6 \cdot (T - 273)^{1.7}$
Mass transfer coefficient	$\beta = \frac{Sh \cdot D}{2 \cdot R}$
Heat transfer coefficient	$h = \frac{Nu \cdot \lambda}{2 \cdot R}$
Effective diffusivity	$\frac{1}{D_{eff}} = \frac{1}{D_p} + \frac{1}{\left(\frac{D_G \varepsilon}{\tau} \right)}$
Reaction coefficient (Boudouard reaction)	$K = 5.4 \times 10^6 \cdot \exp\left(-\frac{220,000}{RT}\right), \text{ m.s}^{-1}$
Reaction coefficient (carbon oxidation reaction)	$K = 7 \times 10^5 \cdot \exp\left(-\frac{160,000}{RT}\right), \text{ m.s}^{-1}$

Table 5.2: Process parameters used in the simulation.

5.8 Simulation Results

The steady state solution of the model is discussed here. The equations (56) & (57) are complex coupled differential equations, where the process parameters i.e. diffusivity, reaction coefficients, effective thermal conductivity; are strongly influenced by the temperature. Solution of the system containing a number of algebraic equations with three coupled differential equations under described boundary conditions has been

achieved using boundary value solver (bvp4c) of Matlab-7 R13. The results given by the model are: the fractional conversion, the particle shrinkage, the variation of O_2 concentration along the radial distance inside the particle and the variation of temperature at the center of the particle with conversion.

5.8.1 Time History of Fractional Conversion and Particle Shrinkage

Figure 5.7 shows comparison of model predictions to the data available in the literature for fractional conversion of a single particle in infinite volume of O_2 and CO_2 [Kilpinen *et al.*]. The model simulation results seem to have the good agreement with experiment. One of the major problems associated with single particle combustion is the experimental measurement of particle shrinkage (r_t/r_0) with time. Figure 5.8 is also used to describe particle shrinkage with time. In Fig. 5.8 we see that the simulation results indicate very similar behavior concerning to the experimental trend. Furthermore, the model has been used to describe process simulation of combustion process where the volume of O_2 available for combustion is not infinite (air excess number~1). Thus, the question is: does the particle reaches to 100% conversion in this condition?

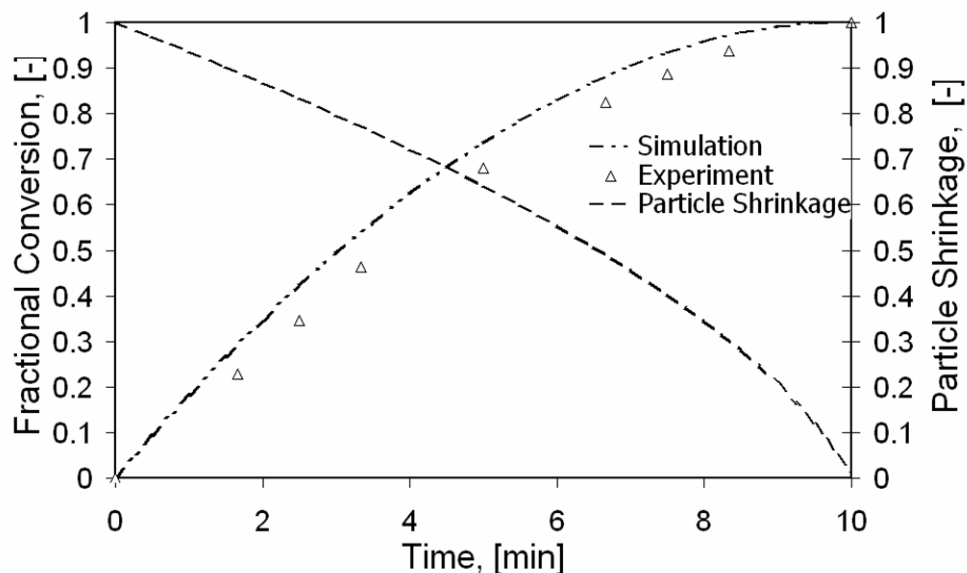


Figure 5.7: History of fractional conversion and particle shrinkage with time at ambient temperature 1123 K with 12 vol% O_2 and 10 vol% CO_2 .

5.8.2 Total Combustion Time

Figure 5.8 shows some simulation results to describe the effect of Boudouard reaction when concentration of O_2 decreases with particle conversion.

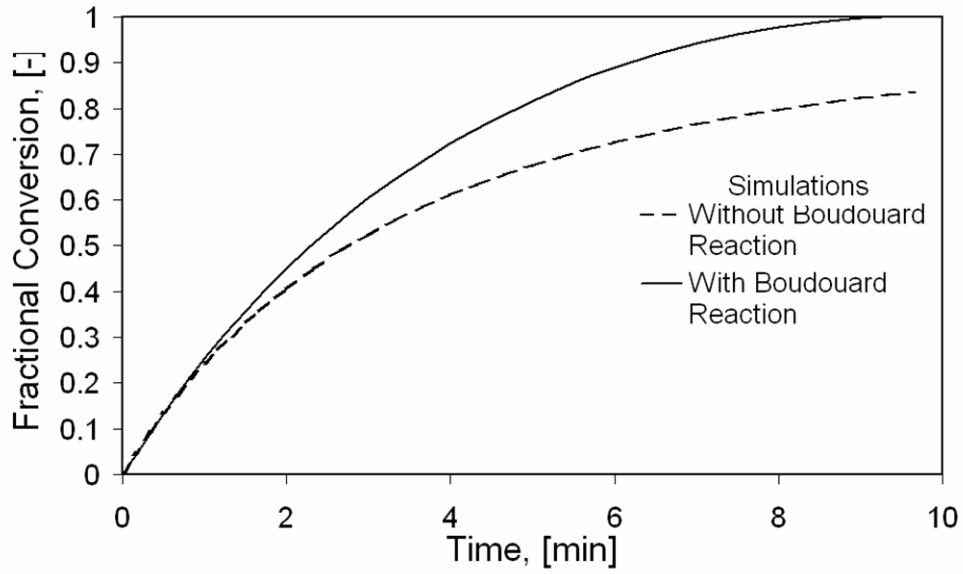


Figure 5.8: Simulation results of fractional conversion as a function of time for a particle at ambient temperature 1123 K in two different conditions: a) with Boudouard reaction, b) without Boudouard reaction.

Comparison of two different simulation results with and without the consideration of Boudouard reaction indicated that the time taken by the particle to achieve 100% conversion without considering Boudouard reaction is infinitely longer than the time it takes while considering the Boudouard reaction. It has also been experienced practically that during such operations that the particle achieves 100% conversion in a short time.

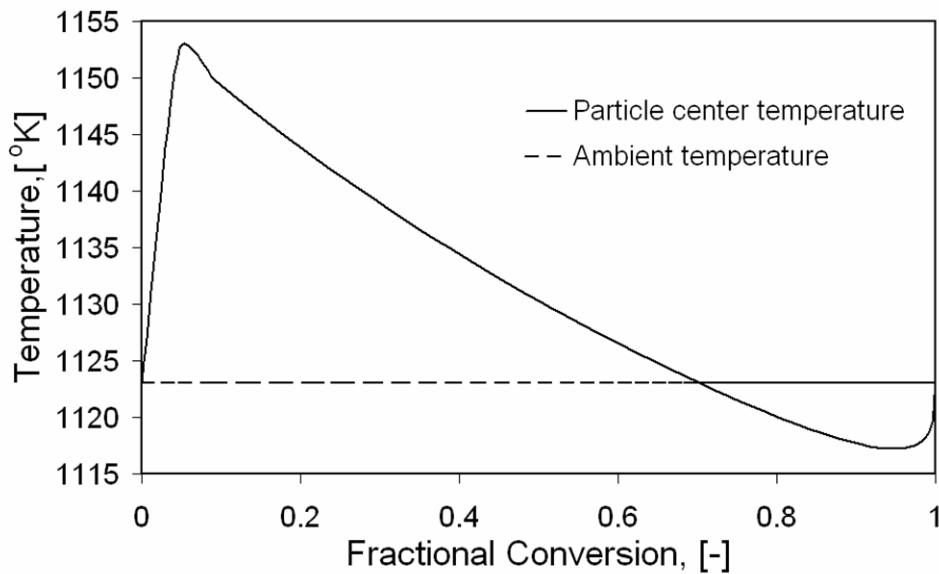


Figure 5.9: Temperature variation at particle center with fractional conversion at ambient temperature 1123 K.

5.8.3 Particle Temperature Variation

Despite the fact that the particle temperature remains approximately constant along the radial distance, it has been found that the temperature at the center of the particle changes with conversion (**Fig. 5.9**). Figure 5.9 shows how the temperature at the center of the particle changes with conversion. A temperature peak was found in the very beginning of the process due to exothermic reaction when particle comes into contact with O_2 . With an increase in particle conversion, O_2 concentration decreases while CO_2 concentration increases. At particle conversion $\sim 70\%$, it was found that the temperature at the particle center reached a value equal to the ambient temperature. Further, this value was decreased below the ambient temperature due to endothermic Boudouard reaction and increases again to the ambient value at $\sim 100\%$ conversion. It is one of the most interesting results of this simulation.

5.8.4 Oxygen Concentration Profile inside the Particle

Figure 5.10 shows O_2 concentration profiles along the radial distance inside the particle with time intervals of 40 seconds between two ensuing curves. It shows how reaction front moves inside the particle along with particle shrinkage. Simulation results explicate well the incomplete conversion of the particle when the concentration of O_2 becomes negligible and illustrate the importance of Boudouard reaction in process modeling.

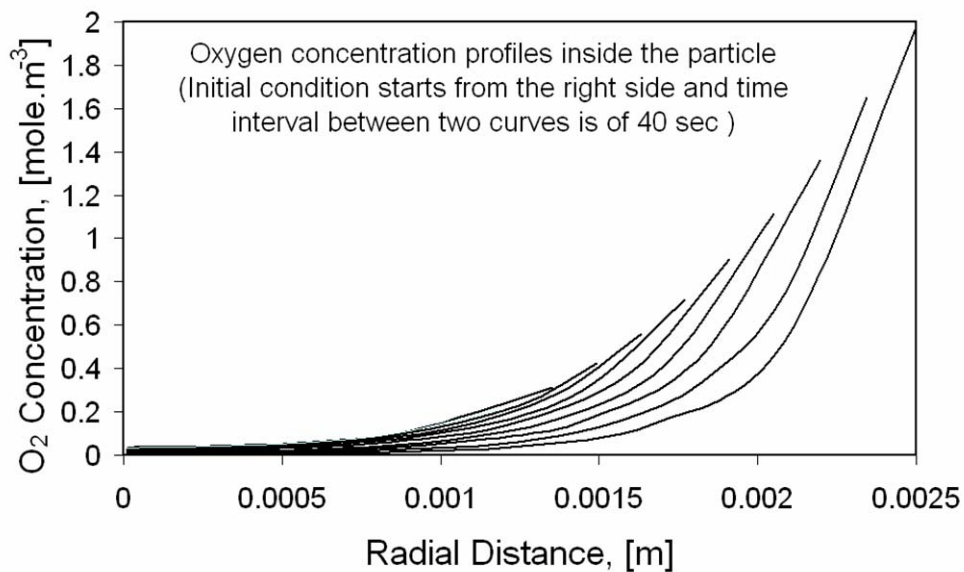


Figure 5.10: Oxygen concentration variation along the radial distance inside the particle of a diameter of 5mm at ambient temperature 1123 K.

5.9 Concluding Remark

The presented continuous film model gives a proper explication of gas phase combustion around the particle. It is verified using simulation results that CO oxidation can take place anywhere inside the boundary layer and non-zero concentrations of O₂, CO and CO₂ exist at particle surface. A possibility of Boudouard reaction to be taken place at the particle's surface is shown and explained with the help of concentration and temperature profiles along the radial distance. The effective values used to solve the mathematical model give a good approximation to the real process dynamics. From the results, it is shown that the concentration of reactant species at the center of the particle is almost zero. The model takes into consideration the possibility of heterogeneous reaction to take place inside the pores within the particle's geometry. For the special case of combustion where air excess number is approximately one, the developed single particle model predictions by taking into account the Boudouard reaction give a good agreement with the available experimental data found in the literature. Different simulations are possible by changing the particle diameter, the ambient temperature and the flow velocity of combustion gas. However, in order to develop a more comprehensive model to predict coke combustion in all conditions, the effect of conversion on internal surface and particle porosity should be considered in future formulation.

Chapter 6

Conclusions and Outlook

This work presented investigations on the behavior of a single coal particle undergoing the devolatilization and combustion. Focus was the experimental and model-based analysis of the coupled heat and mass transfer processes with a possibility of endothermic as well as exothermic heterogeneous and homogeneous chemical reactions. Models developed are shown to be suitable for describing the typical coal behavior in many industrial applications e.g. pulverized coal fired boiler, the combustion chamber to control NO emissions, etc.

Application of the quasi-steady and the transient approach for the isolated droplet combustion in the microgravity has been illustrated in details. The analytical spherically-symmetric model with consideration of unsteady behavior of oxidizer diffusion in addition to quasi steadiness for fuel vapor diffusion yields good estimations for various droplet combustion characteristics such as droplet diameter-squared, flame diameter, flame stand-off ratio, gasification rate and influence of ambient oxygen concentration on flame structure. Model validation is achieved by making simulation runs for two experimental fluids i.e. n-heptane and ethanol. The agreement between the modeling results and the experimental data available in literature is good enough to demonstrate the validity of the model. Furthermore, the behavior of d^2-t curve is similar with experimental observations (classical d^2 -law) for both testing fluids. The model is helpful to enhance the existing knowledge for efficient utilization of fuel and reduction to environmental impact. Consistency of simulation results with the experimental data illustrates that the developed analytical quasi-steady transient model is sufficient enough to describe the fundamental characteristics of single droplet combustion,

though it consists of many simplified assumptions. Finally, the assumption of quasi-steady-transient droplet combustion serves as a basis for subsequent development of the model to accommodate the effects of radiation, non-unity Lewis number, single droplet combustion for a mixture of hydrocarbons and possibility of different chemical reactions during the combustion process.

Analogical approach, based on the modeling of the liquid droplet combustion, to model the coal devolatilization is found to give a better reproduction of the dynamics of the process. The analytical model to describe the devolatilization of a coal particle consists of a few more restrictive assumptions compared to the droplet combustion. The inheritance between the solid coal particle devolatilization and spherically-symmetric droplet combustion in microgravity has been shown to be successfully implemented. Though model predictions are not compared with the experimental data due to non-availability in the literature, the qualitative analysis gives a good explanation of the process dynamics. The temperature of the particle keeps on increasing till the entire volatile matter lasts before the combustion starts. Model predictions show that during the devolatilization the particle temperature increase to a value which is required for the combustion to take place. It has also shown by model predictions that with an increase in amount of volatile matter inside the particle, it is possible to ignite the coal particle easily. Model can successfully give the reason why it is difficult to ignite anthracite coal inside the furnace with no external heating. The reason is the less amount of volatile matter in anthracite coal which is incapable to take the particle to a temperature value which is needed for the ignition. The process parameters e.g. amount of volatile matter, kinetic parameters for devolatilization, etc. used in modeling can not be generalize as these values are dependent on the type of the coal used for simulation purpose.

Potential strategies based on quasi-steady-transient approach to model devolatilization and droplet combustion are sophisticated and fast enough to give information about the dynamics of the processes. For modeling the droplet combustion and coal devolatilization, the model is solved on spatially discrete basis, but fast, hence these analytical models are successfully applied compared to complex transient models with lots of numeric computations. However, an approach of enlarging the presented model with regard to non-zero flame radius for the solution of the surface temperature of the both the droplet and coal particle may prove successful in future formulation.

Due to the crucial role of the kinetic coefficients on a model's dynamic behavior, an experimental analysis of the kinetic coefficients and the effects of the process parameters over the behavior of the coefficients have been carried out subsequently.

The new set of values of reaction and sorption coefficients for a system consists of carbon undergoing gasification in an environment of CO-CO₂-N₂ is obtained on the basis of experimental study. The kinetic analysis provides the values of activation energies and pre exponential factors which are compared to a variety of data available in the literature. Based on experimental investigation, it is concluded that except at low CO partial pressures, a nonlinear influence of CO partial pressure over the reaction rate can be recommended. Moreover, the influence of CO₂ partial pressure over the process can be better described by linear approximation. Experimental investigations implicate that Langmuir-Hinshelwood formulation should be rewritten with modification of exponent partials pressure of both CO and CO₂. Temperature dependencies of the sorption coefficients of CO₂ and CO are investigated experimentally and the mathematical expression to correlate these coefficients with temperature are formulated. Furthermore, the good compatibility of results for surface related reaction coefficients has been observed for a broad range of parameter values. The new value of reaction coefficient for the Boudouard reaction was used in the further modeling of the combustion of a single coal particle.

Focus on coal particle combustion is highlighted with the help of gas phase and solid phase modeling. An assumption of the continuous oxidation of CO over the entire gas boundary layer gives a proper explication of gas phase combustion around the coal particle. A possibility of Boudouard reaction to be taken place at the particle's surface is also shown with the help of concentration and temperature profiles along the radial distance from the particle's surface. Model takes into account a fact that the reaction takes place inside the entire geometry of the particle. The effective values of diffusivity and thermal conductivity are used for simulation purpose and it has been shown that the reaction inside the particle geometry is so high that it's simply impossible for a reactant to penetrate the particle up to its center. For the special case of combustion where air excess number is approximately one, the developed single particle model predictions by taking into account the Boudouard reaction give a good agreement with the available experimental data found in the literature. Different simulations are possible by changing the particle diameter, the ambient temperature and the flow velocity of combustion gas. The predictions of total conversion with the model seem to be in agreement with available experimental data. However, there still remains considerable uncertainty in the use of combustion models including the one used here, and are not sufficiently accurate to predict combustion process in different conditions. Although the dependency of internal surface area and porosity on temperature is not adequately

described, it is demonstrated that reasonable values of these parameters provide approximate agreement with results of experimental measurements.

The models presented in this thesis are reduced models valid for the cases of combustion where an assumption of non-existence of ash over the particle's surface exists. They exhibited short simulation times and hence pose a potential base for further development for the complex model consisting of the diffusion resistance caused by the presence of ash over the surface. However, in order to develop a more comprehensive model to predict coke combustion in all conditions, the effect of conversion on internal surface and particle porosity should be considered in future formulation. Nonetheless, this thesis also showed that the possibility of Boudouard reaction in many industrial applications can not easily be eliminated or even used for improving the performance.

Nomenclature

O_2	Oxygen
CO	Carbon mono-oxide
CO_2	Carbon di-oxide
T_0	Initial temperature of droplet
T	Temperature
q	Amount of heat transferred from the flame interface to the droplet
r	Radius
λ	Thermal conductivity
M	Mass flow rate of the vapor
ΔH	Heat of vaporization
cp	Specific heat of liquid
m_d	Mass of the droplet
ρ	Density of the liquid fuel
t	Time
d_0	Initial droplet diameter
d_t	Time dependent droplet diameter
K	Gasification rate
$P_{v,s}$	Vapor pressure of pure liquid
P	Total pressure
T_{df}	average temperature between the droplet surface and the flame interface
$D_{f,g}$	Diffusion coefficient of the fuel vapor
N	Molar flow rate of the fuel vapor
K_{v0}	Pre-exponential factor
E_v	Activation energy
$-$	Rate of adsorption/desorption of f^{th} species
n	
K_j	Coefficient of adsorption/desorption of f^{th} species
θ	Fraction of the surface covered by f^{th} species
\rightarrow	Reaction coefficient of the forward reaction
K	
\leftarrow	Reaction coefficient of the backward reaction
K	
\rightarrow	Rate of forward reaction
n	
\leftarrow	Rate of backward reaction
n	
n_C	Molar flow rate of the carbon
\overline{M}_i	Molecular mass of f^{th} species
A_p	Surface area of the plate
β	Mass transfer coefficient
ν	Stoichiometric coefficient
K_B	Reaction coefficient of Boudouard reaction
K_{CO_2}	Sorption coefficient of CO_2
K_{CO}	Sorption coefficient of CO
x	Conversion
W	Weight
O_m	Internal surface area

D_{eff}	Effective diffusivity
ρ_c	Density of carbon
C	Concentration

Subscript

∞	Ambient value
f	Flame interface
s	Droplet surface
l	Liquid
g	Gas
v	Vapor
$f-p$	flame interface to the particle surface
ad	Adsorption
de	Desorption

Bibliography

- [1] Abramzon B. and Sirignano W.A., *Droplet vaporization model for spray combustion calculations*, *Int. J. Heat Mass Transfer* 32 (1989), pp. 1605.
- [2] Adanez T., Fuertes A.B., Pis J.J. and Ehrburger P., *Reactivity of lignite chars with CO₂, influence of the mineral matter*, *Int. Chem. Eng.* 33 (1993), pp. 656.
- [3] Adchiri T., Shiraha T., Kojima T. and Furuzawa P., *Prediction of CO₂ gasification rate of char in fluidized bed gasifier*, *Fuel*, 65 (1986), pp. 1688.
- [4] Agrawal A.K. and Sear J.T., *The Coal Char Reactions with CO₂-CO Gas Mixtures*, *Ind. Eng. Chem. Process. Des. Dev.* 19 (1980), pp. 364.
- [5] Alvarez T., Fuertes A.B., Pis J.J. and Ehrburger P., *Influence of coal oxidation upon char gasification reactivity*, *Fuel* 74 (1995), pp. 729.
- [6] Annamalai K. and Ramalingam S.C., *Group combustion of char/carbon particles*, *Combustion and Flame* 70 (1987), pp. 307.
- [7] Anthony D.B. and Howard J., *Rapid Devolatilization and Hydrogasification of Bituminous Coal*, *AIChE J.* 22 (1976), pp. 625.
- [8] Arthur J. R., *Reaction between carbon and oxygen*, *Trans. Faraday Soc.* 47 (1951), pp. 164.
- [9] Austin L.G. and Walker P.L., *Effect of Carbon Mono-oxide in Causing Non Uniform Gasification of Graphite by Carbon Dioxide*, *AIChE J.* 9 (1963), pp. 303.
- [10] Avedsian M. M. and Davidson J. F., *Combustion of carbon particles in a fluidized bed*, *Trans. Inst. Chem. Engg.* 51 (1973), pp. 121.
- [11] Badzioch S. and Hawksley P.G.W., *Kinetics of thermal decomposition of pulverized coal particles*, *Ind. Eng. Chem. Process Des. Dev.* 9 (1970), pp. 521.
- [12] Baldea A. and Niac G., *Kinetics of Lignite Char Gasification with Carbon Dioxide and Steam*, *Revue Roumaine de Chimie* 29 (1984), pp. 175.
- [13] Ballal G. and Zygourakis K., *Gasification of Coal Chars with Carbon dioxide and Oxygen*, *Chem. Eng. Commun.* 49 (1986), pp. 181.
- [14] Basu P., *A review of combustion of single coal particles in fluidized beds*, *Trans. CSME* 9 (1985), pp. 142.
- [15] Basu P., Broughton J. and Elliot D. E., *Combustion of single coal particles in fluidized beds*, *Fluidized Combustion, Inst. Fuel Symp.*, 1 (1975), AD-1 to AD-10.

- [16] Basu P., *Combustion of coal in shallow fluidized beds*, Ph.D. Thesis, University of Aston. Birmingham, 1976.
- [17] Beck N.C. and Hayhurst A.N., *A mathematical model for the **combustion** in air of a single entrained spherical coal*, *Combust. Flame* 79 (1990), pp. 47.
- [18] Beyer H.D., Pückoff U. and Ulrich K.H., *Investigation of Gasification of Coke by a mixture of CO-CO₂ (in german)*, *Archiv für das Eisenhüttenwesen* 43 (1972), pp. 597.
- [19] Blackwood J.D. and Ingeme A.J., *The Reaction of Carbon with Carbon Dioxide at High Pressure*, *Aust. J. Chem.* 13 (1960), pp. 194.
- [20] Borghi G., Saroeim A. F. and Beer J. M., *A model of coal devolatilization and combustion in fluidized bed*, Paper. No. 34c, presented at the A.I.Ch.E. 70th Annual Meeting, New York, 1976.
- [21] Bressan L. and Okeefe L., *Piemsa IGCC Project Environmental and Economical Benefits*, Gasification Technologies Conference, San Francisco, CA, USA, 2001, pp. 7.
- [22] Buttker B, Seifert W., *Syngas and fuel gas from gasification of coal and wastes at Schwarze Pumpe (SVZ) - Germany*. In: 21st world gas conference, Nice, France, 6-9 Jun 2000. Vevey, Switzerland, International Gas Union, 2000, pp. 7.
- [23] Bywater R. J., *The effects of devolatilization kinetics on the injection region of fluidized beds*, *Proc. 6th Int. Conj. Fluidized Bed Combust.*, 3 (1980), pp. 1092.
- [24] Campbell E. K. and Davidson J. F., *The combustion of coal in fluidized beds*, *Fluidized Combustion, Proc. Inst. Fuel Symp.*, Fluidized Combustion Conference, London, September 1975, AZ-I.
- [25] Carslaw H.S. and Jaeger J.C., *Conduction of Heat in Solids*, Oxford University Press, New York, Second Edition, 1959.
- [26] Cavalli L., Laezza G., Biliato G. and Amico F., *The Sulcis IGCC project. In: Gasification 4: the future, proceedings, Noordwijk*, The Netherlands, Rugby, UK, Institution of Chemical Engineers, 2000, pp. 8.
- [27] Cheng H., Reiser B.D. and Dean S., *On the Mechanism and Energies of Boudouard Reaction at FeO (1 0 0) Surface: 2CO→C+CO₂*, *Catalysis Today* 50 (1999), pp. 579.
- [28] Chin G., Kimura S., Tone S., and Otake T., *Gasification of coal char with steam. Part 1. Analysis of reaction rate*, *Int. Chem. Eng.* 23 (1983), pp. 105.
- [29] Cho S.Y. and Dryer F.L., *A numerical study of the unsteady burning behaviour of n-heptane droplets*, *Combust. Theory Model.* 3 (1999), pp. 267.

- [30] Cho S.Y., Yetter R.A. and Dryer F.L., *A computer model for one-dimensional mass and energy transport in and around chemically reacting particles, including complex gas-phase chemistry, multicomponent molecular diffusion, surface evaporation, and heterogeneous reaction*, *J. Comput. Phys.* 102 (1992), pp. 160.
- [31] Choi M.Y., Dryer F.L. and Haggard J.B., *Extinction of a Free Methanol Droplet in Microgravity*, *Proc. Combust. Inst.* 23 (1990), pp. 1597.
- [32] Chukhanov Z.F. and Izvest Z.F., *Chem. Abst.* 49 (1955), pp. 5808.
- [33] Collodi G., Commercial Operation of ISAB Energy and Sarlux IGCC, Gasification Technologies Conference, San Francisco, CA, USA, 2001, pp. 7.
- [34] Dutta S., Wen C.Y. and Belt R.J., *Reactivity of Coal and Char. 1. In Carbon Dioxide Atmosphere*, *Ind. Eng. Chem. Process. Des. Dev.* 16 (1977), pp. 20.
- [35] Elcogas. IGCC Puertollano Power Plant. Puertollano, Spain, Elcogas, 2001, pp. 29.
- [36] Ergun S., *Kinetics of the Reaction of Carbon Dioxide with Carbon*. *J. Phys. Chem.* 60 (1956), pp. 480.
- [37] Faeth G.M., *Evaporation and Combustion of Sprays*, *Prog. Energy Combust. Sci.* 9(1983), pp. 1.
- [38] Faeth G.M., *Mixing, Transport and combustion in sprays*, *Prog. Energy Combustion. Sci.* 13(1987), pp. 293.
- [39] Filho F.F., *An Analytical Solution for the Quasi-Steady Droplet Combustion*, *Combust. Flame* 116 (1999), pp. 302.
- [40] Fuchs W. and Yavorsky P. M., *Symposium on Structure and Reactivity of Coal and Char, 170th National Meeting of the American Chemical Society*, Chicago, August 1987.
- [41] Geertsema, Gas to Synfuels and Chemicals, Sasol Technology (pty) Limited, P. O. Box 1, Sasolburg 9570, South Africa.
- [42] Godsave G.A.E., *Studies of the combustion of drops in a fuel spray*, *Proc. Combust. Inst.* 4 (1953), pp. 818.
- [43] Godsmith M. and Penner S.S., *On the Burning of Single. Drops of Fuel in an Oxidizing Atmosphere*, *Jet Propulsion* 24 (1954), pp. 245.
- [44] Goldberg, P.M. and Essenhigh, R.H., *Proc. Combust. Inst.* 17 (1979), pp. 145.
- [45] Graaf J.D., *The Shell Gasification Process at the AGIP Sannazzaro Refinery*, Gasification Technologies Conference, San Francisco, CA, USA 2001, pp. 7.
- [46] Grabke H.J., *Oxygen Transfer and Carbon Gasification in the Reaction of Different Carbons with CO₂*, *Carbon* 10 (1972), pp. 587.

- [47] Grabke, H.J.; Krajak, R.; Nava Paz, J.C. On the Mechanism of Catastrophic Carburization: 'Metal Dusting'. *Corrosion Sci.* 1993, 35, 1141.
- [48] Grace, J.R., Avidan A.A., and Knowlton, T.M. (eds.), *Circulating Fluidized Beds*, Blackie Academic & Professional, London, 1997.
- [49] Green S., Puertollano Prepares for Syngas Operation. *Mod Power System* 1997, pp. 49.
- [50] Gurgel Veras A., SaasTamoinen J., Carvalho J.A. JR. and Aho M., *Combustion and Flame* 116 (1999), pp. 567.
- [51] Gururajan V.S., Wall T.F. and Truelove J.S., *Combust. Flame* 72 (1988), pp. 1.
- [52] Hara H. and Kumagai S., *The Effect of Initial Diameter on Free. Droplet Combustion with Spherical Flame, Proc. Combust. Inst.* 23 (1990), pp. 1605.
- [53] Hashimoto K., Miura K. and Ueda T., *Factors Affecting the Reactivity of Coal, Fuel* 65 (1986), pp. 1516.
- [54] Hirato M., Utilization System of Biofuel and Coal Gasification Power Generation. vol. 38. Tokyo, Japan: Chemical Daily Co., 1991. No.14.
- [55] Hougen O.A. and Watson K.M., *Chemical process principles, Part III, Kinetics and Catalysis.*, John Wiley, New York, 1947.
- [56] Howard J.B. and Essenhigh R.H., *Pyrolysis of Coal Particles in Pulverized Fuel Flames, Ind. Eng. Chem. Process Des. Dev.* 6 (1967), pp. 74.
- [57] Howard J.B. and Essenhigh R.H., *Combustion Mechanism in Pulverized Coal Flames, Proc. Combust. Inst.* 11 (1966), pp. 399.
- [58] Howard J.B., Williams G.C. and Fine D.H., *Physical Mechanisms in Carbon Formation in Flames, Proc. Combust. Inst.* 14 (1973), pp. 975.
- [59] *IEA World Energy Outlook*, International Energy Agency, Paris, 1998.
- [60] Jost M.E., Leslie I. and Kruger C., *Proc. Combust. Inst.* 20 (1984), pp. 1531.
- [61] Kaczorowski J., "The Boudouard Reaction in Mn-alloy Production Processes", International seminar in materials processing, November-2003.
- [62] Kasaoka S., Sakata Y. and Shimada M., *Importance of Carbon Active Sites in the Gasification of Coal Chars, Fuel* 66 (1987), pp. 697.
- [63] Kassooy D.R. and Williams F.A., *Variable Property Effects in Liquid Droplet Combustion, AIAA Journal* 6 (1968), pp. 1961.
- [64] Kilpinen P., Kallio S., Konttinen J. and Barisic. V., *Char-nitrogen oxidation under fluidised bed combustion conditions: single particle studies, Fuel* 81 (2002), pp. 2349.

- [65] King M.K., *An unsteady-state analysis of porous sphere and droplet fuel combustion under microgravity combustion, Proc. Combust. Inst.* 26 (1996), pp. 1961.
- [66] Kobayashi H., Howard J.B. and Sarofim A.F., *Coal Devolatilization at High Temperatures, Proc. Combust. Inst.* 16 (1976), pp. 411.
- [67] Kovacic G., Chambers A., *Catalytic gasification kinetics of low activity anthracites with carbon dioxide--Isothermal thermo-gravimetric analysis, The Canadian Journal of Chem. Eng.* 69 (1991), pp. 311.
- [68] Kumagai S. and Isoda H., *Combustion of fuel droplets in a falling chamber, Proc. Combust. Inst.* 6 (1957), pp. 726.
- [69] Kumagai S., Sakai T. and Okajima S., *Combustion of free fuel droplets in a freely falling chamber, Proc. Combust. Inst.* 13 (1971), pp. 779.
- [70] Kuo K. and Marsh H., *Fundamental Issues in Control of Carbon Gasification Reactivity, ACS, Div. Fuel Chem. Preprints* 34 (1989), pp. 153.
- [71] Lau C.W. and Niksa, S., *The combustion of individual particles of various coal types, Combust. Flame* 90 (1992), pp. 45.
- [72] Law C.K., *Recent Advances in Droplet Vaporization and Combustion, Prog. Energy Combust. Sci.* 8 (1982), pp. 171.
- [73] Law C.K., *Unsteady droplet combustion with droplet heating, Combust. Flame* 26 (1976), pp. 17.
- [74] Löwe, A. Zum reaktionsmechanismus der vergasung von kohlenstoff mit kohlendioxid-I: Elementarschritte und aktivierungsenergien bei gültigkeit einer langmuir-hinshelwood-kinetik. *Carbon* 12 (1974), pp. 335.
- [75] Lowry H.H. (ed.), *Chemistry of Coal Utilization*, John Wiley, New York, 1945.
- [76] Marchese A.J., Dryer F.L., and Nayagam V., *Numerical Modeling of Isolated N-Alkane Droplet Flames: Initial Comparisons with Ground and Space-Based Microgravity Experiments, Combust. Flame* 116 (1999), pp. 432.
- [77] Matsui I., Kunii D. and Furuzawa T., *Study of char gasification by carbon dioxide. 1. Kinetic study by thermogravimetric analysis, Ind. Eng. Chem.* 26 (1987), pp. 91.
- [78] Mayer R., Der Mechanismus der Primärreakteion Zwischen Sauerstoff und Graphit, *Z. Phvsikal. Chem.* 17 (1932), pp. 385.
- [79] Mendes-Vigo I., *Operational experience of the Puertollano IGCC plant. International conference on clean coal technologies for our future, Cagliari (Sardinia), Italy, London, UK, IEA Clean Coal Centre, CD-ROM, 2002, pp. 25.*

- [80] Mendez-Vigo I., Pena F.G., Karg J., Haupt G. and Zimmermann G., Puertollano IGCC plant: operating Experience and Potential for Further Technology Development Power-Gen Europe, Brussels, Belgium, 2001, pp. 13.
- [81] Molina A. and Mondragon F., *Reactivity of Coal Gasification with Steam and CO₂*, *Fuel* 77 (1998), pp. 1831.
- [82] Montoya A., Mondragon F. and Truong N. T., *CO₂ Adsorption on Carbonaceous Surfaces: A Combined Experimental and Theoretical Study*, *Carbon* 41 (2003), pp. 29.
- [83] Morita Y. Marketability of GTL from Natural Gas, IEEJ, 2001, Sinor Consultants, edj.net/sinor/sfrl.
- [84] Okajima S. and Kumagai S., *Combustion of free fuel droplets in a freely falling chamber*, *Proc. Combust. Inst.* 15 (1975), pp. 401.
- [85] Overholser L. G. and Blakely J. P., *Oxidation of Graphite by Low Concentrations of Water Vapor and Carbon Dioxide in Helium*, *Carbon* 2 (1965), pp. 385.
- [86] P. L. Walker, R. J. Forsti and C.C. Wright, *Effect of Gas Diffusion in Graphitized Carbon Rods on their Gasification Rate with Carbon Dioxide*, *Ind. and Eng. Chem.* 45 (1953), pp. 1703.
- [87] Pena F.G., Coal and Petroleum Coke IGCC Puertollano, The Use of Coal in Mixture with Wastes and Residues, II EU seminar, Cottbus, Germany, 2000, pp. 159.
- [88] Perry R.H. and Green D.W., *Perry's Chemical Engineers' Handbook*, seventh ed., McGraw-Hill, New York, 1997.
- [89] Ploeg J.E.G., Gasification performance of the Demkolec IGCC. In: Gasification 4: the future, proceedings, Noordwijk, The Netherlands, Rugby, UK, Institution of Chemical Engineers, 2000, pp. 11.
- [90] Puri I.K. and Libby P.A., *The Influence of Transport-Properties on Droplet Burning*, *Combust. Sci. Technol.* 76 (1991), pp. 67.
- [91] Rao Y.K. and Jalan B.P., *A Study of the Rates of Carbon-Carbon Dioxide Reaction in the Temperature Range 839 to 1050 °C*, *Metallurgical Transactions* 3 (1972), pp. 2465.
- [92] Reid R.C., Prausnitz J.M. and Poling B.E., *The Properties of Gases and Liquids*, fourth ed., McGraw-Hill, New York, 1995.
- [93] Saastamoinen J. J., Aho M. J. and Linna V. L., *Ash formation in circulating fluidised bed combustion of coal and solid biomass*, *Fuel* 72 (1993), pp. 599.

- [94] Saito M., Sadakata M. and Sakai T., *Swelling behaviour of individual coal particles in the single particle reactor*, *Combust. Sci. Technol.* 51 (1987), pp.109.
- [95] Saxena S. C., *Devolatilization and combustion characteristics of coal particles*, *Prog. Energy Combust. Sci.* 16 (1990), pp. 55.
- [96] Schellberg W., Project Status of the Puertollano IGCC Plant/Spain, Gasification 4-ICHEME conference, Noordwijk, Netherlands, 2000, pp. 11.
- [97] Schellberg W., The Combined Cycle Power Plant in Puertollano/Spain, 14th Annual International Pittsburgh Coal Conference, Taiyuan, China, 1997, pp. 11.
- [98] Schmal M., Monteiro J.L.F. and Toscani H., *Kinetics of coal gasification*, *Ind. Eng. Chem. Proc. Des. Dev.* 22 (1983), pp. 563.
- [99] Sendin U., Gasc M., Schellberg W. and Karg J., Design Construction and Start-Up of the Puertollano 335 MW IGCC Power Plant", EPRI Gasification Conference, San Francisco, CA, USA, 1996, pp. 19.
- [100] Shah M. S., *The combustion of charcoal in oxygen, nitric oxide and nitrous oxide, II: The effect of temperature*, *J. Chem. Soc.* 132 (1929), pp. 2676.
- [101] Shell International Petroleum, The Evolution of the World's Energy System, Shell International Petroleum Company, London, 1996, pp. 1860.
- [102] Sibvonen V., *Über Primarvorgänge Bei der Graphitoxydation*, *Zetsche Electrochemics* 76 (1934), pp. 456.
- [103] Sirignano W.A., *Formulation of spray combustion models: resolution compared to droplet spacing*, *J. Heat Transfer* 108(3) (1986), pp. 633.
- [104] Solomon P.R., Fletcher T.H. and Pugmire R.J., *Progress in coal pyrolysis*, *Fuel* 72 (1993), pp. 587.
- [105] Sorensen L.H., Biedeg O. and Peck R.E., *A Model of the Coal Reburning Process*, *Proc. Combust. Inst.* 25 (1994), pp. 475.
- [106] Spalding D. B., *The combustion of liquid fuels*, *Proc. Combust. Inst.* 4 (1952), pp. 847.
- [107] Spence J., API Energia IGCC Plant Status, Gasification Technologies Conference, San Francisco, CA, USA, October, 2000, pp. 9.
- [108] Stephen N., *Diffusion in packed beds of porous particles*, *AIChE* 34 (1988), pp. 790.
- [109] Stmckland R. F., *Part played by surface oxides in the oxidation of carbon*, *Trans. Faraday Soc.* , 1938, pp. 1074.
- [110] Strange J. F. and Walker P. L., *Carbon-Carbon Dioxide Reaction: Langmuir-Hinshelwood Kinetics at Intermediate Pressures*, *Carbon* 14 (1976), pp. 345.

- [111] Struis R. P. W. J., Scala C., Stucki S. and Prins R., *Gasification Reactivity of Charcoal with CO₂. Part I: Conversion and Structural Phenomena*, *Chemical Engineering Science* 57 (2002), pp. 3581.
- [112] Suuberg E.M., Peters W.A. and Howard J.B., *Product Composition and Kinetics of Lignite Pyrolysis*, *Proc. Combust. Inst.* 17 (1978), pp. 117.
- [113] Szepvölgyi, M.; Kotsis, L.; Marosvölgyi, B. Reaction Kinetics of Miscanthus Pyrolysis Char Gasification with Carbon-dioxide. *Hungarian Agricultural Engineering* 2002, 15, 53.
- [114] Turkdogan E. T. and Vinters J. V., *Kinetics of Oxidation of Graphite and Charcoal in Carbon Dioxide*, *Carbon* 7 (1969), pp. 101.
- [115] Turns S.R., *An Introduction to Combustion: Concepts and Applications*, McGraw-Hill Series, USA, 1996, pp. 319.
- [116] Ubis T., Bressan L., The 800 MW Piensa IGCC Project, Gasification Technologies Conference, San Francisco, CA, USA, October, 2000, pp. 9.
- [117] Unger P.E. and Suuberg E.M., *Internal and external mass transfer limitations in coal pyrolysis*, *Am. Chem. Soc. Div. Fuel Chem. Prepr.* 28 (1983), pp. 278.
- [118] Unsworth, J. F., Barratt, D. J., and Roberts, P. T., *Coal Quality and Combustion Performance: An International Perspective*, Elsevier, Amsterdam, 1991.
- [119] USDoE and Gasification Technology Council, World Gasification Database 2001.
- [120] Visser W., Verbrennung einer umströmten Graphitoberfläche. Dissertation RWTH Aachen 1984.
- [121] Wang H., Dlugogorski B.Z., and Kennedy E.M., *Theoretical analysis of reaction regimes in low-temperature oxidation of coal*, *Fuel* 78 (1999), pp. 1073.
- [122] Weibiao F., Zhang Y., Han H. and Duan Y., *Study on devolatilization of large coal particles*, *Combustion and Flame*. 70 (1987), pp. 253.
- [123] Wen, C. Y.; Wu, N. T. An Analysis of Slow Reactions in a Porous Particle. *AIChE J.* 1976, 22, 1012.
- [124] Williams F.A., *Combustion Theory*, 2nd ed., Addison Wesley, Menlo Park, CA, 1985, p. 5269.
- [125] Yang J.C. and Avedisian C.T., *The combustion of unsupported Heptane/Hexadecane mixture droplets at low gravity*, *Proc. Combust. Inst.* 22 (1988), pp. 2037.
- [126] Yang Y. and Watkinson A. P., *Gasification reactivity of some western Canadian coals*, *Fuel* 73 (1994), pp. 1786.

- [127] Yoshida K. and Kunii D., *Gasification of Porous Carbon by Carbon Dioxide. J. of Chem. Eng. of Japan* 2 (1969), pp. 170.
- [128] Ziegler A., Van H.K., Klein J. and Wanzl W., *proceedings ICCS 97* (1997), Essen, Germany, pp. 1257.

Figure Index

Page

Fig. 1.1	Diagram showing the combustion process of a single coal particle. The left-hand side shows the heterogeneous steps, and the homogeneous reactions are shown on the right-hand side.	3
Fig. 1.2	Application of gasification and possible future role.	5
Fig. 2.1	Schematic diagram of a droplet combustion process.	13
Fig. 2.2	Comparison between experimental [Kumagai <i>et al.</i>] (points) and predicted (lines) data of the droplet diameter and the flame diameter variations with time. Initial conditions: n-heptane; drop diameters, (a) 0.836 mm, (b) 0.92 mm, (c) 0.98 mm; ambient temperature, 298 K; atmosphere, air at 1 atm pressure.	18
Fig. 2.3	Comparison between experimental [Kumagai <i>et al.</i>] (points) and predicted (lines) data of the droplet diameter and the flame diameter variations with time. Initial conditions: ethanol; (a) droplet diameter, 0.93 mm; ambient temperature, 298 K; atmosphere, air at 1 atm pressure; (b) droplet diameter, 0.93 mm, 2.79 mm, 3.41 mm, 5.83 mm; ambient temperature, 298 K; atmosphere, air at 1 atm pressure.	19
Fig. 2.4	Comparison of calculated gasification rate (solid lines) with the experimental results (points) of Kumagai <i>et al.</i> and the model predictions (dotted lines) of Puri and Filho. Points: solid points for n-heptane; empty points for ethanol.	20
Fig. 2.5	Calculated and measured droplet diameter-squared of Kumagai <i>et al.</i> for n-heptane and ethanol droplets in an air at 1 atm. Initial droplet diameter: n-heptane- 0.92 mm; ethanol- 0.93 mm.	21
Fig. 2.6	Variation in flame stand-off ratio for the n-heptane droplets with time. Comparison between experimental [11] (points) and predicted (lines) data for n-heptane droplets burning in atmospheric pressure air.	21
Fig. 2.7	Calculated variations in flame diameter with time for various oxygen concentrations for 0.836 mm n-heptane droplets.	22
Fig. 3.1	Schematic diagram of a single coal particle devolatilization process.	26
Fig. 3.2	Calculated variations in surface temperature of the particle with time: particle diameter: 10mm; volatile matter content: 10, 30 and 50%.	31
Fig. 3.3	Profile of flame to particle diameter ratio for an amount of volatile matter of 50%: particle diameter: (a) 10 mm, (b) 5mm and (c) 10mm.	32
Fig. 4.1	Equilibrium relationship of Boudouard reaction during reduction of iron ore.	35
Fig. 4.2	Comparison of various mass-related reaction coefficients of Boudouard reaction.	41
Fig. 4.3	Schematic diagram of the experimental setup.	44

Fig. 4.4	Specimens used in the experiments. Geometry (from left to right): cylindrical specimen of coke, plate of graphite, plate of aluminum.	45
Fig. 4.5	Comparison of sample thickness before and after the experiment: influence of higher flow rate of CO ₂ .	46
Fig. 4.6	Comparison of sample surface before and after the experiment at a temperature 1000 °C: influence of chemical reaction.	46
Fig. 4.7	Temperature-time plot of aluminum plate at different volumetric flow rates of CO ₂ .	48
Fig. 4.8	Experimental $\ln(T_p - T_g)$ vs. t plot at different volumetric flow rates of CO ₂ .	49
Fig. 4.9	Plot of variation of mass transfer coefficient with temperature.	49
Fig. 4.10	Plot of sample weight vs. time: graphite specimen at atmospheric pressure and temperatures 900, 1000, 1100 and 1200 °C.	50
Fig. 4.11	Experimental history of specimen temperature to describe the influence of endothermic Boudouard reaction.	51
Fig. 4.12	Conversion rate of graphite as a function of the temperature in an environment of CO ₂ .	52
Fig. 4.13	Comparison of experimentally found reaction coefficient with the values available in the literature: Arrhenius plot.	53
Fig. 4.14	Illustrations of the experimental runs with partial pressures of CO ₂ at different temperatures.	54
Fig. 4.15	Temperature dependency of CO ₂ -sorption coefficient on temperature.	54
Fig. 4.16	Comparison of CO ₂ sorption coefficient with the values available in the literature.	55
Fig. 4.17	Influence of CO-partial pressure over the conversion rate.	56
Fig. 4.18	Illustrations of the experimental runs with partial pressures of CO at different temperatures.	56
Fig. 4.19	Comparison of sorption coefficient with the values available in the literature.	57
Fig. 4.20	Particle temperature and weight variations with time at 1100 °C. Specimen used: Poland coke.	60
Fig. 4.21	Temperature and weight loss histories of Czech coke at atmospheric pressure. Curve (A) is the profile of furnace temperature, curve (B) is the profile of sample's temperature and curve (C) is the profile of sample weight loss with time.	61
Fig. 4.22	Surface area variation during the gasification with CO ₂ . Empty circle points: Adschiri <i>et al.</i> , Solid rectangular points: Agarwal <i>et al.</i>	61
Fig. 4.23	Plot of conversion rate vs. conversion. Experimental results: solid rectangles, Poland coke (left ordinate), Czech coke (left ordinate), Solid triangles (right ordinate): Molina <i>et al.</i>	62
Fig. 4.24	Plot of conversion rate variation with temperature. Poland and Czech	63

coke at atmospheric pressure in an environment of CO₂. Empty and filled points correspond to two sets of experiments.

Fig. 4.25	Specimen after completion of experiments. 'A' row: 900 °C, 'B' row: 1000 °C and 'C' row: 1100 °C.	64
Fig. 5.1	Schematic presentation of a typical combustion process of a single coal particle.	66
Fig. 5.2	Combustion model for the burning of a coal particle: concentration profiles of different species.	68
Fig. 5.3	(a) Species concentration profiles along the radial distance from the particle's surface towards the ambience. (b) Gas phase temperature profile along the radial distance from the particle's surface towards the ambience.	74
Fig. 5.4	Schematic diagram of (a) the particle shrinkage with time. (b) Structural change inside the particle geometry.	76
Fig. 5.5	Plot: Ratio of Surface area to Initial Surface area vs. Degree of conversion.	76
Fig. 5.6	Fractional conversion of a coal particle with time. Particle diameter, 2 cm; process temperature, 900, 1000 and 1100 °C.	79
Fig. 5.7	History of fractional conversion and particle shrinkage with time at ambient temperature 1123 K with 12 vol% O ₂ and 10 vol% CO ₂ .	83
Fig. 5.8	Simulation results of fractional conversion as a function of time for a particle at ambient temperature 1123 K in two different conditions: a) with Boudouard reaction, b) without Boudouard reaction.	84
Fig. 5.9	Temperature variation at particle center with fractional conversion at ambient temperature 1123 K.	84
Fig. 5.10	Oxygen concentration variation along the radial distance inside the particle of a diameter of 5mm at ambient temperature 1123 K.	85

Table Index

Page

Table. 1.1	Major electricity producing gasification plants by country. Source: Derived from the World Gasification Database, US DoE and Gasification Technology Council [<i>USDoE and Gasification Technology Council</i>].	6
Table. 4.1	Summary of activation energies of carbon-carbon dioxide reaction.	36
Table. 4.2	Apparent (Poland and Czech coke) and true activation energy (Graphite) of Boudouard reaction.	65
Table. 5.1	Process variables used in simulation.	79
Table. 5.2	Process parameters used in the simulation.	82

Appendix

The BVP Solver

The function `bvp4c` solves two-point boundary value problems for ordinary differential equations (ODEs). It integrates a system of first-order ordinary differential equations,

$$y' = f(x, y),$$

on the interval $[a, b]$, subject to general two-point boundary conditions,

$$bc(y(a), y(b)) = 0.$$

It can also accommodate other types of boundary value problems, such as those that have any of the following:

- Unknown parameters
- Singularities in the solutions
- Multipoint conditions.

In this case, the number of boundary conditions must be sufficient to determine the solution and the unknown parameters.

`bvp4c` produces a solution that is continuous on $[a, b]$ and has a continuous first derivative there. `bvp4c` is a finite difference code that implements the 3-stage Lobatto IIIa formula. This is a collocation formula and the collocation polynomial provides a C^1 -continuous solution that is fourth-order accurate uniformly in the interval of integration. Mesh selection and error control are based on the residual of the continuous solution.

The collocation technique uses a mesh of points to divide the interval of integration into subintervals. The solver determines a numerical solution by solving a global system of algebraic equations resulting from the boundary conditions, and the collocation conditions imposed on all the subintervals. The solver then estimates the error of the numerical solution on each subinterval. If the solution does not satisfy the tolerance criteria, the solver adapts the mesh and repeats the process. The user must provide the points of the initial mesh as well as an initial approximation of the solution at the mesh points.

Curriculum Vitae

Personal Data

Name: Shabi Ulzama
Date of birth: 01.07.1978
Place of birth: Moradabad, India
Nationality: Indian
Marital status: Single

Education

May 2003- April 2007 Doctorate in Engineering (Dr.-Ing.) in Chemical and Process Engineering.
Otto-von-Guericke Universität Magdeburg, Germany
May 2000-Dec. 2001 Master of Technology (M.Tech) in Process Engineering and Design.
Indian Institute of Technology New Delhi, India
May 1996-May 2000 Bachelor of Technology (B.Tech) in Chemical Engineering.
Z.H. College of Engineering and Technology, India

Working Experience

2006– 2007 Wiss. Mitarbeiter, Otto-von-Guericke-Universität Magdeburg,
Institute for Fluid dynamics and Thermodynamics

Publications

- Ulzama S. and Specht E., "An Analytical Study of Droplet Combustion under Microgravity: Quasi-steady-transient Approach", Proceedings of 31st International Symposium on Combustion-2006.
- Ulzama S. and Specht E., "Kinetic Analysis of Boudouard Reaction and its Dependence on Porous Structure", Conference Proceedings of AIChE Spring National Meeting-2006.
- Ulzama S. and Specht E., "Modeling the Reaction Mechanism of Lumped Porous Coke Particles during Industrial Processes", Conference Proceedings of IChE Chemcon-2005.